Robust Switching Recovery Control of a Quadcopter Aerial Vehicle Model

Thesis submitted for the degree of

Doctor of Philosophy

at the University of Leicester

by

Hasan Başak MSc (Manchester)

Control Research Group

Department of Engineering

University of Leicester

2018

Abstract

Robust Switching Recovery Control of a Quadcopter Aerial Vehicle Model

Hasan Başak

This thesis presents recovery control schemes that enable a quadcopter unmanned aerial vehicle (UAV) model to cope with a faulty actuation system.

First, the computational aspects of the design of fixed-order H_∞ controllers are investigated along with the performance they provide for the quadcopter UAV. Double-loop control structures are developed to control the translational velocities of the UAV subject to two different intermittent actuation problems. Fixed-order H_∞ controllers are designed for the nominal and the faulty modes of operation. These closed-loop modes are modelled as a switched system for which stability is analysed using minimum dwell time theory. Average dwell times are also computed by exploiting multiple Lyapunov-like functions that account for the delays in the detection of a fault.

The other key contribution of this thesis is the design of a switched recovery control scheme that does not require the explicit detection of the faults. Sufficient conditions are given in terms of linear matrix inequalities (LMIs) coupled with a scalar, and depend on modified Lyapunov-Metzler inequalities. The switched recovery scheme developed consists of jointly designed state feedback gains switched according to a min-switching strategy that preserves closed-loop stability and satisfy a prescribed H_∞ or H_2 performance.

Finally, the inherent fast switching issue of the min-switching strategy is treated at the expense of conservative reformulated LMIs conditions. Furthermore, the state-dependent switched control scheme is extended to output feedback case. Simulation results demonstrate the potential of the developed switching recovery control schemes to overcome various actuation faults.

ACKNOWLEDGEMENT

Firstly, I would like to express my sincere gratitude to my supervisor, Dr. Emmanuel Prempain, for his continuous moral and technical support, as well as his enthusiasm. I am indebted to him for providing the initial motivation for the research topic of this thesis, for answering all of my questions, constructive suggestions and stimulating discussions. I am grateful to Prof. Matt Turner for providing guidance during my APG transfer. I also wish to acknowledge financial support from Republic of Turkey, Ministry of National Education.

I would also like to thank my friends and their families in Leicester for their friendships and support: Dr. Angeliki Lekka, Dr. Emre Kemer, Dr. Ali Yavuz Polat, Dr. Ioannis Kyriakopoulos, Dr. Caner Gerek, Doğan Güner, Gökmen Durmuş, Hüsamettin Ateş, Erbil Çelik, Edip Demirel. Thanks to friends currently and formerly of the Control Research Group: Dr. Hessam Mahdianfar, Dr. Bharani Chandra, Dr. Peter Norton, Xiaoxing Fu, Teng D. Chollom, Dr. Nkemdilim Ofodile, Tomas Puller, Jahaz Alotaibi, Hao Yang.

Special thanks to Yılmaz Aydemir, Zuhal Aydemir and their families for their continues support.

Finally, I am greatly indebted to my wife for her patience and understanding while I was working evenings and weekends and to my parents who have supported me throughout my studies with their encouragement and love.

Hasan BAŞAK
25 July, 2017

CONTENTS

LIST OF TABLES

LIST OF FIGURES

NOMENCLATURE AND ABBREVIATIONS

Mathematical Symbols

N	an integer
$\mathbb{K}$	set of positive integers
$\mathbb{R}$	set of real numbers
$\mathbb{R}^n$	set of n-tuples of elements belonging to the set $\mathbb{R}$
$\mathbb{R}^{k\times l}$	set of k-by-l real matrices
$\mathcal{C}^1$	the space of continuously differentiable functions
$\mathcal{K}_\infty$	a continuous, strictly increasing and unbounded function f, $f(0) = 0$
$\in$	belongs to
$\forall$	for all
$\Longrightarrow$	implies
A'	transpose of A
$A' = A > 0$	A is symmetric positive definite matrix
$Tr(A)$	trace of a square matrix A
$\mathtt{diag}$	block diagonal matrix
$\dot{x}$	derivative of x with respect to time, $\frac{dx}{dt}$
$\frac{\partial f}{\partial x}$	a partial derivative of a function with respect to x
$\mathbb{N}$	set of natural numbers
$\mathcal{M}$	the class of Metzler matrices
D^+	upper Dini derivative

$\limsup$	limit superior
sup	supremum, the least upper bound
min	minimum
arg $\min$	the argument of the minimum
$He\{.\}$	hermitian operator defined as $He\{M\} = M + M'$
$\equiv$	equivalence
$\|.\|_\infty$	infinity norm
w	reference signals and disturbance
z	performance outputs such as error signals
$\|.\|$	Euclidean norm (vectors) or included spectral norm (matrices)
ρ	H_∞ squared norm
$\doteq$	is equal by definition

Symbols for Quadcopter Dynamics

d	ratio between the drag and thrust coefficients of the blade
I_{xx}, I_{yy}, I_{zz}	the quadcopter moments of inertia about body x, y, z axes, respectively
m	mass of the quadcopter
x_I, y_I, z_I	positions of the quadcopter in inertial frame
g	acceleration due to gravity
L	distance between centre of propeller and centre of the quadcopter
k_t	translational drag coefficient
k_r	rotational drag coefficient
f_i	upward lifting force produced by rotor i
τ_p, τ_q, τ_r	roll, pitch and yaw torques
ϕ, θ, ψ	Euler angles (deg)
p, q, r	body-fixed angular velocities about body x, y, z axes, respectively (deg/sec)
u_f	total upward lifting force
$\hat{u}_x, \hat{u}_y, \hat{u}_z$	virtual inputs
ω_i	the angular speed of rotor i
τ	time constant

Acronyms

UAV	Unmanned Aerial Vehicle
MIMO	Multi-Input-Multi-Outputs
SISO	Single-Input-Single-Output
LMIs	Linear Matrix Inequalities
LPV	Linear Parameter Varying
FTC	Fault Tolerant Control
FDD	Fault Detection and Diagnosis
SMC	Sliding Mode Control
DOF	Degrees of Freedom
LTI	Linear time-invariant
PID	Proportional-Integral-Derivative
LOE	Loss of Effectiveness
BFGS	Broyden-Fletcher-Goldfarb-Shanno algorithm
LQR	Linear Quadratic Regulator

CHAPTER 1

INTRODUCTION

Unmanned aerial vehicles (UAVs) have been gaining in popularity in civil and commercial applications for decades. This popularity is due to advanced technology in microelectromechanical systems and sensors, increasing computational power of microcontrollers, improvements in energy storage in batteries and the decreasing price of UAVs. This offers new application areas for UAVs in various fields. UAVs were originally designed for military applications, and the associated industrial sector has historically constituted an important part of defence commerce. They have been used for surveillance, border patrolling, target acquisition requirements, mine detection, and aerial delivery of payloads. UAVs also have potential applications in civilian usage such as for disaster management during floods, earthquakes, fire, etc., commercial missions like aerial photography, filming for television and cinema, and research and development programs which need flying vehicles to perform various tasks.

Common UAVs are quadcopters (also called quadrotor helicopters) which have six Degrees of Freedoms (DOFs) under-actuated mechanical systems. These vehicles have less control inputs than they have DOFs. In this case, a possible combination of controllable outputs are translational velocities (in x-y-z axes) of the quadcopter with respect to its inertial fixed frame and its yaw angle. The other remaining two DOFs, roll and pitch angles, are determined by the trajectory tracking demands of the translational velocities in the x and y axes. Over the last decade, research has focused on the development of control systems that allow quadcopters to demonstrate effective and robust flight performance.

1.1 Motivation

Flight control system designs need to be robust in the face of disturbances and model uncertainty. H_∞ synthesis can be used to design controllers with robust performance. However, the standard H_∞ controller synthesis algorithm computes an optimal H_∞ controller by solving two Riccati equations [52]. The order of the controller is equal to that of the order of the open-loop plant plus the order of weighting functions, which can be very high in practice and complex in implementation. Simple controllers such as PIDs or control architectures combining PIDs with filters are preferred in practical implementation for their relatively reduced cost and flexibility of implementation. Low-order H_∞ controllers can meet the architecture requirements in embedded control applications [44]. Fixed-order and structured H_∞ optimisation algorithms, such as *hifoo* [13] and *hinfstruct* [13], will be used to synthesize low-order H_∞ controllers. These algorithms can provide satisfactory controllers in terms of bandwidth, disturbance rejection, and robust stability.

Quadcopter UAV systems may encounter loss of effectiveness (LOE) due to motor (actuator) faults, e.g., component failure or damage to the motors, propellers, and so on. A partial LOE in one or more of the motors causes simultaneous loss of thrust and torque. The impact of such a fault can lead to performance deterioration, instability and even unexpected catastrophic accidents. Without any proper recovering action, these endanger personnel on the ground if being operated in a crowded environment. Thus, it is essential to develop effective fault recovery control schemes to accommodate these faults and to ensure a high degree of operational performance for the overall control system in abnormal situations.

Fault tolerant control (FTC) is becoming vital to quadcopter vehicles due to reliability concerns. FTC approaches are classified into passive or active approaches. Passive approaches are those such as the use of a robust controller that can deal with faults of limited severity and are sufficient for dealing with small parameter and signal changes. However, in many practical situations, a variety of the system parameters that can be caused by faults might be of significant magnitudes. Stabilisation of a system with significant changes in parameters is often impossible with a single robust controller. In this instance, an active switching recovery control scheme allows the controller to adapt to different failure situations [146, 161]. One advantage of using switched control is that the faults are taken into consideration in the control law design. As a result, the robust stability of the controlled system in the presence of actuator faults is guaranteed.

The main concern of this thesis is to show how the properties of switched control can be employed to provide a solution to the above considerations and to enhance the capability, reliability and stability of UAV systems. A switching recovery control scheme is shown in Fig. 1.1, where the controllers are precomputed by considering fault situations in advance. The study of stability of switching recovery control schemes is motivated by the possibility of instabilities that might be caused by switching. For example, when all possible subsystems of switched systems are stable, the switched system might possess divergent trajectories for specific switching signals; however, switching carefully between unstable subsystems can lead to stability [31].

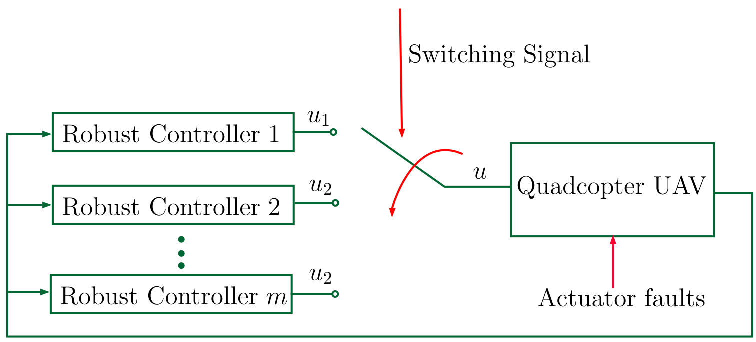

Figure 1.1: Robust switching recovery control structure.

The significant amount of research in the literature involving quadcopter UAVs generally considers pure flight control problems, and has essentially paid no attention to intermittent and time-varying motor faults. A quadcopter subject to intermittent motor faults can be treated as a system switching between faulty and healthy cases. The stability of the resulting closed-loop switched system is an important issue of control design. Lyapunov functions are used to achieve stability under switching by constricting the switching signals through dwell time (time-dependent switching) requirements. The closed-loop stability of the resulting switching system will be analysed using dwell time theories. The problem of a quadcopter UAV system subject to undetected time-varying LOE in motors will be considered as a polytopic switched linear parameter varying problem. A fault tolerant control scheme will be proposed that consists of designing controllers which are switched according to a state-dependent switching strategy. The switched fault tolerant control should thus preserve the stability of the quadcopter system in the presence of time-varying faults.

1.2 Thesis Outline

This thesis is divided into eight chapters.

- Chapter 2 is devoted to literature reviews. The recent works of flight control and FTC approaches to quadcopter UAVs are briefly reviewed. This chapter continues by giving common FTC definitions and terminologies, and noting some typical types of faults. Recent works in field of FTC are discussed including a summary of their advantages and disadvantages.

- Chapter 3 begins with basic definitions of systems and local stability. Stability analysis of switched systems, such as the common quadratic Lyapunov function, multiple Lyapunov functions, and time-dependent and state-dependent switching approaches are presented in detail.

- Chapter 4 presents a non-linear model of the quadcopter UAV used in this thesis. The Newton-Euler approach is applied by including only the most relevant aerodynamic effects within the model. The model is derived from the rigid body dynamics approximation of the quadcopter as influenced by different forces and moments. This non-linear model will be used in subsequent chapters to design control laws and as a demonstration of the capabilities of the controllers through simulation.

- Chapter 5 contributes to the identification of the best simple robust controller for application with the quadcopter by comparing the designs of various low-order robust controllers. H_∞ mixed sensitivity setup is given for shaping sensitivity and complementary sensitivity functions to achieve the control objectives of the closed-loop system. The theoretical backgrounds to various robust control techniques, such as fixed-order, structured H_∞ synthesis, LMI approach and mixed sensitivity H_∞ optimisation, are briefly explained. The computational efficiency and tracking performance of low-order controllers are compared with those of a standard full-order H_∞ controller. We will show time domain simulations of the low-/full-order H_∞ optimisation techniques such that the quadcopter is able to track some given reference attitude and heave position.

- In Chapter 6, the main contribution is to develop a new switching recovery scheme for UAV systems. Here, a double-loop control structure is proposed for this purpose. The inner-loop controller is switched according to pre-assumed available detection information. Switching between controllers has the potential to cause degraded transient responses due to the initial states. In this chapter, we introduce a straightforward method to initialise controller states during switching instants. The proposed structure is applied in case of intermittent actuation problems to enable the quadcopter to autonomously return from missions. Fixed-order H_∞ output feedback controllers are designed for the stabilisation of the vehicle attitudes and for the tracking of the translational velocities. The stability of the resulting synchronous- and asynchronous-switched (due to detection delays) closed-loop systems is analysed using dwell time theory and multiple Lyapunov functions, respectively. Simulation results are provided to demonstrate the potential of the proposed switching control scheme.

- Chapter 7 proposes a novel passive FTC for the problem of time-varying loss of rotor effectiveness. The proposed schemes does not include any FDD to detect the faults that significantly reduces computational complexity and increases the corresponding time of the controller. The passive FTC comprises state feedback gains and a min-switching strategy which are jointly designed. We show that the stability and the performance of the controlled system is maintained despite the fact that there is no fault detection mechanism involved in the design. State-dependent switched control strategy has inherent chattering behaviour. To address this issue, a relaxed minimum switching strategy is proposed. Sufficient conditions of controller synthesis are given under this relaxed minimum switching strategy by means of LMIs. Proposed switched recovery control schemes with relaxed minimum switching rules are performed using a non-linear model of the quadcopter model to demonstrate how chattering has been reduced. Moreover, a dynamic output feedback switched controller is proposed to eliminate the dependence of the min-switching strategy on full-state measurements. The responses of state-dependent switched control strategy are also compared to those produced with a switched and a constant H_2 state feedback controllers. Simulation results are included to demonstrate the potential of the proposed solutions.

- Finally, Chapter 8 discusses the contributions of this thesis to current research and possible directions for future work.

1.3 Publications

1. Hasan Basak and Emmanuel Prempain, Low order H_∞ controllers for a quadrotor UAV. IEEE UKACC International Conference on Control (CONTROL),(pp. 127-132), 2014.

2. Hasan Basak and Emmanuel Prempain, Switching recovery Control of Quadrotor Drones Subject to Intermittent Motor failures. Poster session presented at :11^{th} University of Leicester Festival of Postgraduate Research, 6^{th} of july 2015; Leicester, UK

3. Hasan Basak and Emmanuel Prempain, Switching recovery control of a quadcopter UAV. IEEE European Control Conference (ECC), (pp. 3641-3646), 2015.

4. Hasan Basak and Emmanuel Prempain, Switched fault tolerant control of a quadrotor UAV. IFAC World Congress, vol. 20, no. 1, (pp. 10363-10368), 2017.

CHAPTER 2

LITERATURE REVIEW

2.1 Introduction

This chapter begins with a literature review of flight control and FTC approaches to quadcopter UAVs. Key definitions and certain important concepts from fault tolerant control are introduced. To understand the main features of recovery control schemes, an initial background into related research and proposed approaches to fault tolerant control in the literature are also presented. This chapter is organised as follows: Section 2.2 will review the literature on flight control and FTC approaches to quadcopter UAVs. Section 2.3 introduces various definitions of different types of faults and failures; different fault tolerant control approaches are also presented. Finally, Section 2.4 gives a summary of this chapter.

2.2 Review on Control Apporaches to Quadcopter UAVs

The following survey provides a brief overview to related research published in recent years.

2.2.1 Flight Control Approaches

The dynamics of quadcopters are non-linear and multi-variable. A variety of approaches to fault-free quadcopter UAVs have been proposed to improve the flight control performance in the literature. Altug et al. [3] presented feedback linearisation and backstepping control methods for a quadrotor. The vision feedback system is used as a sensor to estimate the position and orientation of the helicopter. Flight experiments show that the helicopter could perform vertical and yaw motions. Bouabdallah et al. [19] designed a small-size quadrotor and stabilised angular rotations using a pole placement method. Proportional Integral Derivative (PID) and Linear Quadratic Regulator (LQR) controllers were designed in [20]. Experimental results showed that a classical PID controller is able to control angular orientations of a quadcopter in the presence of a disturbance. Hoffmann et al. [63] designed the Stanford Testbed of Autonomous Quadrotor for Multi-Agent Control (STARMAC). Here, the altitude is controlled by sliding mode control and LQR techniques. The experiment was undertaken manually by eliminating wind disturbance. Castillo et al. [23] proposed a controller based on Lyapunov analysis where global stability achieved. Real-time experiments illustrate that the tasks of taking off, landing and hovering are autonomously performed. Backstepping and a sliding-mode techniques were applied by Bouabdallah and Siegwart [17] to an autonomous quadrotor. Experimental results demonstrated that the backstepping technique is better at control in the presence of relatively large disturbances. Tayebi and McGilvray [139] proposed a quaternion-based feedback controller based on compensating for the coriolis and gyroscopic torques for attitude stabilisation. They conclude that compensating for the coriolis and gyroscopic torques does not make an important difference owing to the initial conditions and the relatively low speeds considered. Bouabdallah and Siegwart [18] provided a collision-avoidance controller using an integral backstepping method for the control of attitude, altitude and positions. This approach is not sufficient to perform free flight. Hoffmann et al. [64] analysed the various aerodynamic effects that result in moments influencing attitude and altitude control. The quadrotor hovers for about 50 seconds with a circle of 0.8 m using a PID controller. Dynamic inversion with zero-dynamics stabilisation was proposed by Das et al. [26], where the controller so designed was effective in the presence of perturbations, whilst Lyapunov theory ensures stability and tracking performance. Experimental results illustrate that a quadrotor is autonomously navigating in indoor environments in [54]. Hoffmann et al. [65] presented a trajectory-tracking control so that a quadrotor follows a desired path and dynamically feasible trajectories, where the algorithms consist of obstacle avoidance and computation of control inputs.

The trajectory-tracking algorithm demonstrates that the quadrotor is able to track a path indoors with a 10 cm accuracy and outdoors with a 50 cm accuracy. A model reference adaptive control was applied to a quadrotor in the presence of actuator uncertainties and non-linearities in [136]. More recently, Raffo et al. [110] present a state-space predictive controller and integral robust controller to deal with the tracking problem under parameter uncertainty. The simulation results show that robust performance is provided by the designed controller in the case of parametric uncertainties in the mass and inertia terms. An L_1-optimal controller is designed and implemented by Aykut et al. [11] where the controller rejects persistent disturbance in experiments, and the performance of the controller is compared with the backstepping method. Leishman et al. [83] demonstrate how accelerometer measurements can be used from an improved dynamic model of a quadrotor to estimate velocity and attitude. Ma et al. [92] propose a solution to a trajectory tracking problem of quadcopter experiencing disturbances using an active disturbance rejection and predictive control. Jia et al. [73] develop an integral backstepping sliding mode controller in the presence of constant and stochastic disturbances. Due to the combination of the advantages of backstepping and sliding mode controllers, the proposed controller achieves better trajectory tracking performance than the PID, LQR and backstepping approaches. However, all above cited works have been proposed to deal with control of UAVs under normal flight conditions without the further consideration of potential actuator faults. The next section will take a closer look at the work published relating to FTC of quadcopter UAVs over the last decade.

2.2.2 Fault-Tolerant Control Approaches

Research into the FTC of unmanned aerial vehicles has become increasingly important to allow UAVs to fly safely. Numerous contributions have been made regarding the reliability of quadcopter vehicles over the past decade. However, most fault tolerant control methods with application to quadcopters cope with constant actuator faults and the availability of research in the literature on quadcopter time-varying actuator faults is still quite limited. Sharifi et al. [128] represented a sliding mode controller design method in the presence of external disturbances and a fixed 50 % loss of effectiveness (LOE) in an actuator. A Luenberger linear observer is employed to estimate the outputs of actuators to allow the detection of possible faults. The fault detection mechanism subtracts the estimation of each output from the rotor output demanded, as computed by the control law. If the error between these two values is greater than a set threshold for longer than some given minimum time, the corresponding rotor is deemed to be faulty. Ranjbaran and Khorasani [112] developed an adaptive feedback linearisation recovery strategy which enhances the capabilities of the quadrotor system to operate under 25 % and 50 % partial LOE of an actuator. The proposed fault recovery mechanism is also validated in the instance of any delay in recovery. The recovered longitudinal response settles in 70 seconds under a 25% LOE of the first actuator when there is some delay in the detection and isolation of the fault. Ranjbaran and Khorasani [111] extended the work presented in [112], where multiple LOE faults in different actuators are considered by assuming that a fault detection and diagnosis (FDD) unit is available. A constant 20 % LOE fault in an actuator at 20 seconds and a constant 30 % LOE fault in another actuator at 35 seconds occur sequentially in the flight conditions. Simulation results show that this control method reduces the tracking error. Zhou et al. [163] designed an FTC based on feedback linearisation control assuming that the mode dynamics are known. In the practice, nominal systems remain highly vulnerable to uncertainties. Therefore, this FTC does not guarantee robust stability of the controlled system in the presence of uncertainty.

Sadeghzadeh et al. [119] propose a Model Reference Adaptive Control (MRAC) technique to address the presence of faults in one or more actuators. A variety of scenarios are taken into consideration, such as 14 % LOE fault in all four actuators and physical damage of 15 % to one of the four propellers during autonomous flight. The developed FTC method does not handle major changes in the system dynamics well. The simulation results showed that there is almost 80 % undershoot in response to the height position of a quadrotor in the case of 14 % LOE in all actuators. Dydek et al. [35] propose a direct and indirect model reference adaptive control for a quadrotor. The robustness is compared with a baseline controller; the adaptive controller increases robustness against parametric uncertainties by accounting for any uncertainties inherent to the control law design, and reduces the effects of any loss-of-thrust anomaly. A combined model reference adaptive controller (CMRAC) is a combination of direct and indirect adaptive control. For a 25% collective thrust reduction, CMRAC provides better performance over MRAC and a baseline controller as it can adapt to both estimation and tracking errors. If one of the propellers is damaged by cutting both tips in flight, which results in an approximate

40% LOE of the associated actuator, the model reference adaptive controller recovers the UAV from the fault. Büyükkabasakal et al. [22] developed a mixing adaptive control that blends the outputs of a set of predesigned adaptive controllers. The loss in vertical position is observed in the simulation and experimental results. Although this control scheme provided robust stability, the parameters of the estimation algorithms have to be re-tuned to achieve better tracking performance.

Besnard et al. [16] developed a sliding mode control to deal with partial LOE, while a sliding mode disturbance observer is employed to estimate the effects of any disturbances. Simulation results have showed that the sliding variable has a chattering problem, and hence has to be filtered to obtain an equivalent control law. Barghandan et al. [14] combined an adaptive fuzzy control with a sliding mode control to overcome model uncertainties and actuator faults. It was assumed that rotors imposed a small range of constant faults. A conventional quadrotor UAV is modified in [120] by adding two actuators to the quadrotor. These redundancy actuators rendered the control re-allocation method capable of dealing with severe actuator faults. When faults occur in the actuator located underneath an extra upward actuator, the modified quadrotor can remain at hover when a piece of a propeller is cut off under flight conditions without the need for control re-allocation. The vehicle can maintain its stability at the levelled position with control re-allocation under conditions of severe damage to an actuator. Chamseddine et al. [25] propose a flatness-based flight trajectory planning/ replanning method, assuming that an FDD scheme is present to detect the fault. This method redefines the reference trajectory to allow it to function under 25 % LEO in an actuator and requires an online solution to the given optimization problem. A gain-scheduled PID control technique is developed in [118], where the parameters of the controller change by considering operating conditions; however, the single PID could not manage to maintain the desired height of the quadrotor when a fault with an 18% loss in control effectiveness occurred. The gain-scheduled PID prevents the quadrotor from hitting the ground after fault occurrence as new control parameters are scheduled based on information from an FDD. Rotondo et al. [114] presented a fault-tolerant control strategy based on an LPV system. The passive and active FTCs are compared under the fault scenario of constant 50 % LEO of an actuator, and also of two actuators. Simulation results show that the fault-tolerant controllers designed specifically for a single actuator fault provide better performance than the nominal controller. The results with the fault-tolerant controllers designed for two actuator faults show a deterioration in performance when compared to the nominal and the single fault cases. Yu et al. [152] compared two control algorithms based on a linear quadratic regulator (LQR) and model predictive control under an actuator LEO. Simulations results showed that the LQR method cannot handle 30 % and 50 % LEO in actuators. The model predictive controller can handle a 30% LEO in an actuator with an excellent degraded performance.

Recently, Lanzon et al. [82] presented a robust feedback linearisation control in the presence of a permanent rotor fault in a quadrotor vehicle. The proposed control strategy enables the vehicle to use the remaining three functional rotors to deal with a rotor failure. The quadrotor spins in yaw direction to maintain its stability. To deal with a similar problem, Lippiello et al. [89] propose a backstepping approach such that the quadrotor can land in case of a permanent propeller fault. In addition to the cited works, Mueller and D'Andrea [102] provided periodic solutions when a quadrotor loses either a single, two opposing, or three propellers. Merheb et al. [98] proposed an active FTC using sliding mode control and sliding mode observers, where a saturation function is used to design the discontinuous control law that causes chattering problems for certain rotor speeds. The sliding mode controller is reconfigured using the estimated fault information. In addition, the authors developed a passive FTC using sliding mode control theory in [99] to deal with a partial LOE affecting all motors simultaneously. Segui-Gasco et al. [126] increased the complexity of convectional quadrotor architectures to overcome a complete actuator failure by using dual axis tilting propellers. A collection of different approaches designed to address the reliability and safety of quadrotors under constant loss of actuator effectiveness is given by Zhang et al. [158]. More recently, researchers have focused on the problem of sensor faults. For instance, López-Estrada et al. [91] proposed an LPV model-based FTC for a quadcopter in the presence of external disturbances, where a bank of robust LPV observers is used to detect and isolate possible sensor faults. Asymptotic stability under external disturbance is guaranteed by means of sufficient conditions. For a similar problem, Avram et al. [10] presented a fault detection and accommodation algorithm by employing non-linear adaptive estimators. A non-linear fault detection estimator and a bank of non-linear adaptive fault isolation estimators are considered in order to obtain a diagnosis architecture. Adaptive thresholds for fault detection and isolation are considered to avoid false alarms within the diagnostic algorithm. The fault parameters determined by the isolation estimator are used to recover the system from a sensor fault condition. However, the quadcopter actuation systems are vulnerable to time-varying faults due to damage to the motors, loosening of soldered joints, and so on. The occurrence of such time-varying actuator faults results in a deterioration of tracking performance and even instability of the controlled system.

2.3 Review on Fault Tolerant Control

In this section, we describe the different types of faults and failures that can occur in actuators. Later, current approaches of Fault Tolerant Control (FTC) will be presented. The technical committee in [69] make the following definitions to avoid confusion amongst researchers.

Fault *is an unpermitted deviation of at least one characteristic property or parameter of the system from the acceptable/ usual/ standard conditions.* ***Failure*** *is a permanent interruption of a system's ability to perform a required function under specified operating conditions.*

More precisely, a failure is a much worse condition than fault. For instance, when an actuator experiences a fault, the actuator can be still usable but may become less effective or have a slower response. However, when a failure occurs, the actuator needs replacing with a new one to produce the desired effect.

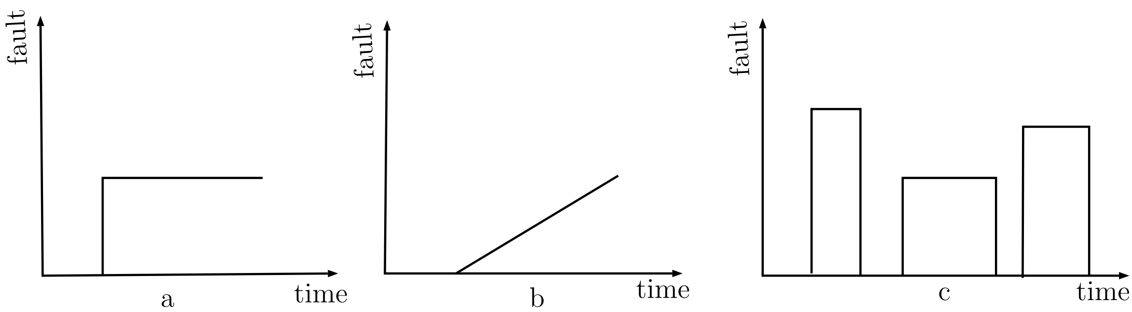

Figure 2.1: Faults with respect to time (a) abrupt; (b) incipient; (c) intermittent (adopted from [68]).

Faults/ failures can be classified in terms of time that illustrated in Fig. 2.1. *Abrupt fault* (**a**) represents a very severe situation and this fault might affect stability of the system. These types of faults usually occur due to hardware damage. *Incipient fault* (**b**) represents a situation whereby the fault characteristics vary slowly due to for instance gradual component wear. *Intermittent fault* (**c**) is a combination of impulses with different amplitudes. It represents a repetitive malfunction. Intermittent faults, as their name suggests, happen only intermittently with respect to time and can be due to intermittent contact or aged wiring in some part of the circuitry, for instance. These type of faults are not necessarily repeatable during maintenance testing [125].

2.3.1 Modelling Multiplicative Actuator Faults/ Failures

Multiplicative modelling is commonly employed to represent actuator faults/ failures. Multiplicative faults/ failures may not explicitly influence the dynamics of the controlled system. These faults can affect the closed-loop system, and hence may result in uncontrollability of the system. Actuators are the interface between the controller signals and the plant. An actuator fault is defined as a loss of effectiveness, i.e., reduced capability, as compared to the fault-free operating condition. In the case of a fault situation, an actuator will only partially achieve the required controller demand, and might result in a degraded performance. Actuator faults may stem from, for instance, a drop in voltage supply, increased resistance, etc [59]. One representation of an LTI system subject to actuator faults or failures is

$$\dot{x}(t) = Ax(t) + B\Omega u(t) \tag{2.1}$$

where $A \in \mathbb{R}^{n\times n}, B \in \mathbb{R}^{n\times m}$ and $\Omega = \text{diag}(k_i, ...k_m)$ is a diagonal weighting matrix. The scalars $k_i, ...k_m$ represent the loss of actuator effectiveness. If $k_i = 1$, it means that the corresponding i^{th} actuator has no fault and is working perfectly, whereas if $1 > k_i > 0$, an actuator fault is present. On the other hand, $k_i = 0$, represents a complete loss of effectiveness, or the failure, of a particular actuator. This representation has been used by other researchers in the FTC field, for instance [4, 59, 159].

2.3.2 Current FTC Approaches

Faults/ failure in actuators may lead to an unsatisfactory performance, or even instability with a standard feedback controller. In order to enhance the capability of the control system against such weaknesses, new methods to control system design have been proposed in order to maintain desired stability and performance properties in the presence of component malfunctions [160].

FTC systems can be categorised into passive fault tolerant control systems and active fault tolerant control systems [106]. In passive FTC systems, controllers are designed to be robust against presumed faults and uncertainty. Therefore, passive FTCs are generally robust controllers that cope with faults without requiring information from a Fault Detection and Diagnosis (FDD) module. Their fault tolerance capabilities are thus limited. Furthermore, there is no guarantee of stability and performance since impaired signals are used in the closed-loop system.

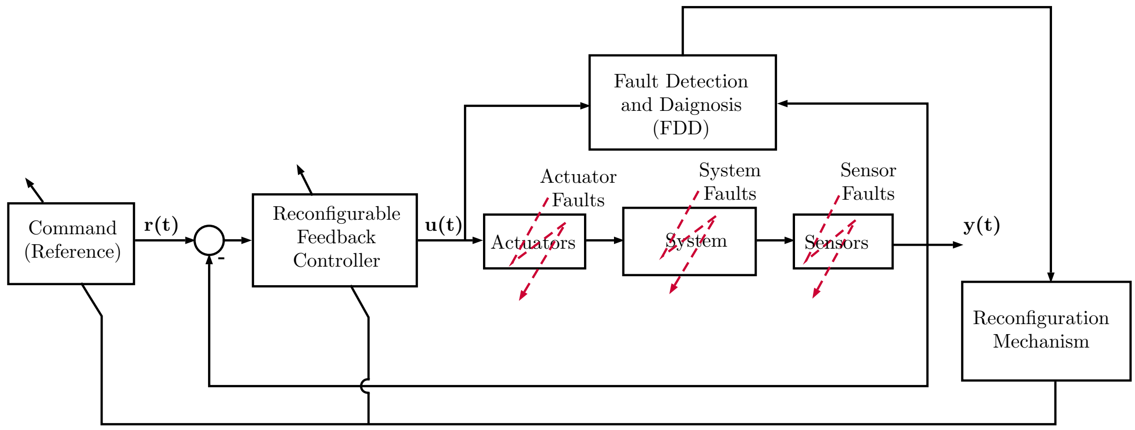

Figure 2.2: A structure of an active fault tolerant control system (adopted from [160]).

Active FTC typically needs a FDD which provides some information on occurrence of the faults/failures. A typical active FTC system is shown in Fig. 2.2. The FDD module should detect and isolate any fault in the system as quickly as possible. Fault parameters, system state/output variables, and post-fault system models need to be estimated online in real time. The reconfigurable controller should be designed to automatically maintain stability, desired dynamic performance and steady-state performance based on the on-line information. In addition to a reconfigurable controller, a command/reference may also need to be designed to adjust the command input or reference trajectory automatically. This avoids potential actuator saturation and degraded performance after the occurrence of any fault. In the literature, the survey papers [74, 106, 153, 160] and books [5, 36] give extensive bibliographical reviews of various FTC approaches. A general overview of the implementation of FTC is presented in Fig. 2.3. Active FTC can be divided into two sub-groups: projection- based FTC and online reconfiguration/adaptation.

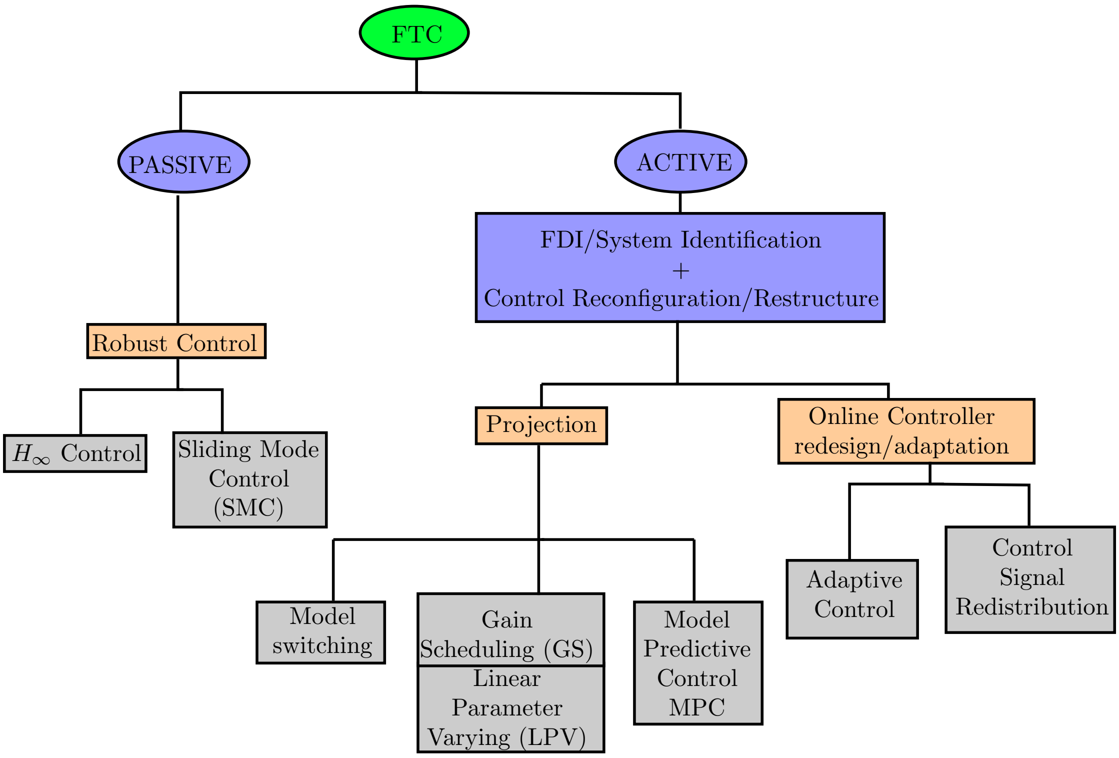

Figure 2.3: Classification of fault tolerant control (adopted from [5]).

H_∞ Control

H_∞ control has been developed for many applications ranging from industrial process control to aircraft control problems. The main objective of H_∞ control is to design feedback control laws which are robust against plant dynamic uncertainties and disturbances. Since partial actuator faults can be considered a type of uncertainty, an H_∞ control approach can be used to address it. This controller can be categorised as passive FTC, which does not need information regarding faults online and hence works in normal and abnormal conditions. The designed controller has a limited capability to deal with faults by minimising the effect of uncertainty or disturbances on the system [96]. H_∞ control theory has been built based on the minimisation of the peak values of given system transfer functions over frequency; this minimisation can be chosen by the designers to meet particular given design objectives. H_∞ optimisation approaches allow designers to satisfy stability and performance specifications in the instance of modelling errors, uncertainty and perturbations due to disturbances or noise. Frequency-dependent weighting functions are used to shape input and output signals such that performance and robustness specifications can be attained [72, 94, 133]. Consider an LTI continuous time system described by

$$\dot{x}(t) = Ax(t) + Bu(t) \tag{2.2}$$
$$y(t) = Cx(t) + Du(t) \tag{2.3}$$

where $x(t) \in \mathbb{R}^n$ is the state vector, $u(t) \in \mathbb{R}^m$ the input vector and $y(t) \in \mathbb{R}^p$ is the output vector. A transfer function matrix corresponding to the system in (2.2) and (2.3) can be given as

$$G(s) := C(sI_n - A)^{-1}B + D. \tag{2.4}$$

The sensitivity and the complementary sensitivity transfer functions are defined as $S(s) = (I + G(s)K(s))^{-1}$ and $T(s) = I - S(s)$. Various important relationships, as

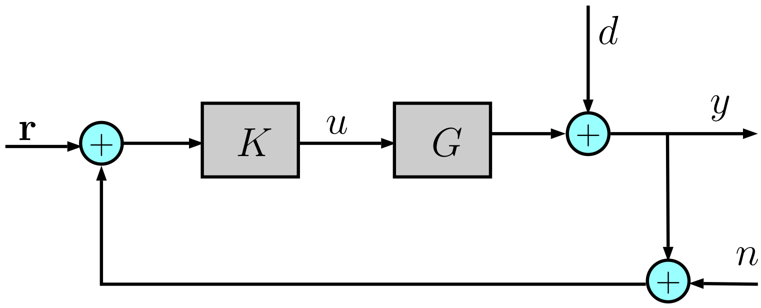

Figure 2.4: Closed-loop system.

given below, can be derived from the closed-loop system shown in Fig. 2.4:

$$y(s) = T(s)\mathbf{r}(s) + S(s)d(s) - T(s)n(s) \tag{2.5}$$
$$u(s) = K(s)S(s)\left[\mathbf{r}(s) - n(s) - d(s)\right] \tag{2.6}$$

The closed-loop system is determined from relationships (2.5) and (2.6): $|S(j\omega)|$ and $|T(j\omega)|$ must be chosen to be small for disturbance rejection and noise attenuation, respectively. $|K(j\omega)S(j\omega)|$ should be chosen to be small for reduced control energy. $|T(j\omega)| \simeq I$ should be optimised for good reference tracking.

One drawback of H_∞ controller is that the final controller is usually of a higher order than the system [96]. In practice, low-order controllers are preferred to make them implementable. The following subsection gives an overview of recent work on low-order robust control methods.

Low-order H_∞ Optimal Control Synthesis

First ideas and necessary conditions for fixed-order dynamic compensation are given by Hyland and Bernstein [67], which are based on two modified Riccati and Lyapunov equations. Gahinet and Apkarian [42] show that if the rank minimisation problem under linear matrix inequalities (LMIs) constraints is satisfied, then a reduced-order controller can be computed. Iwasaki [70] proposes a dual iteration method for low-order H_∞ synthesis that uses state feedback and the observer gain variables. This method is not guaranteed to converge to the global minimum and it crucially depends on the initial feedback and observer used. Grigoriadis and Skelton [53] solve H_∞ synthesis problems described by LMIs using alternating projections. At each iteration, the control order is decreased, such that a low-order controller is ultimately obtained. The algorithm is very efficient for small- and medium-size problems, and only local convergence is guaranteed. A cone complementarity linearisation method is given by El Ghaoui et al. [37], which computes stabilising low-order controllers. However, it is reported that this algorithm could not find the lowest order controller in all cases. More recently, Orsi et al. [104] present an algorithm is to solve non-convex feasibility problems using LMI constraints with rank constraints. This method is implemented in the software, LMIrank. In comparison, Apkarian and Noll [7] do not use the LMI formulation and Lyapunov variables; instead, their algorithm uses generalised gradients and bundling techniques. Therefore, large size problems can be solved using this algorithm. The authors report that this algorithm is efficient even for systems with several hundred states. Descent directions are computed by solving quadratic programs, and line search direction is carried out. This algorithm is now available as code, *hinfstruct* in MATLAB/Robust Control Toolbox. At the same time, a code package, fixed-order H_∞ optimisation, *hifoo* is proposed by Gumussoy et al. [58]. *hifoo* has been successfully applied to different benchmark examples in [56, 57]. Arzelier et al. [8] extend *hifoo* to H_2 performance criteria and developed it for mixed H_2 /H_∞ synthesis. *hifoo* has been used for the lateral control of high-capacity passenger aircraft in [61]. Gahinet and Apkarian [45] report that *hinfstruct* is significantly faster than *hifoo*. In addition to this, Puyou and Ezerzere [109] claim that the *hinfstruct* method has yielded more reliable results.

Sliding Mode Control

Sliding Mode Control (SMC) is a form of robust control technique that can deal with uncertainties and disturbance [115]. The robustness property of SMC makes it a good candidate for providing satisfactory closed-loop performance in the event of any system fault. The idea of SMC consists of two stages. At the first stage, a sliding surface is defined. At the second stage, a controller-based on this surface is developed, that results in the sliding motion of states on the slide surface, and then states converge to the desired trim point. Let us consider the following single-input linear system

$$\dot{x}(t) = Ax(t) + Bu(t) \tag{2.7}$$

where the scalar $x(t)$ is the output of a system, and the scalar $u(t)$ is the control input. The sliding mode function is defined in [107] as $s(x) = Sx = 0$, where S is a full rank matrix. A sliding motion is assumed to occur on the surface. In sliding mode, $s(x,t) \equiv 0$, and we only need to differentiate s once such that the input u appears,

$$\dot{s} = SAx(t) + SBu(t) = 0. \tag{2.8}$$

Assuming that SB is invertible, the equivalent control is $u_{eq}(t) = -(SB)^{-1}SAx(t)$.

According to [66], the dynamics of the sliding mode function are specified by the differential equation as $\dot{s} = -Qsgn(s) - Rs$, where *sgn*(.) is the signum function. The sliding mode control law is solved directly from $\dot{s} = SAx(t) + SBu(t) = -Qsgn(Sx(t)) - RSx(t)$ as follows:

$$u(t) = -(SB)^{-1}(SAx(t) + Qsgn(Sx(t)) + RSx(t)) \tag{2.9}$$

where matrices S, Q and R are experimentally chosen.

One of the drawbacks of SMC is that SMC is not able to deal with failures directly; additionally, a mechanism is required to redistribute control inputs among redundant healthy actuators. That is, if there is enough redundancy in the system, SMC can deal with total actuator failures [59]. Papers [4, 16, 128, 129, 144] and books [5, 60] represent some of the recent work in the framework of field of FTC.

Adaptive Control

Adaptive control systems are comprised of a controlled plant, controller parameters and adaptive law to adjust the control parameters to achieve the desired performance. The adaptive control is classified as being of two types: indirect adaptive control and direct adaptive control [34]. In indirect adaptive control, the system parameters need to be estimated in case of any change (e.g., faults/ failures) in the operational conditions. This information is then used to design the indirect adaptive controller. However, a direct adaptive controller is designed directly rather than initially determining the model parameters [34, 77, 150]. One of the more popular adaptive control approaches is Model Reference Adaptive Control (MRAC), which forces the plant output to be equal to that of a reference model. A block diagram of MRAC is depicted in Fig. 2.5(a), where the control objectives are given in terms of a reference model and the controller parameters are adjusted directly to obtain those objectives. Another form of adaptive control is Self Tuning Control (STC), whose block diagram is given in Fig. 2.5(b). The plant parameters are estimated by an estimator and this information is then used to compute the parameters of the controller. For the purposes of FTC, adaptive controllers lack the capability to handle unanticipated

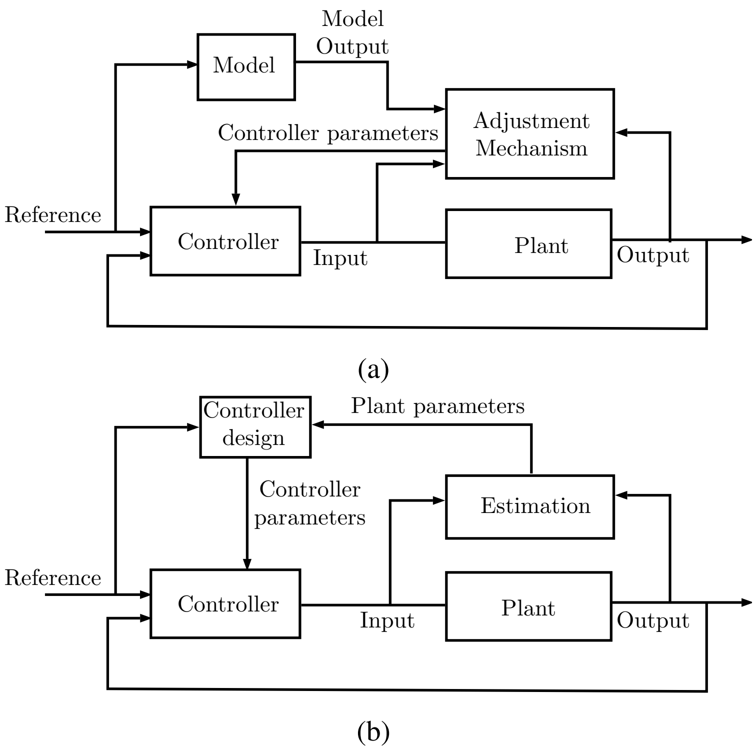

Figure 2.5: Adaptive control systems (a) MRAC, (b) STC (adopted from [9]).

faults or major system change in system dynamics alone [96], and a combination of other methods is required as given in [79].

Model Predictive Control

The development of Model Predictive Control (MPC) began in the process industry due to its simplicity and easy to be understood by engineers. The main idea of MPC is to allow the production process to run as close as possible to process limits in order to maximise production. MPC performs control signal redistribution while satisfying any constraints for redundant dynamics. MPC is an alternative approach to flight control and especially FTC because of its ability to handle limits and constraints. However, similar to most FTC methods, MPC depends on an FDD to provide information regarding any abrupt change in system parameters due to fault occurrence. In the case of actuator faults, an online parameter estimation is required to compute faulty model parameters from online input and output. As a result, a new constraint can be included in the optimisation process. Some papers discussing MPC as a form of flight control are [1, 71, 78, 93]. FTC described in the literature [78, 93] comprises three components: an FDD that identifies a fault magnitude, a 'Reference Model' which uses pilot commands to generate a reference trajectory for the aircraft's state vector, and an MPC controller whose objective is to track the reference trajectory, using the output of the FDD to update its internal model, constraints, etc. Recently, [151] proposes an FTC scheme where a bank of MPC controllers for different possible faults and state estimators to estimate the fault situation. Fault information from the FDD is used to activate the appropriate MPC controller. A drawback of MPC is the requirement of an online solution to the constrained optimisation problem. Online optimisation is hard to obtain in current computing hardware, where systems require fast responses [96].

Control Signal Redistribution

One of the most cited control signal redistribution methods is that of Pseudo-Inverse Modelling (PIM) because of its computational simplicity [47, 137]. The basic idea of PIM is to reduce the distance between the closed-loop of the faulty system and the nominal system. Consider a linear system given by

$$x(t) = Ax(t) + Bu(t). \tag{2.10}$$

with the control law that defined as $u(t) = Kx(t)$ for a given state feedback gain K. The closed-loop corresponding to the nominal system is

$$x(t) = (A + BK)x(t) \tag{2.11}$$

and the closed-loop corresponding to faulty system can be written as

$$x_f(t) = (A_f + B_f K_f)x_f(t) \tag{2.12}$$

K_f is found so that the closed-loop performance of the faulty system will be similar to that of the nominal one. The purpose is to make $x_f(t) = x(t)$, hence a requirement is to assure $(A + BK) = (A_f + B_f K_f)$ and then $K_f = B_f^{\dagger}(A - A_f + BK)$, in which $B_f^{\dagger}$ denotes the pseudo-inverse of B_f. The matrices A, B and K are assumed to be known in advance. Fault system parameters (A_f,B_f) can be estimated through an FDD and the feedback gain is updated online [106]. Although the method given above is quite simple, the pseudo-inverse method has several drawbacks such as its lack of stability analysis, and the assumption of available state measurements [106]. [149] also points out that there is a lack of robustness when the system pair (A_f, B_f) has not been perfectly identified.

The other method of control signal redistribution is Control Allocation (CA). This method has the capability to redistribute control demand signals to the remaining healthy actuators based on the limits of those actuators. Let us consider an overactuated system, which can be represented by a linear system as:

$$\dot{x} = Ax + B_u u \tag{2.13}$$

where B_u can be factorised as $B_u = B_v B$. Hence, the linear system can be rewritten as

$$\dot{x} = Ax + B_v v \tag{2.14}$$

where v is the virtual control given as $v := Bu$. For a given v, the control signal $u(t)$ is

$$u = B^{\dagger} v \tag{2.15}$$

where $B^{\dagger} = WB^T(BWB^T)^{-1}$ is the weighted right pseudo-inverse of B, where matrix W provides a certain degree of design freedom. Some papers discussing the framework of FTC are [97, 120].

The pseudo-inverse and CA methods seem to be similar in the sense that both employ a pseudo-inverse that yields a degree of design freedom. However, one of the main differences between them is that CA is based on a virtual control signal when designing the controller. CA maps the virtual control to the actual control demand to the actuators. The advantage of this is that the controller design does not depend on the CA scheme. On the other hand, the CA requires the pure factorisation $B_u = B_v B$, which is very difficult to obtain. In the case of optimal control, linear or quadratic programming is necessary. This is a difficult requirement to obtain online in real time due to the associated computational complexity and numerical sensitivity during the optimisation [75].

Gain-scheduling Control

Gain-scheduling (GS) is one of the most popular approaches to non-linear control design and has been widely and successfully applied in fields ranging from aerospace to process. GS approaches are often described as being a divide and conquer-type design procedure, where the non-linear control design task is decomposed into a series expansion linearisation of a system about its trim points [84]. The term GS also refers to the scheduling of linear models, and its controllers are associated by parameters or states in order to deal with non-linear control problems due to any change in the operating conditions. GS is also based on pre-calculated control laws. In some flight conditions, there is no requirement for the controller structure to be changed. Only the gains of the controller need to be changed according to the flight conditions or the severity of the faults/ failures. Predefined gains are chosen for specific flight conditions or specific parameters instead of adaptive tuning. This can be presented in the form of a simple logic switch between two gains, or more commonly through the use of lookup tables or curve fitting. One of the advantages of GS is that it is easily understood and implemented. However, in some cases, GS cannot cope with significant faults and controller reconfiguration is required

[84]. GS papers in the field of FTC are [118, 145].

Linear Parameter Varying Control

Linear parameter varying (LPV) control has been proposed in the context of gain-scheduling design. The idea in LPV control is to attain smooth semi-linear models that are varied or scheduled using a parameter such as altitude or speed. As a result, the LPV model can imitate real non-linear dynamics. Instead of selecting a combination of defined linear models, the models change based on a parameter. The structure of the LPV model consists of a linear system with (A, B, C) matrices, but each matrix is varied based on the selected parameter [46]. A representative LPV system can be given by

$$\begin{aligned} \dot{x}(t) &= A(\alpha)x(t) + B(\alpha)u(t) \\ y(t) &= C(\alpha)x(t) + D(\alpha)u(t) \end{aligned} \tag{2.16}$$

where α is the varying parameter, e.g., speed or altitude. If α is a constant, then the LPV system becomes a linear time invariant (LTI) system. The LPV controller synthesis involves finding an output feedback controller $K(p)$ such that the closed loop system achieves stability and the $\mathcal{L}_2$ gain of u to y is minimised.

The family of the linear models is characterised by one or two variables with respect to the trim point. The resulting state space matrices fitted to a polynomial that is continuous throughout the trim points [12]. In the field of FTC, LPV-type ideas have been used to deal with actuator faults [46]. The LPV control method can guarantee stability and performance when compared to classical gain scheduling. On the other hand, scheduling parameters are often not independent and, particularly in the field of FTC, the admissible parameter set is larger than required [81]. Such a large value in the parameter set leads to conservatism and complexity in scheduling multivariable controllers and in implementation. Some LPV papers in the field of FTC are [113, 130, 134] and [131].

Method	H_∞ Control
Advantages	(i) Robust stability of the controlled systems in the presence of uncertainties and disturbance. (ii) Direct applicability to problem of MIMO systems.
Disadvantages	(i) Difficulty of practical implementation of high-order controllers.
Method	Sliding Mode Control
Advantages	(i) Robustness against parametric uncertainties and disturbances.
Disadvantages	(i) Chattering problem and hence requirement for the high bandwidths of control laws. (iii) Requirement for the entire state variables for the controller design.
Method	Adaptive Control
Advantages	(i) The enhancement of system stability with adaptation of the controller parameters for the operating conditions.
Disadvantages	(i) Incapability to handle unanticipated faults or major system change in system dynamics. (ii) Requirement of on-line estimation.
Method	Model Predictive Control
Advantages	(i) Simplicity and ease of understanding.
Disadvantages	(i) Requirement of an online solution to the constrained optimisation problem.
Method	Control Allocation
Advantages	(i) Compensation of actuator faults without reconfiguring the control laws.
Disadvantages	(i) Requirement of online optimisation. (ii) Limitations of actuators after faults are not taken into consideration in control law.
Method	Pseudo-Inverse Modelling
Advantages	(i) Computational simplicity.
Disadvantages	(i) Its lack of stability analysis. (ii) The assumption of available state measurements.
Method	Gains-scheduling Control
Advantages	(i) Easy implementation.
Disadvantages	(i) It is not sufficient to deal with significant faults.
Method	Linear Parameter Varying Control
Advantages	(i) Guarantee stability and performance.
Disadvantages	(i) Conservatism and complexity in scheduling controllers. (ii) Difficulty in implementation.

Table 2.1: Summary of the advantages and disadvantages of FTC approaches.

2.4 Conclusions

This chapter has reviewed the flight control and FTC approaches to quadcopter UAVs in the literature. A number of control approaches to fault-free quadcopter UAVs have been proposed to improve the flight control performance without the further consideration of potential actuator faults. In addition, the research results for quadcopter time-dependent actuator faults are still limited. This chapter has also shed light on types of faults and failures that may occur in actuators. The advantages and disadvantages of different fault tolerant control approaches were briefly discussed, which ranged from passive to active fault tolerance control schemes. An active FTC approach can cope with various types of faults; however the handling quality of the FTC depends on a timely and correct fault identification by the FDD. Any detection delay in the FDD may result in the deterioration of the performance of an active FTC. By contrast, a passive FTC approach does not require an FDD unit or a reconfiguration scheme.

CHAPTER 3

BACKGROUND ON STABILITY OF SWITCHED SYSTEMS

3.1 Introduction

This chapter will begin by giving various definitions of systems and stability. In particular, we present the stability conditions of switched systems under the constraints of both average dwell-time requirements and state-dependent switching rules. The stability and stabilisation of the quadcopter UAV subject to time-varying actuation problems will be built upon the switched stability results presented herein. This chapter is organised as follows: Section 3.2 describes basic concepts of system linearisation and local stability in the sense of Lyapunov. Section 3.3 presents arbitrary and constrained switching stability results. Finally, Section 3.4 gives a summary of this chapter.

3.2 Linearisation and Local Stability

The objective of this section is to introduce basic definitions of systems and stability. Linear systems are categorised as being either time-varying or time-invariant based on whether the system matrix A varies with time, or otherwise. These categorisations are replaced by ”autonomous” and ”non-autonomous” in the context of non-linear systems.

Definition* 3.2.1** ([135]):*** A non-linear system $\dot{x}(t) = f(x, t)$ is referred to as being autonomous if f does not depend on time, that is, if the state equation of the system can be written as

$$\dot{x}(t) = f(x(t)), \tag{3.1}$$

otherwise, the system is referred to as being non-autonomous.

Definition* 3.2.2** ([135]):*** A state x_e is an equilibrium point or equilibrium state of a system if, once $x(t)$ is equal to x_e, it remains equal to x_e indefinitely. This means that when the constant vector x_e satisfies

$$f(x_e) = 0 \tag{3.2}$$

then the equilibrium points can be determined by solving (3.2).

Most stability problems are formulated with respect to equilibrium points. A non-linear system may have several (or infinitely many) equilibrium points.

3.2.1 Linearisation

Consider an autonomous system in the form of

$$\dot{x}(t) = f(x, u), \tag{3.3}$$

where $f(x, u)$ is assumed to be continuously differentiable. Then the associated system dynamics can be written as

$$\dot{x} = \left.\frac{\partial f}{\partial x}\right|_{(x=x_e, u=u_e)} x + \left.\frac{\partial f}{\partial u}\right|_{(x=x_e, u=u_e)} u + f_{h.o.t}(x, u) \tag{3.4}$$

where $f_{h.o.t}(x, u)$ are higher-order terms in x and u, which are neglected. The above Taylor expansion starts directly with the first order term since $f(x_e, u_e) = 0$ with the equilibrium input, u_e. If A is the Jacobian matrix of f with respect to x at (x_e, u_e) and B denotes the Jacobian matrix of f with respect to u at the same point, i.e.,

$$A = \left.\frac{\partial f}{\partial x}\right|_{(x=x_e, u=u_e)}, \qquad B = \left.\frac{\partial f}{\partial u}\right|_{(x=x_e, u=u_e)} \tag{3.5}$$

then the system $\dot{\tilde{x}} = A\tilde{x} + B\tilde{u}$ is called linear approximation of the original non-linear system at the equilibrium point (x_e, u_e) [135].

3.2.2 Classical Stability Concepts

The concept of stability is the most important system specification when one designs a control law for dynamic systems. For an unforced system, the stability concepts can be defined as follows.

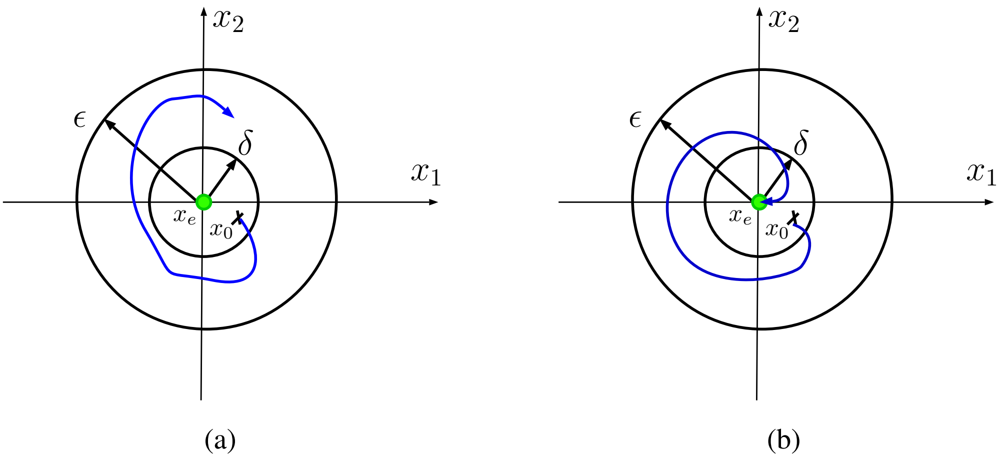

Figure 3.1: Illustrations of (a) a stable equilibrium in the sense of Lyapunov, and (b) an asymptotically stable equilibrium.

Definition* 3.2.3** ([80]):*** The equilibrium state x_e of (3.1)

(a) is *stable* if for any $\epsilon > 0$, there exists $\delta = \delta(\epsilon) > 0$ such that if $\|x(0)\| < \delta$ then $\|x(t)\| < \epsilon$ for all $t \geq 0$. Otherwise, the equilibrium point is *unstable.*

(b) is asymptotically stable if, as well as being stable, there exists some $\delta > 0$ such that $\|x(0)\| < \delta$ implies that $x(t) \longrightarrow 0$ as $t \longrightarrow \infty$. Furthermore, it is globally asymptotically stable if (3.1) is satisfied for any initial state $x(0)$.

(c) is exponentially stable if in addition to being stable there exists two strictly positive numbers α and λ such that $\forall t > 0$, $\|x(t)\| \leq \alpha\|x(0)\|e^{-\lambda t}$ and is globally exponentially stable if (3.1) is satisfied for any initial states $x(0)$.

Asymptotic stability means that the equilibrium is stable and the states converge to zero as $t \longrightarrow \infty$. The concept of exponentially stability can be used to estimate how fast the states of the system converge to zero.

Definition* 3.2.4** ([80]):*** If the positive definite function $V(x)$ has continuous partial derivatives and its time derivative, along any state trajectory of the system (3.1) is negative semi-definite, i.e.,

$$\dot{V}(x) \leq 0$$

then the system (3.1) is stable (Definition 3.2.3(a)). If its time derivative, along any state trajectory of the system (3.1) is negative definite, i.e.,

$$\dot{V}(x) < 0$$

then the system (3.1) is asymptotically stable (Definition 3.2.3(b)).

Consider a quadratic Lyapunov function candidate, $V(x) = x'Px$, where P is a real symmetric positive definite matrix. The derivative of V along the trajectories of the linear system, $\dot{x} = Ax$, is given by

$$\dot{V}(x) = \dot{x}'Px + x'P\dot{x} = x'(PA + A'P)x = -x'Qx. \tag{3.6}$$

If there exists $Q = Q' > 0$ such that

$$PA + A'P = -Q \tag{3.7}$$

then the linear system is asymptotically stable and the equation (3.7) is referred to as the *Lyapunov equation*.

3.3 Stability of Switched Systems

A family of continuous time dynamical systems can be represented by a switched system with a switching rule. This rule determines each instance at which the dynamic system is responsible for the time evolution. Consider a family of dynamical systems,

$$\dot{x}(t) = f_{\sigma(t)}(x(t)), \quad \sigma(t) \in \{1, \ldots, N\}. \tag{3.8}$$

The easiest case to consider is that all these systems are linear:

$$\dot{x}(t) = A_{\sigma(t)}x(t), \quad \sigma(t) \in \{1, \ldots, N\} \tag{3.9}$$

where $\sigma(t)$ is a piecewise continuous function and represents the switching rule between matrices $A_i \in \mathbb{R}^{n\times n}, \quad i = 1, ..., N$. The problem is to ensure that the switched linear system (3.9), satisfies certain given stability properties for $\sigma(t) > 0$. In the following subsections, we will give sufficient conditions for stability under arbitrary and constrained switching.

3.3.1 Common Quadratic Lyapunov Functions

Common quadratic Lyapunov functions (CQLF) are employed to verify the stability of a switched system under arbitrary switching signals. Indeed, there has been considerable effort to derive the conditions for the existence of a common quadratic Lyapunov function due to its importance in practice. Suppose that we are given a family of real Hurwitz $n \times n$ matrices $A_1, ..., A_N$, where n and N are positive integers. If there exists a matrix $P > 0$ which satisfies

$$A_i'P + PA_i < 0 \qquad i = \{1, ..., N\}, \tag{3.10}$$

then this means that the quadratic function $V(x) = x'Px$ is a common Lyapunov function for the family of asymptotically stable linear systems

$$\dot{x} = A_i x \qquad i = \{1, ..., N\}. \tag{3.11}$$

By fixing an arbitrary matrix $Q = Q' > 0$, if one can prove the existence of the positive definite symmetric matrix P satisfying the CQLF:

$$A_i'P + PA_i + Q \leqslant 0 \qquad i = \{1, ..., N\}, \tag{3.12}$$

then the CQLF is $V(x) = x'Px$ which is satisfied for all A_i. The existence of CQLF for a given switching system ensures global uniform exponential stability under arbitrary switching [85, 87].

3.3.2 Multiple Lyapunov Functions

The common quadratic Lyapunov function approach, however, may not guarantee stability. In other words, looking for a CQLF may be conservative. In such a case, the stability analysis can be pursued within the framework of multiple Lyapunov functions (MLFs). MLFs can be described by

$$V_i(x) = x' P_i x. \tag{3.13}$$

The basic idea is to find a Lyapunov-like function V_i corresponding to f_i for all i which are positive definite and decreasing whenever the ith individual system is active. The Lyapunov-like function might not monotonically decrease along the state trajectories [88]. We need to impose restrictions on switching by assuring that V_i is non-increasing on an appropriate sequence of switching times. A multiple Lyapunov-like function satisfies the following conditions: $V_i(x) > 0 \ \ \forall x \neq 0$ and $V_i(0) = 0$; the derivative of the each V_i function satisfies $\dot{V}_i \leq 0$ when the ith sub-system is active.

In order to ensure stability, assume that there are candidate Lyapunov functions V_i corresponding to f_i for all i. It can be said that they satisfy the sequence for a non-increasing condition for a trajectory $x(.)$ if $V_{i_{j+1}}(x(t_{j+1})) < V_{i_j}(x(t_j))$, where sub-indices represent switching times. Whereas each V_i decreases when the ith subsystem is active, it may similarly increase when the ith subsystem is inactive. This is illustrated in Fig. 3.2. MLFs are the most well-studied area in the switched system literature [86].

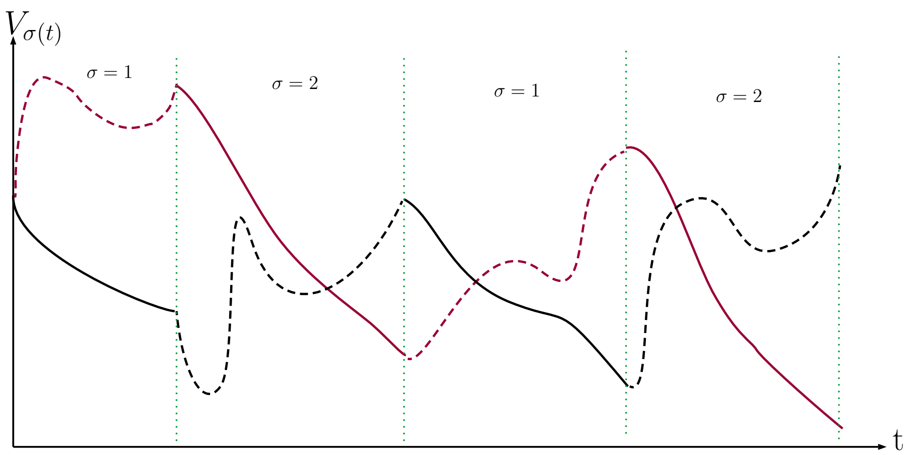

Figure 3.2: Multiple Lyapunov function values versus time $(N = 2)$. Solid/dotted denotes corresponding system activity/inactivity (adopted from [21]).

3.3.3 Dwell Time Switching

In this section, the stability of a switched system is considered under slow switching. A switched system is stable if all individual subsystems are stable and switching is sufficiently slow. The method of dwell-time switching has been widely used in the literature for stability analysis and control of switched systems (e.g., [62, 147, 155]). The dwell-time estimate essentially provides an upper bound on the frequency of switching occurring during a finite interval.

***Definition* 3.3.1** ([85])*:* A switching signal is said to have a dwell-time T_d if $t_{k+1} - t_k \geq T_d, \ \forall k \in \mathbb{N}$ where t_k and t_{k+1} denotes the switching instants.

***Definition* 3.3.2** ([62])*:* For a switching signal σ and any $t \geq \tau \geq 0$, let $N_\sigma(t, \tau)$ denote the number of switching of σ in the open internal (τ, t). For a given N_0, $T_a > 0$, if $N_\sigma(t,\tau) \leq N_0 + \frac{t-\tau}{T_a}$ holds for the set of all switching signals, then T_a is referred to as the average dwell-time and N_0 is the chatter bound.

The following theorem gives the stability results for switched linear systems under average dwell-time.

***Theorem* 3.3.1** ([85])*:* Consider the switched dynamical system $\dot{x}(t) = f_\sigma(x(t))$, $\sigma \in \mathbb{K}$ and let $\alpha > 0, \ \mu > 1$ be given constants. Assume that there exist $\mathcal{C}^1$ function $V_{\sigma}(t) : \mathbb{R}^n \to \mathbb{R}$, $\sigma(t) \in \mathbb{K}$ and two classes $\mathcal{K}_\infty$ function k_1 and k_2 such that $\forall i \in \mathbb{K}$,

$$k_1(\|x(t)\|) \leq V_i(t) \leq k_2(\|x(t)\|) \tag{3.14}$$

$$\dot{V}_i(x(t)) \leq -\alpha V_i(x(t)) \tag{3.15}$$

and $\forall (i,j) \in \mathbb{K} \times \mathbb{K}, i \neq j$,

$$V_i(x(t)) \leq \mu V_j(x(t)) \tag{3.16}$$

then the system is globally asymptotically stable for any switching signal with an average dwell-time $T_a > T_a^* = \ln \mu / \alpha$.

Average dwell-time (ADT) switching has been recognised to be more flexible than the minimum dwell-time switching (e.g, see [2]) in system stability analysis and control syntheses.

3.3.4 Minimum Lyapunov function Switching Strategy

Consider a switched linear system of the general form

$$\dot{x}(t) = A_{\sigma(t)}x(t), \quad x(0) = x_0, \tag{3.17}$$

defined for all $t \geq 0$, where $x(t) \in \mathbb{R}^n$ is the state, $\sigma(t)$ is the switching rule. Considering a given set of matrices $A_i \in \mathbb{R}^{n\times n}, i = 1, ..., N$, the switching rule $\sigma(t)$, for each $t \geq 0$, is such that

$$A_{\sigma(t)} \in \{A_1, ..., A_N\}, \tag{3.18}$$

The main difference with respect to time-dependent switching is that it is considered that the state vector $x(t)$ is available for feedback for all $t \geq 0$. The purpose is to find the function such that

$$\sigma(t) = u(x(t)) \tag{3.19}$$

makes the equilibrium point $x = 0$ of (3.17) asymptomatically stable [49]. In this case, each matrix of the set $\{A_1, ..., A_N\}$ is not required to be asymptotically stable. Using the following simplex, defined as:

$$\wedge := \left\{ \lambda \in \mathbb{R}^N : \sum_{i=1}^{N} \lambda_i = 1, \lambda_i \geq 0 \right\} \tag{3.20}$$

and the set of positive definite matrices $\{P_1, \ldots, P_N\}$, the following piecewise quadratic Lyapunov function can be defined by

$$V(x) := \min_{i=1,\ldots,N} x'P_i x = \min_{\lambda\in\wedge} \left(\sum_{i=1}^{N} \lambda_i x' P_i x \right). \tag{3.21}$$

This Lyapunov function is important for the stability analysis but it is not differentiable everywhere. Here, the set $\mathcal{I}(x) = \{i : V(x) = x'P_i x\}$ plays a key role as the piecewise quadratic Lyapunov function fails to be differentiable on $x \in \mathbb{R}$ when $\mathcal{I}(x)$ contains more than one element. Before giving the following theorem, let the class of Metzler matrices be denoted by $\mathcal{M}$ and consist of all matrices $\Pi \in \mathbb{R}^{N\times N}$ with elements π_{ij}, such that

$$\pi_{ij} \geq 0 \quad \forall i \neq j, \quad \sum_{i=1}^{N} \pi_{ji} = 0 \quad \forall j. \tag{3.22}$$

***Theorem* 3.3.2:** [49] If a set $\{P_1, ..., P_N\}$ of positive definite matrices and $\Pi \in \mathcal{M}$ satisfy the Lyapunov-Metzler inequalities

$$A_i' P_i + P_i A_i + \sum_{j=1}^{N} \pi_{ji} P_j < 0, i = 1, ..., N, \tag{3.23}$$

the state-switching control (3.19) with

$$u(x(t)) = \arg \min_{i=1,\dots,N} x(t)' P_i x(t) \tag{3.24}$$

makes the equilibrium solution $x = 0$ of (3.17) globally asymptotically stable.

Proof. The Lypunov function (3.21) is not differentiable for all $t \geq 0$. Hence, the Dini derivative

$$D^+V(x(t)) = \limsup_{h \longrightarrow 0^+} \frac{V(x(t+h)) - V(x(t))}{h} \tag{3.25}$$

is used, assuming that the state switching control is given by $\sigma(t) = u(x(t)) = i$ for some $i \in \mathcal{I}(x(t))$ at an arbitrary $t \geq\ 0$ where $\mathcal{I}(x(t))$ is the index of the active subsystem. Hence, using (3.25) with the system dynamic equation (3.17), one obtains

$$\begin{aligned}
D^+V(x(t)) &= \limsup_{h \longrightarrow 0^+} \frac{V(x(t) + hA_i x(t)) - V(x(t))}{h} \\
&= \min_{l \in I(x(t))} \limsup_{h \longrightarrow 0^+} \frac{\cancel{x'P_l x} + hx'P_l A_i x + hx'A_i' P_l x + h^2 \cancelto{0}{x'A_i' P_l A_i x} - \cancel{x'P_l x}}{h} \\
&= \min_{l \in I(x(t))} x(t)'(A_i' P_l + P_l A_i) x(t) \\
&\leq x(t)'(A_i' P_i + P_i A_i) x(t)
\end{aligned} \tag{3.26}$$

where the index $l = \sigma(0)$ may be involved in an optimisation, but a good choice would be $l = i \in \mathbb{K}$ [51]. The last inequality is satisfied and $x(t)' P_j x(t) \geq x(t)' P_i x(t)$ for all $j \neq i = 1, \dots, N$ due to the fact that $i \in \mathcal{I}(x(t))$. Consider the Lyapunov-Metzler inequalities (3.23). We have

$$\begin{aligned} D^+V(x(t)) &< -x(t)'\left(\sum_{j=1}^{N}\pi_{ji}P_j\right)x(t) \\ &< -\left(\sum_{j=1}^{N}\pi_{ji}\right)x(t)'P_ix(t) \\ &< 0, \end{aligned} \tag{3.27}$$

where $\left(\sum\limits_{j=1}^{N}\pi_{ji}\right) = 0$, which then proves the theorem because the Lyapunov function $V(x(t))$ defined in (3.21) is radially unbounded.

It can be seen that the switching rule, (3.24), may result in stable sliding modes (chattering). Actually, switching from any mode $i \in \mathcal{I}(x(t))$ to $j \in \mathcal{I}(x(t))$ is possible only if $x(t)'(A_j'P_j + P_jA_j)x(t) \leqslant x(t)'(A_i'P_i + P_iA_i)x(t) < 0$. Consequently, (3.21) is strictly decreasing along the system's trajectories even under sliding modes. The stabilisation of switched systems using the min-switching strategy is illustrated in Fig. 3.3, where the solid line indicates the active system and dotted line denotes the inactive system.

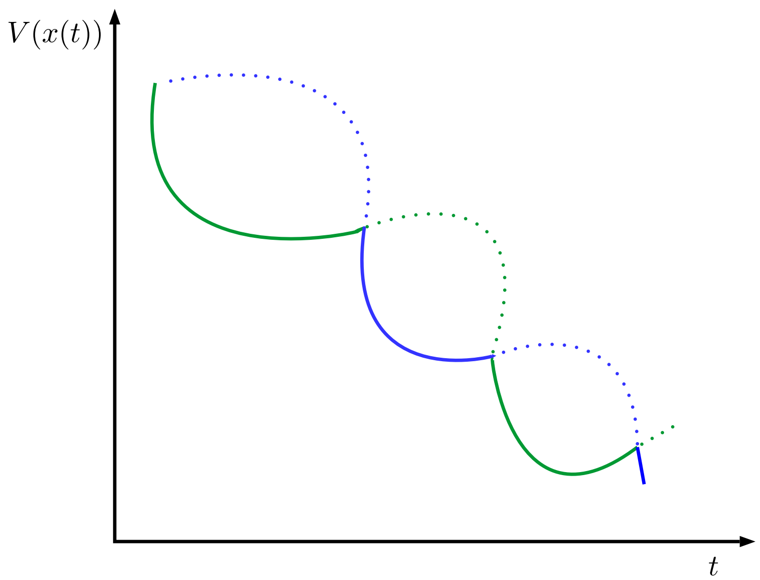

Figure 3.3: Lyapunov function values versus time ($N = 2$) with the min-switching strategy.

Remark* 1*: A necessary condition for the Lyapunov-Metzler inequalities to be feasible with respect to $\{P_1, ..., P_N\}$ is matrices $A_i + (\pi_{ii}/2)I$ for all $i = 1, ..., N$ need to be asymptotically stable, since $\pi_{ii} \leqslant 0$.

The numerical solution of the Lyapunov-Metzler inequalities given in Theorem 3.3.2 with respect to the variables $(\Pi, \{P_1, ..., P_N\})$ is not trivial because of the products of variables. The following theorem is given to overcome this difficulty and to obtain simpler stability conditions that can be expressed in terms of LMIs and are thus solvable.

Theorem* 3.3.3*: [49] Let $Q \geq 0$ be given. If a set of positive matrices $\{P_1, ..., P_N\}$ and a scalar $\gamma > 0$ hold the modified Lyapunov-Metzler inequalities:

$$A_i' P_i + P_i A_i + \gamma(P_j - P_i) + Q < 0, i = 1, ..., N \tag{3.28}$$

then the state-switching control (3.19) with $u(x(t))$ given by (3.24) makes the equilibrium solution $x = 0$ of (3.17) globally asymptotically stable, and

$$\int_0^\infty x(t)' Q x(t) dt < \min_{i=1,...,N} x_0' P_i x_0. \tag{3.29}$$

The basic theoretical features of Theorem 3.3.4 is still present in Theorem 3.3.3. Furthermore, the most important point is that the asymptotic stability of the set of matrices $\{A_1, ..., A_N\}$ is still not required. The convexity makes it possible to solve the following problem,

$$\min_{\gamma>0, P_i>0,...,P_N>0} \left\{ \sum_{i=1}^{N} x_0' P_i x_0 : (3.28) \right\} \tag{3.30}$$

by using LMI solvers and a line search.

3.4 Conclusions

This chapter has given a brief introduction to classical stability concepts. Simple but conservative results of common quadratic Lyapunov functions have been presented under arbitrary switching. Estimates of average dwell-time for constrained switched systems have been represented by means of a set of quadratic Lyapunov functions. In addition, the stability criteria for a switched system under the state-dependent switching rule have been given in terms of the Lyapunov Metzler inequalities and, additionally, in terms of LMIs coupled with a scalar satisfying the Lyapunov Metzler inequalities.

CHAPTER 4

SYSTEM DESCRIPTION

4.1 Introduction

Quadcopter UAVs can be classified as a rotary-wing VTOL aircraft because they are powered by rotors. Quadcopters are symmetrically equipped with four rotors in a cross configuration. They have a relatively simple mechanical design, hovering capability, high maneuverability and low maintenance costs. Therefore, these UAVs are prominent autonomous aerial vehicles in various academic and commercial sectors. Quadcopter UAVs have been used in tasks such as search and rescue, building exploration, security and inspection in dangerous and inaccessible environments.

In the literature, several papers have addressed the problem of dynamic modelling for the quadcopter vehicle. A comprehensive model of the quadcopter is studied in [18] considering rigid body dynamics, propeller pyroscopic effect and several aerodynamic forces. The Euler-Lagrange approach is employed to obtain the dynamical model in [48, 121]. In [110], the Euler-Lagrange approach is also used by assuming the quadcopter structure to be symmetric. Furthermore, it assumes that centre-of-mass of vehicle and the body-fixed frame origin are matched. In [95, 139], the Newton-Euler approach is used to derive the model by including the most relevant aerodynamic effects. Aerodynamic effects and blade flapping are considered in [108] for the quadcopter vehicle. In [40] the model is obtained using the Euler-Lagrange and Newton-Euler approaches and including the aerodynamic effects experienced by quadcopters. All the modelling approaches cited above assume that the quadcopters have a rigid body subject to forces and moments. This chapter presents a dynamic model of a quadcopter vehicle. The main modelling approach adopted in this thesis is similar to the one given in [139].

This chapter is structured as follows. Section 4.2 presents a description of motions, the assumptions behind the model developed and angular velocities as expressed by using standard Euler angle relationships. In Section 4.3, rotational dynamics and translational dynamics are expressed using the Newton-Euler approach. Section 4.4 gives information about sensors that can be emplyed with quadcopters. Finally, Section 4.5 gives some concluding remarks.

4.2 Quadcopter Kinematics

The quadcopter vehicle depicted in Fig. 4.1 is controlled by varying the angular speeds of four electric motors. All rotors are located at an angle of 90 degrees with respect to each other. Each rotor produces a thrust force which is directed along the vertical body axis. The front rotor M_1 and rear rotor M_3 rotate in a clockwise direction, whilst the other two rotors, M_2 and M_4, rotate in an anticlockwise direction.

Motions described in Fig. 4.2 are attained through the orientations of roll, pitch and yaw angles. Roll (ϕ) is obtained by increasing (reducing) the speed of the rotor M_2 and reducing (increasing) the speed of the rotor M_4 while the speeds of the rotors M_1 and M_3 are kept the same. Similarly, pitch (θ) is achieved by increasing (reducing) the speed of the rotor M_1 and reducing (increasing) the speed of the rotor M_3 while the speeds of the rotors M_2 and M_4 are kept the same. Yaw (ψ) is obtained by increasing (decreasing) the speed of rotors M_1 and M_3 and decreasing (increasing) the speed of rotors M_2 and M_4. In order words, the difference in the counter-torque between the pair of rotors M_1-M_3 and the pair of rotors M_2-M_4 creates yaw (ψ) [26]. The model developed here is based on some assumptions [18, 40]:

- The structure of the quadcopter is rigid.
- The quadcopter is designed symmetrically.
- Propellers are rigid.
- Free stream air velocity is zero.

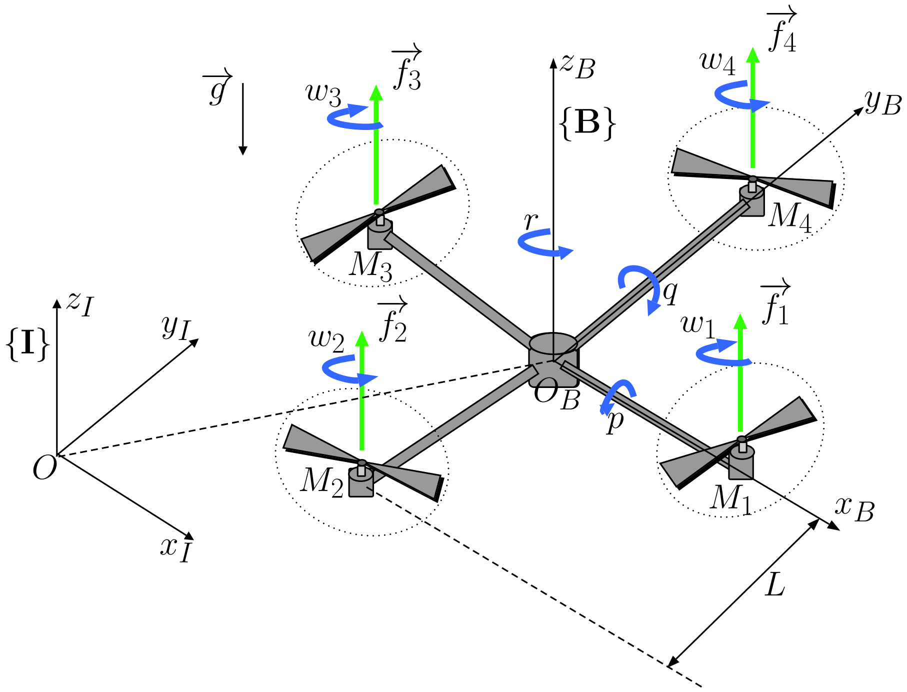

Figure 4.1: Body-fixed and inertial-fixed frames for a quadcopter UAV model.

- The propellers are not very flexible thus can be neglected.
- Drag is considered to be linear, hence obeying Stoke's law.
- Motor dynamics are assumed to be a first-order transfer function $(\tau s + 1)^{-1}$.

These assumptions are mostly considered for the quadcopter models studied in the literature. The rotor M_i produces a thrust force, f_i, that is proportional to the square of the angular speed, that is, $f_i = k\omega_i^2$. The forces are directed along the positive z_B-axis and at distance L from the centre-of-mass of the quadcopter. Let $\{\mathbf{I}\}$ $(O,\ x_I,\ y_I,\ z_I)$ be the inertial frame and $\{\mathbf{B}\}$ $\{O_B,\, x_B,\, y_B,\, z_B\}$ be the body-fixed frame, where O_B is located at the centre-of-mass of the quadcopter vehicle.

The position vector of the quadcopter centre-of-mass is given in the inertial frame:

$$\boldsymbol{\xi} = \begin{bmatrix} x_I \\ y_I \\ z_I \end{bmatrix}. \tag{4.1}$$

The body-fixed angular velocity about the body x_B, y_B and z_B axes, respectively, is $\boldsymbol{w} =$

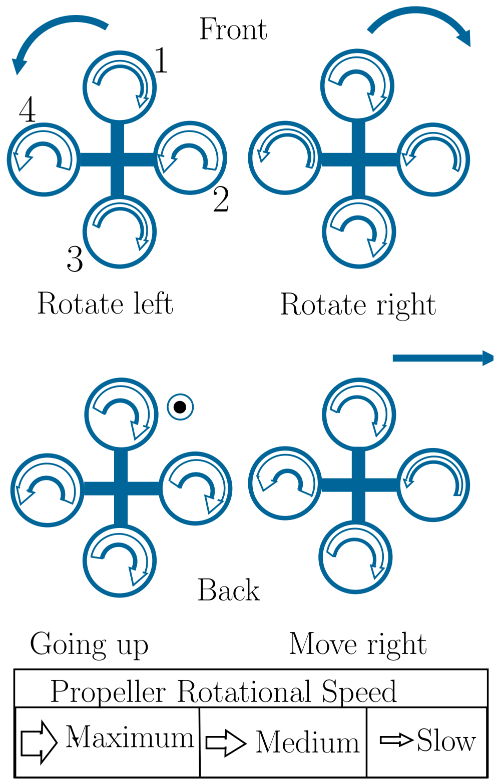

Figure 4.2: The motions of quadcopter UAVs.

$[p\ q\ r]'$. The orientation of the body-fixed frame $\{\mathbf{B}\}$ $\{\ O_B,\ x_B,\ y_B,\ z_B\}$ with respect to the inertial frame $\{\mathbf{I}\}$ $(O,\ x_I,\ y_I,\ z_I)$ is expressed by a vector of three independent angles as:

$$\boldsymbol{\eta} = \begin{bmatrix} \phi \\ \theta \\ \psi \end{bmatrix}. \tag{4.2}$$

An orthonormal rotation matrix $\boldsymbol{R_{B\to I}}$ is obtained through three successive rotation matrices $R_z(\psi)$, $R_y(\theta)$ and$R_x(\phi)$. The first is given by a rotation around the z_B axis by an angle ψ. The second is followed by a rotation of the pitch angle around the new y_B axis. Finally, a rotation of the roll angle is carried out around the newest x_B axis in order to rotate the quadcopter to its final position. These angles are bounded as: roll angle, ϕ, by $(-90^o < \phi < 90^o)$; pitch angle, θ, by $(-90^o < \theta < 90^o)$; yaw angle, (ψ), by $(-180^o < \psi < 180^o)$. The heading of the vehicle is unrestricted, but the pitch and roll angles can not assume a value resulting in reverse flight.

The transforming of the body-fixed frame coordinates into the inertial frame coordinates can be obtained as follows [140],

$$\boldsymbol{R_{B\rightarrow I}} \doteq R_z(\psi).R_y(\theta).R_x(\phi)$$

$$= \begin{bmatrix} cos\psi & -sin\psi & 0 \\ sin\psi & cos\psi & 0 \\ 0 & 0 & 1 \end{bmatrix} \begin{bmatrix} cos\theta & 0 & sin\theta \\ 0 & 1 & 0 \\ -sin\theta & 0 & cos\theta \end{bmatrix} \begin{bmatrix} 1 & 0 & 0 \\ 0 & cos\phi & -sin\phi \\ 0 & sin\phi & cos\phi \end{bmatrix} \tag{4.3}$$

$$\boldsymbol{R_{B\rightarrow I}} \doteq \begin{bmatrix} cos\theta\, cos\psi & cos\psi\, sin\theta\, sin\phi - cos\phi\, sin\psi & cos\phi\, cos\psi sin\theta + sin\phi\, sin\psi \\ cos\theta\, sin\psi & sin\theta\, sin\phi\, sin\psi + cos\phi\, cos\psi & cos\phi\, sin\theta\, sin\psi - cos\psi\, sin\phi \\ -sin\theta & cos\theta\, sin\phi & cos\theta\, cos\psi \end{bmatrix} \tag{4.4}$$

The kinematic equations of the rotational and translational motions are attained through the rotation matrix. The kinematic translation can be written as;

$$\boldsymbol{v_I} = \boldsymbol{R_{B\rightarrow I} v_B} \tag{4.5}$$

where $\boldsymbol{v_I}$ and $\boldsymbol{v_B}$ are linear velocities of the centre-of-mass of the quadcopter in the inertial frame and body-fixed frame, respectively. The angular velocity vector is given as $\boldsymbol{\omega} = [p\ q\ r]^T$, where $p,\ q$ and r represent the direct angular velocities around the x_B, y_B and z_B-axes, respectively. Let W_η be a Jacobian matrix representing a rotation matrix that transforms body-fixed angular velocities into inertial-fixed angular velocities, and which can be obtained as follows [140]:

$$\begin{bmatrix} p \\ q \\ r \end{bmatrix} = \begin{bmatrix} \dot{\phi} \\ 0 \\ 0 \end{bmatrix} + R_x(\phi)^T \begin{bmatrix} 0 \\ \dot{\theta} \\ 0 \end{bmatrix} + R_x(\phi)^T R_y(\theta)^T \begin{bmatrix} 0 \\ 0 \\ \dot{\psi} \end{bmatrix} \tag{4.6}$$

$$\begin{bmatrix} \dot{\phi} - \dot{\psi}\, sin\theta \\ \dot{\theta}\, cos\phi + \dot{\psi} sin\phi\, cos\theta \\ -\dot{\theta}\, sin\phi + \dot{\psi} cos\phi\, cos\theta \end{bmatrix} \equiv W_\eta \begin{bmatrix} \dot{\phi} \\ \dot{\theta} \\ \dot{\psi} \end{bmatrix}. \tag{4.7}$$

The Jacobian matrix is

$$W_\eta = \begin{bmatrix} 1 & 0 & -sin\theta \\ 0 & cos\phi & sin\phi\, cos\theta \\ 0 & -sin\phi & cos\phi\, cos\theta \end{bmatrix}. \tag{4.8}$$

The desired rotation matrix is the inverse of the Jacobian matrix and can be given by:

$$W_\eta{}^{-1} = \begin{bmatrix} 1 & sin\phi\, tan\theta & cos\phi\, tan\theta \\ 0 & cos\phi & -sin\phi \\ 0 & sin\phi\,(cos\theta)^{-1} & cos\phi\,(cos\theta)^{-1} \end{bmatrix}. \tag{4.9}$$

Then angular velocities are

$$\begin{bmatrix} \dot{\phi} \\ \dot{\theta} \\ \dot{\psi} \end{bmatrix} = W_\eta{}^{-1} \begin{bmatrix} p \\ q \\ r \end{bmatrix}. \tag{4.10}$$

Substituting $W_\eta{}^{-1}$ in (4.10) results in

$$\begin{bmatrix} \dot{\phi} \\ \dot{\theta} \\ \dot{\psi} \end{bmatrix} = \begin{bmatrix} 1 & sin\phi\, tan\theta & cos\phi\, tan\theta \\ 0 & cos\phi & -sin\phi \\ 0 & sin\phi\,(cos\theta)^{-1} & cos\phi\,(cos\theta)^{-1} \end{bmatrix} \begin{bmatrix} p \\ q \\ r \end{bmatrix} \tag{4.11}$$

and the roll, pitch and yaw angular velocities are

$$\dot{\phi} = p + q\, sin\phi\, tan\theta + r\, cos\phi\, tan\theta, \tag{4.12}$$

$$\dot{\theta} = q\, cos\phi - r\, sin\phi, \tag{4.13}$$

$$\dot{\psi} = q\, sin\phi\,(cos\theta)^{-1} + r\, cos\phi\,(cos\theta)^{-1}. \tag{4.14}$$

4.3 Newton-Euler Equations

The rotational motion of the quadcopter referring to the body frame coordinates can be expressed both by using the Newton-Euler formalism or the Lagrange approach. In fact, the Lagrange approach needs the direct use of inertial frame coordinates, and which involves a much heavier symbolism. On the other hand, the same model can be obtained by using a different notation by employing the Newton-Euler formulation. Hence, the Newton-Euler approach is used to derive the rigid body dynamics of the quadcopter model in this section, as given in [139].

First, the rotational dynamics are formulated in terms of the body frame coordinates and then given in terms of the inertial frame coordinates using a kinematics transformation [38]. The rotational dynamics of the rigid body, when external forces are applied to the centre-of-mass and expressed in the inertial frame, are given by

$$\mathbb{I}\dot{\boldsymbol{\omega}} = -\boldsymbol{\omega} \times (\mathbb{I}\boldsymbol{\omega}) + \tau_B \tag{4.15}$$

where " $\times$ " represents the vector cross product. The inertia matrix in the body frame is defined in [38] as

$$\mathbb{I} := \begin{bmatrix} I_{xx} & -I_{xy} & -I_{xz} \\ -I_{yx} & I_{yy} & -I_{yx} \\ -I_{zx} & -I_{zy} & I_{zz} \end{bmatrix} \tag{4.16}$$

where I_{xx}, I_{yy}, I_{zz} are the moments of inertia about the x_B, y_B and z_B axes. $I_{xy} = I_{xy}$, $I_{xz} = I_{zx}$, $I_{yz} = I_{zy}$ are the products of inertia. Quadcopter vehicles are usually designed symmetrically about the body axes, with the centre of gravity close to the geometric centre and the rotors located at a distance L from the centre of gravity. Due to the body axis choice, (4.16) can be given as

$$\mathbb{I} = \begin{bmatrix} I_{xx} & 0 & 0 \\ 0 & I_{yy} & 0 \\ 0 & 0 & I_{zz} \end{bmatrix}. \tag{4.17}$$

Torques due to aerodynamic forces are

$$\tau_B = \begin{bmatrix} \tau_p \\ \tau_q \\ \tau_r \end{bmatrix} = \begin{bmatrix} L(f_4 - f_2) \\ L(f_3 - f_1) \\ d(f_1 - f_2 + f_3 - f_4) \end{bmatrix}. \tag{4.18}$$

Considering the rotational drag force, Stoke's law is used for the rotational drag terms.

The rotational drag term k_r is proportional to the angular velocity, which is supposed to be constant in all directions. Now, the rotational dynamics of the rigid body under external forces given in [40] as:

$$\tau_B - k_r\,\boldsymbol{\omega} = \mathbb{I}\,\dot{\boldsymbol{\omega}} + \boldsymbol{\omega} \times (\mathbb{I}\,\omega). \tag{4.19}$$

Substituting the required matrices, eq. (4.19) is equal to

$$\begin{bmatrix} \tau_p \\ \tau_q \\ \tau_r \end{bmatrix} = \begin{bmatrix} I_{xx} & 0 & 0 \\ 0 & I_{yy} & 0 \\ 0 & 0 & I_{zz} \end{bmatrix} \begin{bmatrix} \dot{p} \\ \dot{q} \\ \dot{r} \end{bmatrix} + \begin{bmatrix} p \\ q \\ r \end{bmatrix} \times \begin{bmatrix} I_{xx} & 0 & 0 \\ 0 & I_{yy} & 0 \\ 0 & 0 & I_{zz} \end{bmatrix} \begin{bmatrix} p \\ q \\ r \end{bmatrix} + k_r \begin{bmatrix} p \\ q \\ r \end{bmatrix} \tag{4.20}$$

The roll pitch and yaw torques are

$$\begin{aligned} \tau_p &= I_{xx}\,\dot{p} + q\,r(I_{zz} - I_{yy}) + k_r\,p, && (4.21)\\ \tau_q &= I_{yy}\,\dot{q} + p\,r(I_{xx} - I_{zz}) + k_r\,q, && (4.22)\\ \tau_r &= I_{zz}\,\dot{r} + p\,q(I_{yy} - I_{xx}) + k_r\,r, && (4.23) \end{aligned}$$

and thus the angular accelerations are

$$\begin{aligned} \dot{p} &= \frac{1}{I_{xx}}[L(f_4 - f_2) - q\,r(I_{zz} - I_{yy}) - k_r\,p], && (4.24)\\ \dot{q} &= \frac{1}{I_{yy}}[L(f_3 - f_1) - p\,r(I_{xx} - I_{zz}) - k_r\,q], && (4.25)\\ \dot{r} &= \frac{1}{I_{zz}}[d(f_1 - f_2 + f_3 - f_4) - p\,q(I_{xx} - I_{zz}) - k_r\,r]. && (4.26) \end{aligned}$$

The translational equations of motion for the quadcopter can be derived in the inertial frame by taking into consideration the weight, the thrust forces and the drag terms acting on it. The weight is applied to the centre of gravity and is directed along the negative z-axis in the inertial frame. The translational drag is assumed to be proportional to the linear velocity [40]. Using the Newton-Euler approach, the translational dynamics of a rigid body under external forces applied to the center-of-mass and expressed in an earthfixed frame are:

$$\dot{\boldsymbol{\xi}} = \boldsymbol{v_I} \tag{4.27}$$

$$m\ddot{\boldsymbol{\xi}} = F \tag{4.28}$$

where F denotes the vector of the external forces acting on the quadcopter including thrusts, the gravitational force and translational drag terms. The gravitational force applied to the vehicle is

$$F_g = mgi_3 \tag{4.29}$$

where $i_3 = [0\ 0\ 1]'$. The upward-lifting forces generated by the propellers are f_1, f_2, f_3 and f_4 and the force in the z_B direction can be written as $u_f = f_1 + f_2 + f_3 + f_4$, which yields

$$F = \boldsymbol{R_{B\to I}} i_3 u_f - k_t \dot{\boldsymbol{\xi}} - mgi_3. \tag{4.30}$$

Substituting (4.30) into (4.28) which results in

$$m\ddot{\xi} = \boldsymbol{R_{B\to I}} i_3 u_f - k_t \dot{\boldsymbol{\xi}} - mgi_3. \tag{4.31}$$

Now, the simplified eq. (4.31) can be given as

$$\begin{bmatrix} \ddot{x}_I \\ \ddot{y}_I \\ \ddot{z}_I \end{bmatrix} = \frac{u_f}{m} \begin{bmatrix} cos\phi\, cos\psi\, sin\theta + sin\phi\, sin\psi \\ cos\phi\, sin\theta\, sin\psi - cos\psi\, sin\phi \\ cos\theta\, cos\psi \end{bmatrix} - \frac{k_t}{m} \begin{bmatrix} \dot{x}_I \\ \dot{y}_I \\ \dot{z}_I \end{bmatrix} - \begin{bmatrix} 0 \\ 0 \\ g \end{bmatrix}. \tag{4.32}$$

Accelerations of the centre-of-mass of the quadcopter with respect to inertial fixed frame can be given as:

$$\ddot{x}_I = \frac{1}{m}(f_1 + f_2 + f_3 + f_4)(cos\phi\, cos\psi\, sin\theta + sin\phi\, sin\psi) - \frac{k_t}{m}\dot{x}_I, \tag{4.33}$$

$$\ddot{y}_I = \frac{1}{m}(f_1 + f_2 + f_3 + f_4)(cos\phi\, sin\theta\, sin\psi - cos\psi\, sin\phi) - \frac{k_t}{m}\dot{y}_I, \tag{4.34}$$

$$\ddot{z}_I = \frac{1}{m}(f_1 + f_2 + f_3 + f_4)(cos\theta\, cos\psi) - \frac{k_t}{m}\dot{z}_I - g, \tag{4.35}$$

Parameters	Values	Unit
d	3.793×10^{-2}	
I_{xx}	4.9×10^{-3}	kg.m^2
I_{yy}	4.9×10^{-3}	kg.m^2
I_{zz}	8.8×10^{-3}	kg.m^2
m	0.468	kg
g	9.81	m/s^2
L	0.255	m
k_r	5.8×10^{-2}	N/rad/s
k_t	5.8×10^{-2}	N/m/s
τ	0.2	s

Table 4.1: Quadcopter parameters [139].

in which k_t donates the translational drag coefficient, which is assumed to be equal in all directions. Unmanned quadcopter vehicles usually operate at low flight speeds to carry out any task or mission and are built with small propellers of reduced flexibility. Hence, flapping angles are close to zero and gyroscopic effects are negligible [40].

The set of equations for the quadcopter UAV model can be given as

$$\dot{\phi} = p + q\,\sin(\phi)\tan(\theta) + r\,\cos(\phi)\tan(\theta), \tag{4.36}$$

$$\dot{\theta} = q\,\cos(\phi) - r\,sin(\phi), \tag{4.37}$$

$$\dot{\psi} = q\frac{sin(\phi)}{\cos(\theta)} + r\frac{\cos(\phi)}{\cos(\theta)}, \tag{4.38}$$

$$\dot{p} = \frac{1}{I_{xx}}\left[L(f_4 - f_2) - q\,r(I_{zz} - I_{yy}) - k_r\,p\right], \tag{4.39}$$

$$\dot{q} = \frac{1}{I_{yy}}\left[L(f_3 - f_1) - p\,r(I_{xx} - I_{zz}) - k_r\,q\right], \tag{4.40}$$

$$\dot{r} = \frac{1}{I_{zz}}\left[d(f_1 - f_2 + f_3 - f_4) - p\,q(I_{yy} - I_{xx}) - k_r\,r\right], \tag{4.41}$$

$$\ddot{x}_I = \frac{(f_1 + f_2 + f_3 + f_4)}{m}[\cos(\phi)\cos(\psi)\sin(\theta) + \sin(\phi)\sin(\psi)] - \frac{k_t}{m}\dot{x}_I, \tag{4.42}$$

$$\ddot{y}_I = \frac{(f_1 + f_2 + f_3 + f_4)}{m}[\cos(\phi)\sin(\theta)\sin(\psi) - \cos(\psi)\sin(\phi)] - \frac{k_t}{m}\dot{y}_I, \tag{4.43}$$

$$\ddot{z}_I = \frac{(f_1 + f_2 + f_3 + f_4)}{m}[cos(\theta)\cos(\phi)] - \frac{k_t}{m}\dot{z}_I - g. \tag{4.44}$$

where $f_i = k\omega_i^2$ and $\omega_i = \frac{1}{\tau s+1}\omega_d$, ω_d and ω_i are the desired angular speed and actual angular speed of the rotors, respectively.

The model described by the set of equations (4.36)-(4.44) can be used to describe the majority of the dynamics of a quadcopter vehicle. Whenever numerical results are given, they refer to this model, with appropriate parameters reported in Table 4.1.

4.4 Sensors

The quadcopter vehicles could be equipped with inertial measurement units (IMU), Global Positioning Systems (GPS) and barometric pressure sensors. The IMU sensor contains an accelerometer, a gyroscope and a magnetometer. As the name suggests, the accelerometer is used to measure the acceleration, whereas the gyroscope measures the angular velocity and the magnetometer estimates the yaw angle. These sensors estimates real values through with a degree of time delay, e.g., 15 ms as reported in [122]. Furthermore, the positional information from the IMU might be affected by drift and measurement noise. Any noise or drift in acceleration might result in a significant deviation in position. The drift is at low frequencies, whereas the noise is at high frequencies. Hence, a high-pass filter is used to significantly reduce the effects of drift at lower frequencies and noise can be reduced by a low-pass filter [139]. Integrating measurements is another issue, because double integration requires an initial velocity and position from the raw measurements; however, the requirement for initial conditions is not possible in many situations. To overcome this issue, a high-pass filter is used to remove the DC components in the results. First, linear acceleration is low-pass filtered to eliminate the noise at high frequency. Then, the resulting measurement is high-pass filtered to remove the drift at low frequency and then integrated to find the linear velocity. This velocity is high-pass filtered to eliminate DC components, which removes the requirement for information on initial conditions. The resulting data is again integrated to gain position values and is high-pass filtered to remove the DC component, as mentioned earlier [127].

A GPS can provide accurate measurements around 2-3 meters in terms of position x_I and y_I [124]. However, this candidate system has a number of weakness under certain environmental and flight conditions such as cloudy weather and during low altitude flight. As a result, it does not provide accurate measurements. Alternative methods (e.g., see [101]) have been developed to estimate the translational position and velocity to enable autonomous navigation where the GPS signal is not possible. The low measurement rate and heavy computational demands of the GPS lead to a time delay in measurement which might result in a deterioration in system stability. To overcome this issue, the delayed output observer is developed in [156]. For the indoor environment, optical flow sensors were employed by [1] to estimate x-y translational velocities with respect to the inertial frame. However, optical flow sensors offer little robustness under various lighting conditions and require considerable computational resources [142]. A barometric pressure sensor is used to measure the altitude with deviation and noise in a timely fashion. This measurement can be improved by using a low-pass filter. Another issue with respect to this sensor is that the atmospheric pressure varies rapidly at certain locations due to weather conditions and other influences. A reference ground barometer can be employed to deal with pressure fluctuations [138]. Practical sensor issues are outside the scope of this research, and we will thus assume ideal dynamics for the sensors.

4.5 Conclusions

In this chapter, a non-linear model of the quadcopter aircraft has been presented using the Newton-Euler equations based on the force and moments acting on the body. Quadcopters operate at low speed and are equipped with small propellers of reduced flexibility. Therefore, blade gyroscopic effects are omitted due to the essentially zero flapping angles. The translational drag is proportional to the linear velocity, and the rotational drag is proportional to the angular velocity. The most relevant aerodynamic effects are included in the model in order to derive a set of equations that are more suitable for simulation purposes. The model given here will be used in later chapters for designing flight control laws corresponding to attitude stabilisation and inertial velocity trajectory tracking. This chapter also has been provided information regarding sensors which can be used for requirement measurements.

CHAPTER 5

INVESTIGATION OF LOW-ORDER H_∞ CONTROL OPTIMISATION TOOLS

5.1 Introduction

Simple controllers, e.g., PID controllers, are preferred in practical implementation for flexibility of implementation. At the same time, PID controllers have some drawbacks; the performance of these controllers relies on the precisely estimation of system models and parameters; PID gain parameters are difficult to tune for MIMO systems; the PID controller is less robust than robust controllers when the system imposes disturbances and uncertainties under operational conditions, and PID parameters have to be retuned in the presence of disturbances or in the instance of payload change [105]. Consequently, simple robust controllers are needed to overcome the drawbacks of PID controllers.

This chapter investigates the designs of fixed-order and structured H_∞ controllers for the quadcopter UAV and discusses their advantages/ drawbacks over a standard H_∞ controller design. The Glover-Doyle approach computes an optimal H_∞ controller by solving two Riccati equations [52]. The order of the controller is equal to the order of the open-loop plant plus the order of the weighting functions, which can be very high in practice. The fixed-order and structured H_∞ optimisation algorithms, namely, *hifoo* [13] and *hinfstruct* [13], are used to synthesise low-order H_∞ controllers. These new methods can provide satisfactory controllers in terms of bandwidth, disturbance rejection and robust stability. Simpler H_∞ controllers could potentially replace higher-order H_∞ controllers during practical implementation. They can also meet the architectural requirements of embedded applications [44]. *hifoo* has been successfully applied to different benchmark examples [56].

Our objective here is to compute simple H_∞ controllers and compare their performance to the performance of a standard H_∞ controller obtained with the Glover-Doyle algorithm. This chapter describes the designs of various H_∞ controllers for the stabilisation of vehicles's altitude and attitude, and also sheds some light on the performance and computational efficiency of low-order H_∞ controllers.

This chapter is structured as follows: in Section 5.2, the general H_∞ problem is described, and the mixed sensitivity H_∞ setup is given. Section 5.3 briefly presents the H_∞ non-smooth optimisation algorithms, the H_∞ mixed sensitivity and LMI approach to H_∞ optimisation. Section 5.4 presents the control objectives and the low- and full-order H_∞ controller designs. Simulation results are analysed and discussed in terms of the advantages/ drawback of control approaches in Section 5.5. Finally, Section 5.6 gives some concluding remarks.

5.2 General Control Configuration

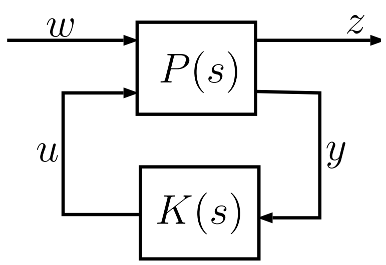

Figure 5.1: Standard feedback system.

The H_∞ synthesis is based on the standard feedback system of Fig. 5.1 where the signals ($z,\ w,\ y,\ u$) represent, respectively, the output objectives, the exogenous inputs such as disturbance and reference, and the measured outputs and control inputs. The open-loop system $P(s)$ of Fig. 5.1, which is a generalised plant model that includes weighting functions and a plant model, is given as

$$\begin{bmatrix} z \\ y \end{bmatrix} = \left[\begin{array}{c|c} P_{11} & P_{12} \\ \hline P_{21} & P_{22} \end{array}\right] \begin{bmatrix} w \\ u \end{bmatrix} = P \begin{bmatrix} w \\ u \end{bmatrix}. \tag{5.1}$$

The transfer function from w to z is given by:

$$\mathcal{F}_l(P, K) = P_{11} + P_{12}K(I - P_{22}K)^{-1}P_{21}. \tag{5.2}$$

State-space realisation of generalised plant, $P(s)$, is

$$P(s) \stackrel{s}{=} \left(\begin{array}{c|cc} A & B_1 & B_2 \\ \hline C_1 & D_{11} & D_{12} \\ C_2 & D_{21} & D_{22} \end{array}\right) \tag{5.3}$$

where $A \in \mathbb{R}^{n\times n}, D_{12} \in \mathbb{R}^{p_1\times m_2}, D_{21} \in \mathbb{R}^{p_2\times m_1}$ and other matrices have compatible dimensions. State-space realisation of the controller is

$$K(s) \stackrel{s}{=} \left(\begin{array}{c|c} A_K & B_K \\ \hline C_K & D_K \end{array}\right) \tag{5.4}$$

where $A_K \in \mathbb{R}^{n_K\times n_K}$ and B_K, C_K, D_K have compatible dimensions with A_K and the generalised plant matrices.

The optimal H_∞ controller design objective is

$$\inf_{K \text{ stabilising}} \|\mathcal{F}_l(P, K)\|_\infty \tag{5.5}$$

where K is a stabilising controller. The stabilising controller optimally achieves the minimum closed-loop norm $\|T_{wz}\| = \gamma_{opt}$. A stabilising controller that achieves the closed-loop norm $\gamma > \gamma_{opt}$ is said to be sub-optimal.

5.2.1 H_∞ Mixed Sensitivity Setup

Denote that W_1, W_2 and W_3 are the performance, the penalizing control input and the stability weighting functions, respectively. The purpose here is to find a stabilising controller K such that

$$J_\infty = \left\| \begin{matrix} W_1 S \\ W_2 K S \\ W_3 T \end{matrix} \right\|_\infty \tag{5.6}$$

is minimised, where

$$|S(j\omega)| \leq \frac{1}{|W_1(j\omega)|}, \quad \forall\omega \tag{5.7}$$

$$|T(j\omega)| \leq \frac{1}{|W_3(j\omega)|}, \quad \forall\omega \tag{5.8}$$

Consequently, if $\|J\|_\infty < 1$ then the frequency domain specifications will be met and the Lyapunov stability of $\mathcal{F}_l(P, K)$ is guaranteed. Weighting functions can be chosen as [133]:

$$W_1(s) = \left(\frac{s/M_S + \omega_{BS}^*}{s + \omega_{BS}^* A_s} \right) \tag{5.9}$$

$$W_2(s) = \text{constant} \tag{5.10}$$

$$W_3(s) = \left(\frac{s/\omega_{BT}^* + 1/M_T}{A_T s/\omega_{BT}^* + 1} \right) \tag{5.11}$$

where M_S and M_T impose limits on the maximum peak values. In fact, if M_S or M_T are less than 2 (6 dB), sufficient gain and phase margins can be obtained according to:

$$\begin{aligned} GM &\geq \tfrac{M_S}{M_S - 1} \quad PM \geq 2\arcsin(\tfrac{1}{2M_S}) \\ GM &\geq 1\tfrac{1}{M_T} \quad\ \ PM \geq 2\arcsin(\tfrac{1}{2M_T}) \end{aligned} \tag{5.12}$$

A large value of M_S or M_T (larger than 12 dB) may lead to poor performance and poor closed-loop robustness. A_S and A_T can be set to zero to impose pure integral action. However, this will lead to numerical problems as rank conditions to be violated in this case. Hence, A_S and A_T will typically be small positive numbers.

The gain crossover frequency, ω_c, is the frequency where an open-loop system first crosses 0 dB from above. It is generally a value between ω_{BS}^* and ω_{BT}^* ($\omega_{BS}^* \leq \omega_c \leq$

ω_{BT}^*). The bandwidth of the sensitivity function approximately determines the closed-loop bandwidth frequency requirement [55, 133].

When the main concern is disturbance rejection, ω_{BS}^* is increased as much as possible. However, if ω_{BS}^* is unnecessarily increased, this results in a peak in the sensitivity transfer function curve and overshoot in the time domain response. The complementary transfer function, $T(j\omega)$, is shaped to achieve tracking and noise attenuation requirements. In order to reduce the influence of the measurement noise, a high roll-off rate at high frequencies is desirable. Hence, ω_{BT}^* is decreased, but unnecessarily decreasing ω_{BT}^* leads to poor tracking performance [103].

5.3 H_∞ control Approaches

In this section, fixed-order H_∞ optimisation, structured H_∞ optimisation, LMI-based H_∞ optimisation and mixed sensitivity H_∞ optimisation algorithms are presented to compute a stabilising controller K for orientations and vertical position tracking of the quadcopter aircraft system.

5.3.1 Fixed-order H_∞ Optimisation

A free MATLAB Toolbox *hifoo* computes a fixed-order output feedback H_∞/H_2 controller. *hifoo* uses a hybrid algorithm for non-smooth, non-convex optimisation based on standard quasi-Newton (BFGS optimisation) and gradient sampling techniques.

The algorithm has a two-stage approach: stabilisation, and performance optimisation to search for local minimisers. In the first stage, the standard quasi-Newton technique is used to minimise the maximum of the real parts of the eigenvalues found for the closed-loop system matrix. This process terminates as soon as a controller is found that provides an initial point for the subsequent phase; if a stabilising controller is not found, *hifoo* terminates with an error message. In the second phase, *hifoo* utilises a gradient sampling method. Gradients are randomised around the current iteration to locally minimise the H_∞ performance of the closed-loop system.

Both stages benefit considerably from the *hanso* supporting software package in terms of non-smooth, non-convex optimisation. This supporting package involves three optimisations. The quasi-Newton algorithm efficiently searches for the approximation of a local minimum at the first stage. Next, a local minimum for the best point found by the quasi-Newton algorithm is verified by a local bundle. If this verification is not achieved, a gradient sampling phase attempts to approximate the local minimiser and returns a locally optimal controller.

This approach looks for a local minimiser to the optimisation problem. *hifoo* uses randomised starting points and, furthermore, the gradient sampling phase also involves randomisation. The same results are not obtained every execution. For this reason, *hifoo* is run at least 10 times to obtain the minimum closed-loop H_∞ norm. The reader should consult [8, 56, 58] for more details.

5.3.2 Stuctured H_∞ Synthesis

hinfstruct is available in the MATLAB Robust Control Toolbox [13], and synthesises structured H_∞ controllers based on the work of [7]. The standard representation of Fig. 5.1 is utilised, where a fixed-order diagonal structured controller of the form

$$K(s) = \begin{pmatrix} C_1(s) & \cdots & 0 \\ \vdots & \ddots & \vdots \\ 0 & \cdots & C_N(s) \end{pmatrix} \tag{5.13}$$

is considered, where $C_1(s), ..., C_N(s)$ are linear time-invariant systems of a prescribed structure.

hinfstruct uses the same problem formulations as *hifoo* but solves them using different techniques. Stuctured H_∞ synthesis requires a solution to semi-infinite, non-convex and non-smooth problems of the form

$$\underset{K}{\text{minimise}} \;\; \|\mathcal{F}_l(P, K)\|_\infty \Leftrightarrow \underset{x \in \mathbb{R}^k}{\text{minimise}} \;\; \max_{\omega \in [0,\, \infty]} \;\; \bar{\sigma}(\mathcal{F}_l(\hat{P}(j\omega), x)) \tag{5.14}$$

where the vector x contains all low-level tunable parameters in $K(s)$. The right-hand side function in (5.14) consists of non-smooth function $\max_\omega \bar{\sigma}(.)$ and non-convex but differentiable mapping $x \longrightarrow (\mathcal{F}_l(\hat{P}(j\omega), x))$. Therefore, the Clarke sub-differential is utilised by *hinfstruct* at each iteration. For simplicity, the problem (5.14) is written as follows:

$$\underset{x \in \mathbb{R}^k}{\text{minimise}} \quad f_\infty(x) := \underset{\omega \in [0,\ \infty]}{\max} \quad f(\omega, x)) \tag{5.15}$$

To solve (5.15), a tangent model around the current iteration x is constructed that consists of a quadratic first-order local approximation of the original problem. Then, a search direction is computed and a line search is carried out. There is the minimal requirement that some finite set of frequencies should contain the active frequencies ω_a that achieve the peak value in (5.14): $f_\infty(x) = f(\omega_a, x))$. This requirement is adequate in order to make the algorithm converge to a local minimum. In addition, a few extra well-chosen frequencies improve the quality of the tangent model and the length of the steps achieved at each iteration. In particular, including frequencies that achieve peak values can speed up the convergence considerably. Fig. 5.2 illustrates this strategy.

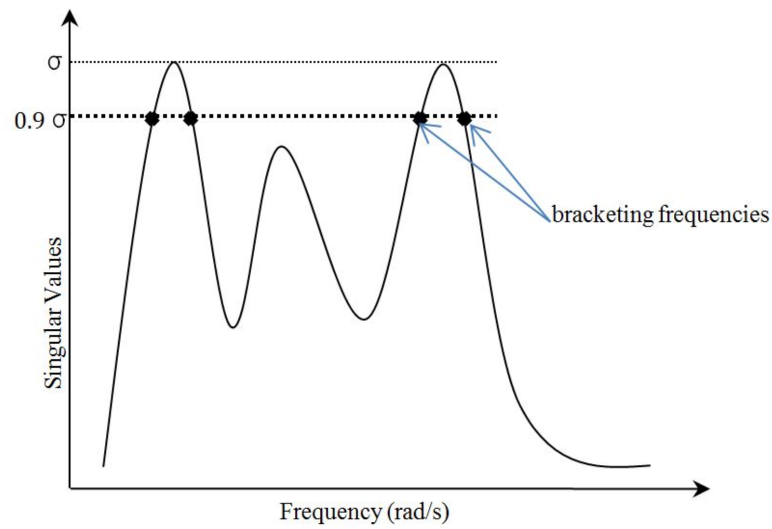

Figure 5.2: Frequencies at current iteration to build a tangent model [44].

hinfstruct is a deterministic approach that does not involve any randomisation apart from extra starting points. The *hinfstruct* algorithm automatically executes multiple optimisations, setting random starting points. This improves the speed at which parameter values that meet the design requirements are found. (see for details [43–45]).

5.3.3 Linear Matrix Inequality (LMI) Approach

The Linear Matrix Inequality (LMI) approach is an alternative to the state-space characterisation and available as *hinflmi* in MATLAB Robust Control Toolbox. The standard H_∞ Riccati equations are replaced by Riccati inequalities. The set of pairs (X, Y) of symmetric matrices satisfying the system matrix inequities are used to compute suboptimal H_∞ and reduced-order controllers.

The suboptimal H_∞ problem is solvable under the following assumptions:

1. (A, B_2, C_2) is stabilisable and detectable so that the plant can be stabilised by output feedback
2. $D_{22} = 0$ to simplify the calculation without loss of generality

and if, and only if, there exist symmetric matrices R, S that satisfy the following LMI system [42]:

$$\left(\begin{array}{c|c} N_R & 0 \\ \hline 0 & I \end{array}\right)' \left(\begin{array}{cc|c} AR+RA' & RC_1' & B_1 \\ C_1R & -\gamma I & D_{11} \\ \hline B_1' & D_{11} & -\gamma I \end{array}\right) \left(\begin{array}{c|c} N_R & 0 \\ \hline 0 & I \end{array}\right) < 0 \tag{5.16}$$

$$\left(\begin{array}{c|c} N_S & 0 \\ \hline 0 & I \end{array}\right)' \left(\begin{array}{cc|c} A'S+SA & SB_1 & C_1' \\ B_1'S & -\gamma I & D_{11}' \\ \hline C_1 & D_{11} & -\gamma I \end{array}\right) \left(\begin{array}{c|c} N_S & 0 \\ \hline 0 & I \end{array}\right) < 0 \tag{5.17}$$

$$\begin{pmatrix} R & I \\ I & S \end{pmatrix} \geq 0 \tag{5.18}$$

where N_R and N_S are the null spaces of $(B_2',\ D_{12}')$ and $(C_2,\ D_{21})$, respectively.

Once computing some solution $(R,\ S)$ for the system LMIs (5.16)-(5.18), there then exist some γ-suboptimal reduced-order controller ($k < n$) if, and only if,

$$Rank(I - RS) \leq k. \tag{5.19}$$

Computational steps follow to construct a suboptimal H_∞ controller [41]. Two full-column rank matrices $M,\ N \in \mathbb{R}^{n\times k}$ are computed via SVD (Singular Value Decomposition) such that

$$MN' = I - RS. \tag{5.20}$$

The positive definite matrix $X_{cl} \in \mathbb{R}^{(n+k)\times(n+k)}$ is obtained as the unique solution of the linear equation:

$$\begin{bmatrix} S & I \\ N' & 0 \end{bmatrix} = X_{cl} \begin{bmatrix} I & R \\ 0 & M' \end{bmatrix}. \tag{5.21}$$

Solving the (5.22) inequality for the control parameters:

$$\Psi_{X_{cl}} + Q'\Theta' P_{X_{cl}} + P'_{X_{cl}}\Theta Q < 0 \tag{5.22}$$

where

$$\Psi_{X_{cl}} := \begin{pmatrix} \begin{pmatrix} A & 0 \\ 0 & 0 \end{pmatrix} X_{cl} + X_{cl} \begin{pmatrix} A' & 0 \\ 0 & 0 \end{pmatrix} & X_{cl}\begin{pmatrix} B_1 \\ 0 \end{pmatrix} & \begin{pmatrix} C_1' \\ 0 \end{pmatrix} \\ \begin{pmatrix} B_1' & 0 \end{pmatrix} X_{cl} & -\gamma I & D_{11}' \\ \begin{pmatrix} C_1 & 0 \end{pmatrix} & D_{11} & -\gamma I \end{pmatrix},$$

$$P_{X_{cl}} = \left[\begin{bmatrix} 0 & I' \\ B_2' & 0 \end{bmatrix} X_{cl} \left| \begin{matrix} 0 & 0 \\ 0 & D_{12}' \end{matrix} \right. \right],$$

$$Q = \begin{bmatrix} 0 & I & 0 & 0 \\ C_1 & 0 & D_{11} & 0 \end{bmatrix}, \tag{5.23}$$

the controller is obtained as

$$\Theta = \left(\begin{array}{c|c} A_K & B_K \\ \hline C_K & D_K \end{array} \right). \tag{5.24}$$

The minimum order of the controller is significantly affected by the size of X_{cl} or the rank of $(I - RS)$.

The rank minimisation problem can be expressed as an optimisation problem under LMI constraints for a feasible H_∞ norm. The amount by which the order is reduced can be calculated with the objective function:

$$\sum_{i=1}^{n-k} \lambda_i \begin{pmatrix} R & I \\ I & S \end{pmatrix} \tag{5.25}$$

where $\lambda_i(.) \leq \cdots \leq \lambda_{n-k}(.)$ are the $n-k$ smallest eigenvalues of $\begin{pmatrix} R & I \\ I & S \end{pmatrix}$.

There exist reduced-order suboptimal controllers if, and only if, the global minimum of the objective function is zero. Global convergence is not guaranteed [42].

5.3.4 Mixed Sensitivity H_∞ Optimisation Approach

Necessary and sufficient conditions are derived by Glover and Doyle [52] for the existence of an H_∞ control solution. The optimal H_∞ controller minimises the maximum singular value based on the following assumptions for the generalised plant, (5.3):

- (A, B_2, C_2) is stabilisable and detectable
- D_{12} and D_{21} are full rank
- $\begin{bmatrix} A - j\omega I & B_2 \\ C_1 & D_{12} \end{bmatrix}$ has full column rank for all ω
- $\begin{bmatrix} A - j\omega I & B_1 \\ C_2 & D_{21} \end{bmatrix}$ has full column rank for all ω

The first assumption is necessary for the existence of stabilising controllers K, and the second is required to ensure that the optimal controller is proper and hence realisable. The last two assumptions guarantee that the optimal controller does not cancel poles or zeros on the imaginary axis that causes closed-loop instability. For specified γ, optimal H_∞ algorithms find a K-stabilising controller such that $\|\mathcal{F}_l(P, K)\|_\infty < \gamma$ if all the following conditions are fulfilled

1. $X_\infty \geq 0$ is a solution to the algebraic Riccati equation.

$$A'X_\infty + X_\infty A + C_1'C_1 + X_\infty(\gamma^{-2}B_1B_1' - B_2B_2')X_\infty = 0 \tag{5.26}$$

   such that $Re\,\lambda_i\left[A + (\gamma^{-2}B_1B_1' - B_2B_2')X_\infty\right] < 0, \quad \forall i.$

2. $Y_\infty \geq 0$ is a solution to the algebraic Riccati equation.

$$AY_\infty + Y_\infty A' + B_1B_1' + Y_\infty(\gamma^{-2}C_1'C_1 - C_2'C_2)Y_\infty = 0 \tag{5.27}$$

   such that $Re\,\lambda_i\left[A + Y_\infty(\gamma^{-2}C_1'C_1 - C_2'C_2)\right] < 0, \quad \forall i$; and

3. $\rho(X_\infty Y_\infty) < \gamma^2$

then

$$K(s) \stackrel{s}{=} \left(\begin{array}{c|cc} A + \gamma^{-2}B_1{B_1}'X_\infty + B_2F_\infty + Z_\infty L_\infty C_2 & -Z_\infty L_\infty & Z_\infty B_2 \\ \hline F_\infty & 0 & I \\ -C_2 & I & 0 \end{array}\right) \tag{5.28}$$

with $F_\infty = -B_2'X_\infty, L_\infty = -Y_\infty C_2', Z_\infty = (I - \gamma^{-2}Y_\infty X_\infty)^{-1}$ is admissible. Finding an optimal H_∞ controller requires the solution of equations (5.26) and (5.27). This solution yields a central controller with the same state dimension as as the generalised plant $P(s)$. The Glover-Doyle algorithm can solve $\|\mathcal{F}_l(P, K)\|_\infty < \gamma$ efficiently by reducing γ iteratively, through which an optimal solution can be found [94].

5.4 Control Laws Designs

The output feedback controller is designed to stabilise the attitudes $\phi,\ \theta,\ \psi$ as well as tracking the desired height position, z_I. The control structure proposed to control the Euler angles and the heave position of the quadcopter UAV is given in Fig. 5.3. Control objectives are to regulate the Euler angles via a maximum 30% overshoot and a 2% steady-state error in no more than 10 seconds. In addition, the quadcopter is expected to reach the desired vertical position, without overshoot and with less than 2% steady-state error, in 10 seconds (Table 5.1).

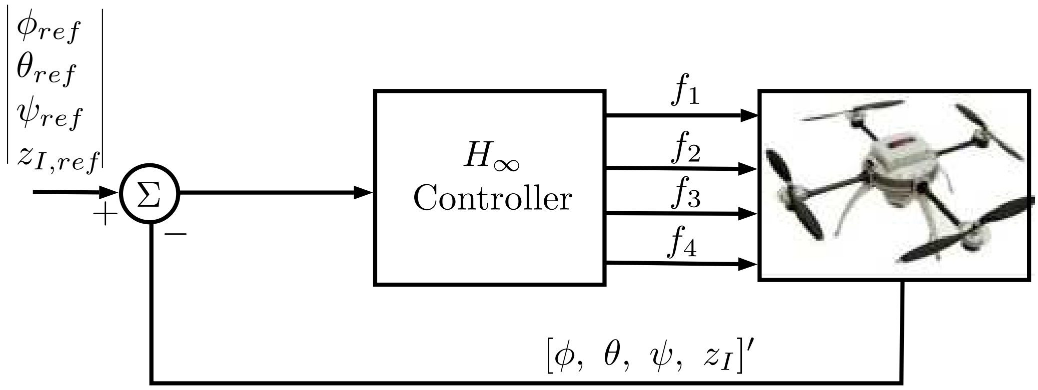

Figure 5.3: Closed-loop control structure.

	Overshoot (%)	Steady-state error (%)	Settling time (s)
roll	30	2	10
pitch	30	2	10
yaw	30	2	10
height	0	2	10

Table 5.1: Control objectives.

In order to design the controller, the non-linear equations (4.36)-(4.41) and (4.44) are first written in a state-space form with the state vector:

$$x = [x_1 \ldots x_8]' = [\phi\ \theta\ \psi\ z_I\ p\ q\ r\ \dot{z}_I]' \tag{5.29}$$

$$\tag{5.30}$$

and input vector:

$$u = [f_1\ f_2\ f_3\ f_4]' \tag{5.31}$$

where

$$\dot{x}_1 = x_5 + x_6 \sin(x_1)\tan(x_2) + x_2\cos(x_1)\tan(x_2) \tag{5.32}$$

$$\dot{x}_2 = x_6\cos(x_1) - x_7\sin(x_1) \tag{5.33}$$

$$\dot{x}_3 = x_6\frac{\sin(x_1)}{\cos(x_2)} + x_7\frac{\cos(x_1)}{\cos(x_2)} \tag{5.34}$$

$$\dot{x}_4 = x_8 \tag{5.35}$$

$$\dot{x}_5 = \frac{1}{I_{xx}}[L(f_4 - f_2) - x_6 x_7 (I_{zz} - I_{yy}) - k_r\, x_5] \quad (5.36)$$
$$\dot{x}_6 = \frac{1}{I_{yy}}[L(f_3 - f_1) - x_4 x_6 (I_{xx} - I_{zz}) - k_r\, x_6] \quad (5.37)$$
$$\dot{x}_7 = \frac{1}{I_{zz}}[d(f_1 - f_2 + f_3 - f_4) - x_4 x_5 (I_{yy} - I_{xx}) - k_r\, x_7] \quad (5.38)$$
$$\dot{x}_8 = \frac{(f_1 + f_2 + f_3 + f_4)(\cos(x_1)\cos(x_2))}{m} - \frac{k_t}{m} x_8 - g \quad (5.39)$$

The measurable output is $y(t) = [x_1\ x_2\ x_3\ x_4]'$=$[\phi\ \theta\ \psi\ z_I]'$. This non-linear system can be written in a more compact form:

$$\begin{aligned} \dot{x}(t) = &\ f(x(t), u(t)) \\ y(t) = &\ h(x(t)) \end{aligned} \quad (5.40)$$

These equations are linearised around the origin $\phi,\ \theta,\ \psi,\ z_I = 0$. The input at equilibrium is

$$u_{eq} = [f_1\ f_2\ f_3\ f_4]^T = [\frac{gm}{4}\ \frac{gm}{4}\ \frac{gm}{4}\ \frac{gm}{4}]'. \quad (5.41)$$

Using the Jacobian linearisation, the linear system approximation to attitude and altitude non-linear dynamics is

$$\begin{aligned} \dot{\delta x} = &\ \frac{\partial f}{\partial x}\Big|_{x_e, u_{eq}} \delta x + \frac{\partial f}{\partial u}\Big|_{x_e, u_{eq}} \delta u \\ y = &\ \frac{\partial h}{\partial x}\Big|_{x_e, u_{eq}} \delta x \end{aligned} \quad (5.42)$$

Defining a new state vector $\tilde{x} = \delta x$ and input $\tilde{u} = \delta u$ yields

$$\begin{aligned} \tilde{x} = &\ A\tilde{x} + B\tilde{u} \\ y = &\ C\tilde{x} \end{aligned} \quad (5.43)$$

where the state-space matrices A and B are given by

$$A := \left.\frac{\partial f}{\partial x}\right|_{x_e,u_{eq}} = \begin{bmatrix} 0 & 0 & 0 & 0 & 1 & 0 & 0 & 0 \\ 0 & 0 & 0 & 0 & 0 & 1 & 0 & 0 \\ 0 & 0 & 0 & 0 & 0 & 0 & 1 & 0 \\ 0 & 0 & 0 & 0 & 0 & 0 & 0 & 1 \\ 0 & 0 & 0 & 0 & -\frac{k_r}{I_{xx}} & 0 & 0 & 0 \\ 0 & 0 & 0 & 0 & 0 & -\frac{k_r}{I_{yy}} & 0 & 0 \\ 0 & 0 & 0 & 0 & 0 & 0 & -\frac{k_r}{I_{zz}} & 0 \\ 0 & 0 & 0 & 0 & 0 & 0 & 0 & -\frac{k_t}{m} \end{bmatrix}$$

$$B := \left.\frac{\partial f}{\partial u}\right|_{x_e,u_{eq}} = \begin{bmatrix} 0 & 0 & 0 & 0 \\ 0 & 0 & 0 & 0 \\ 0 & 0 & 0 & 0 \\ 0 & 0 & 0 & 0 \\ 0 & -\frac{L}{I_{xx}} & 0 & \frac{L}{I_{xx}} \\ -\frac{L}{I_{yy}} & 0 & \frac{L}{I_{yy}} & 0 \\ \frac{d}{I_{zz}} & -\frac{d}{I_{zz}} & \frac{d}{I_{zz}} & -\frac{d}{I_{zz}} \\ \frac{1}{m} & \frac{1}{m} & \frac{1}{m} & \frac{1}{m} \end{bmatrix}. \tag{5.44}$$

Assuming that the Euler angles ($\phi,\ \theta,\ \psi$) and the position (z_I) are measurable, then the output matrix C is

$$C := \left.\frac{\partial h}{\partial x}\right|_{x_e,u_{eq}} = \begin{bmatrix} I_{4,4} & 0_{4,4} \end{bmatrix} \tag{5.45}$$

Various controllers will be computed using the functions *hifoo*, *hinfstruct*, *hinflmi* for low-order controllers and the Glover-Doyle algorithm (*mixsyn* function) for full-order controller on a 64-bit PC with a 3.2 GHz Intel® Core i5-3470 processor and 16 GB of RAM. First, loop-shaping requirements are obtained with the *hifoo* algorithm because *hifoo* is sensitive to initial weight selections. The trial-and-error method is used to adjust the parameters of the formulae (5.9)-(5.11). Afterwards, other controllers will be designed with the same weighting functions. The weighting function parameters are reported in Table 5.2 following the procedure described in Section 5.2.1. The value M_S is inversely proportional to robustness thus, smaller M_S provides better robustness [133].

$M_S = 2$ specifies that gain and phase margins are greater than 2 and 29^o, respectively. Similarly, $M_T = 2$ specifies that gain and phase margins are greater than 1.5 and 29^o, respectively. Attitudes and altitude have different time constants and thus different band-

	A_S	A_T	M_T	M_S	ω^*_{BS} (rad/s)	ω^*_{BT} (rad/s)	W_2
roll	$3e^{-4}$	0.05	2	2	1	10	1
pitch	$3e^{-4}$	0.05	2	2	0.25	10	1
yaw	$3e^{-4}$	0.05	2	2	0.8	10	1
height	$3e^{-4}$	0.05	2	2	3	10	1

Table 5.2: Weight function parameters.

widths. Controller orders and times are reported in Table 5.3. The computational time has been computed using the *tic* and *toc* commands in MATLAB. Table 5.3 shows that the *hifoo* algorithm has the highest computational time and sensitivity to initial weight selection. As reported in [45], *hinfstruct* obtains the same size order controller, even though computational time is shorter in comparison. The lowest H_∞ stabilising controller has been obtained as a 6^{th} order controller by the *hifoo* and the *hinfstruct* algorithms. The size of the controller order is not reduced by the LMI approach to the same degree as the *hifoo* and the *hinfstruct* algorithms. The LMI approach could represent an alternative to the Glover-Doyle optimisation technique; however, this method is not adequate to obtain the lowest order H_∞ controller.

The frequency responses obtained with *hifoo* and *hinfstruct* algorithms are shown in Figs. 5.4 - 5.7. The peak gains of the output sensitivity functions are 7.87 dB at 3.24 rad/s and 7.37 dB at 4 rad/s, respectively. The peak gains of the output complementary sensitivity functions are 6.87 dB at 2.87 rad/s and 4.87 dB at 3.57 rad/s, respectively. The output feedback controller will reduce disturbances to the frequency at less than 0.5 rad/s, although the disturbance is amplified between 0.5 rad/s and 19.1 rad/s when the controller designed by the *hifoo* algorithm is employed. Furthermore, there are good

Algorithms	*hifoo*	*hinfstruct*	LMI	Glover-Doyle
Order	6	6	11	20
Closed-loop H_∞ norm	3.88	1.936	2.23	1.18
Sensitivity to initial point	✓	✗	✗	✗
Computing time (s)	420	10.2	4.9	1.6

Table 5.3: Comparison of control law designs.

tracking characteristics for a command with a frequency of less than 0.4 rad/s. However, the *hinfstruct* controller provides good tracking characteristics for a command with a frequency of less than 0.1 rad/s. Similarly, an examination of the frequency responses obtained the LMI and the Glover-Doyle approaches from Fig. 5.8 to 5.11 show that the peak gains of the output sensitivity functions are 2.28 dB at 3 rad/s and 2.6 dB at 2.2 rad/s, respectively. The peak gains of the output complementary sensitivity functions are 1.37 dB at 0.417 rad/s and nearly 0 dB over the range of frequency, respectively. The LMI and Glover-Doyle controllers achieve good disturbance rejection until 0.5 rad/s and 1.0 rad/s, respectively. There is good command tracking until 0.1 rad/s with the LMI controller, but the command tracking property is increased to a frequency of 0.5 rad/s by the Glover-Doyle controller. Consequently, it is expected that the Glover-Doyle controller will provide better closed-loop responses than the LMI controller.

Comparing the results in the Figs. 5.4, 5.6, 5.8 and 5.10, it can be seen that the *hinfstruct* controller amplifies disturbance over a larger range of frequencies than the *hifoo* and Glover-Doyle controllers. It can be seen that the peak gain of the closed-loop sensitivity function with the *hifoo* controller is the highest amongst these controllers. Therefore, it might be expected that the *hifoo* controller will provide a larger overshoot than others. Furthermore, a comparison of the frequency responses of closed-loop complementary sensitivity functions from Figs. 5.5, 5.7, 5.9 and 5.11 shows that the Glover-Doyle controller achieves the best tracking property amongst these controllers. In the next section, we will present time domain simulation results obtained with the non-linear dynamic model of the quadcopter given in Chapter 4.

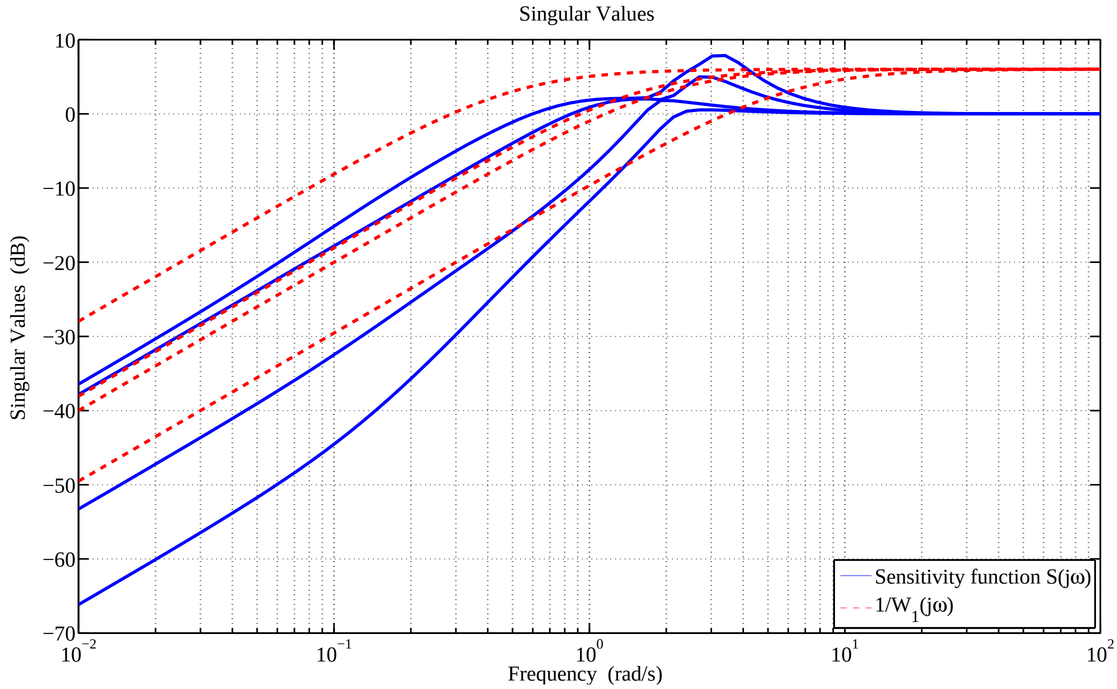

Figure 5.4: Singular value plots of the sensitivity function and inverse of the performance weight with the controller designed using the *hifoo*.

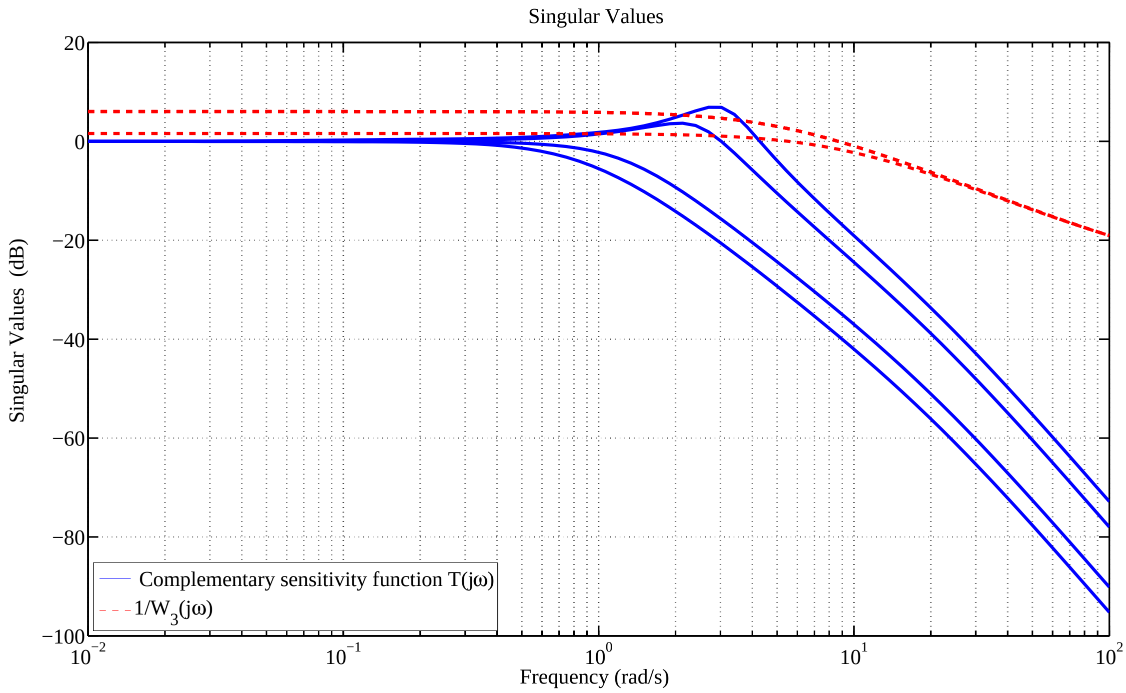

Figure 5.5: Singular value plots of the complementary sensitivity function and inverse of the stability weight with the *hifoo*.

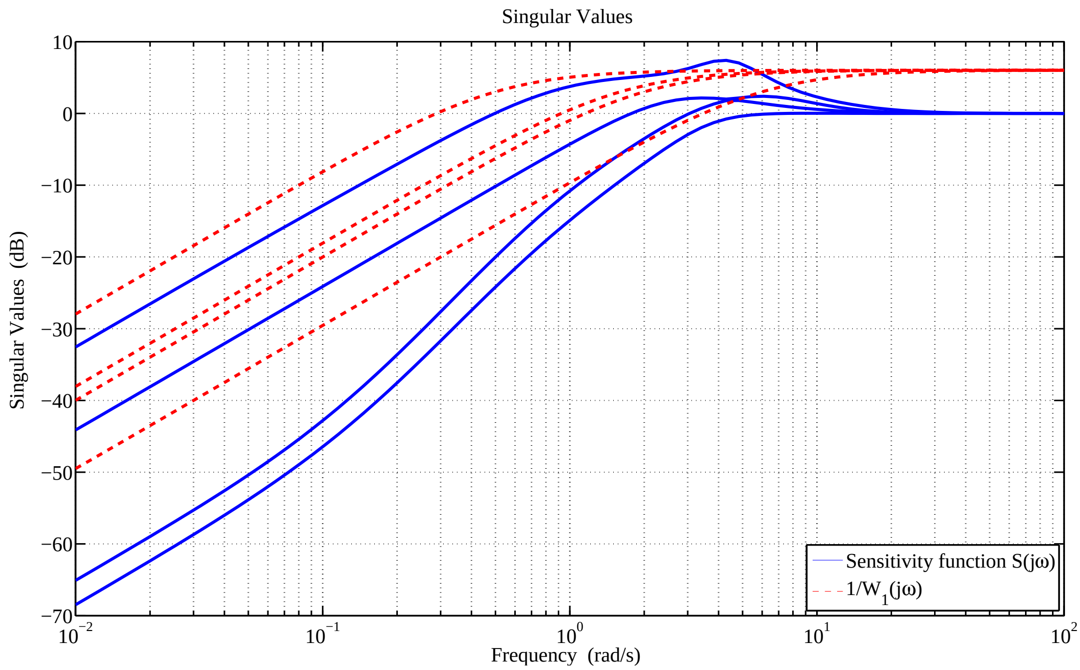

Figure 5.6: Singular value plots of the sensitivity function and inverse of the performance weight with the *hinfstruct*.

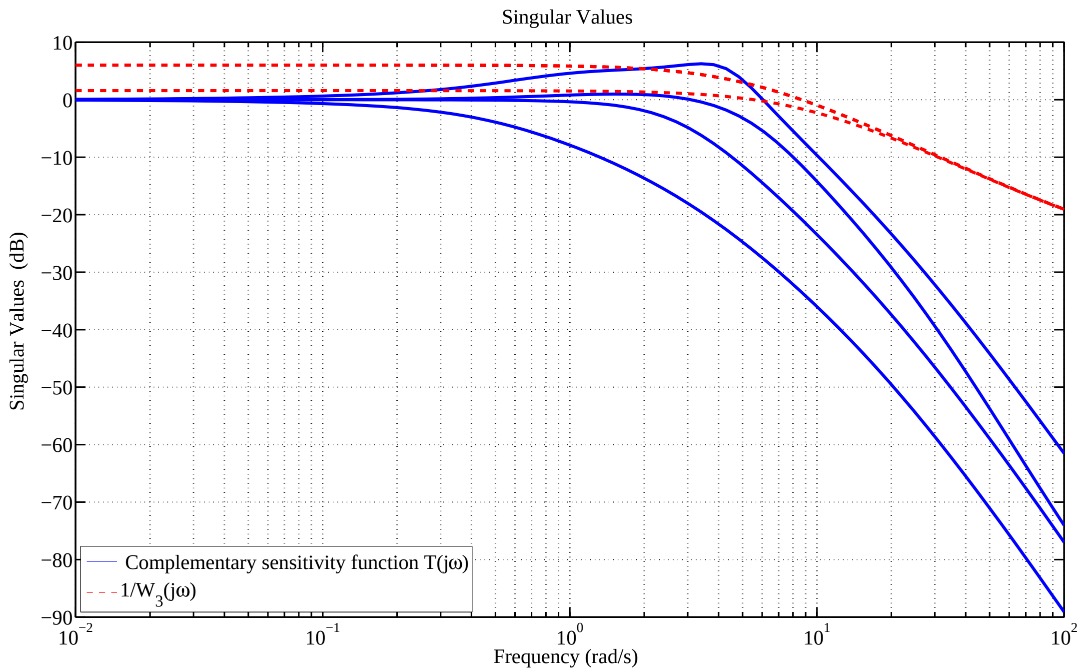

Figure 5.7: Singular value plots of the complementary sensitivity function and inverse of the stability weight with the *hinfstruct*.

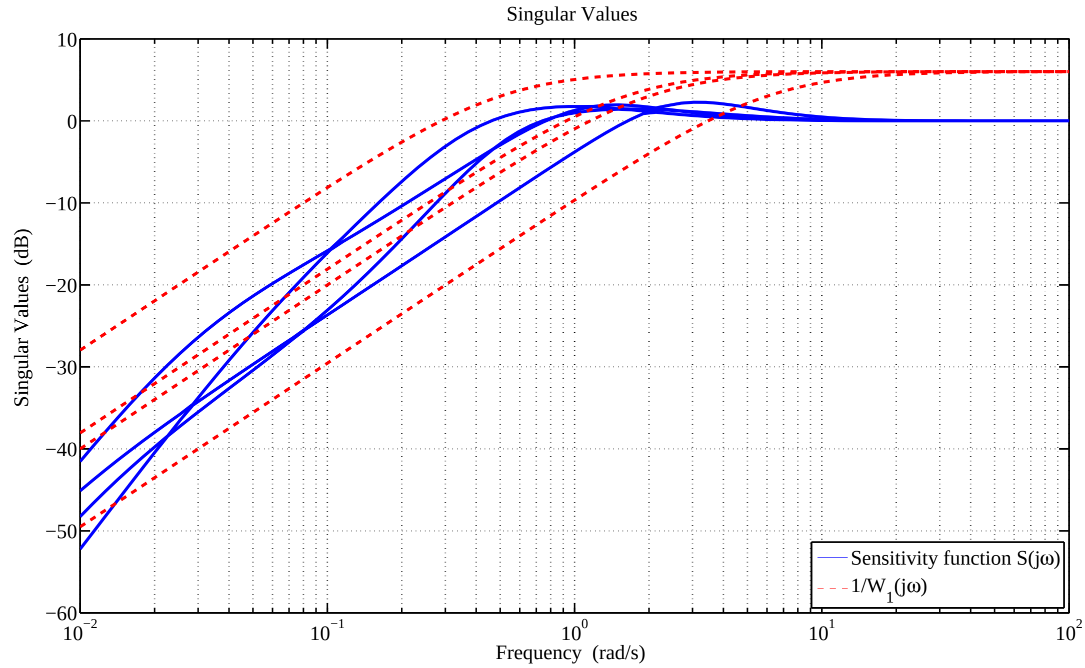

Figure 5.8: Singular value plots of the sensitivity function and inverse of the performance weight with the LMI.

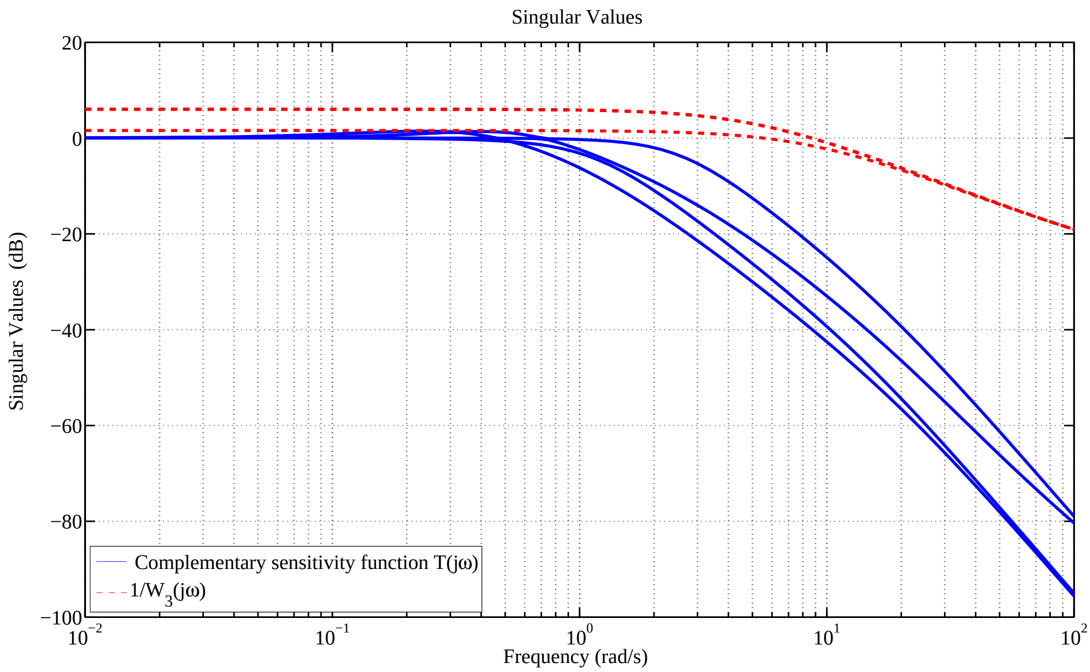

Figure 5.9: Singular value plots of the complementary sensitivity function and inverse of the stability weight with the LMI.

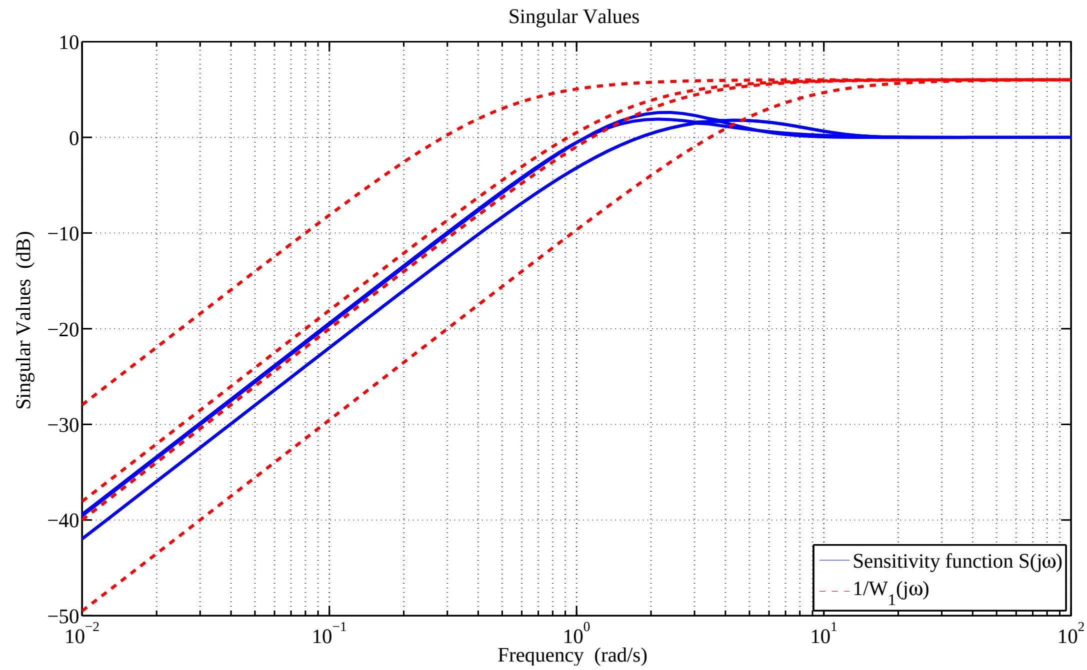

Figure 5.10: Singular value plots of the sensitivity function and inverse of the performance weight with the Glover-Doyle.

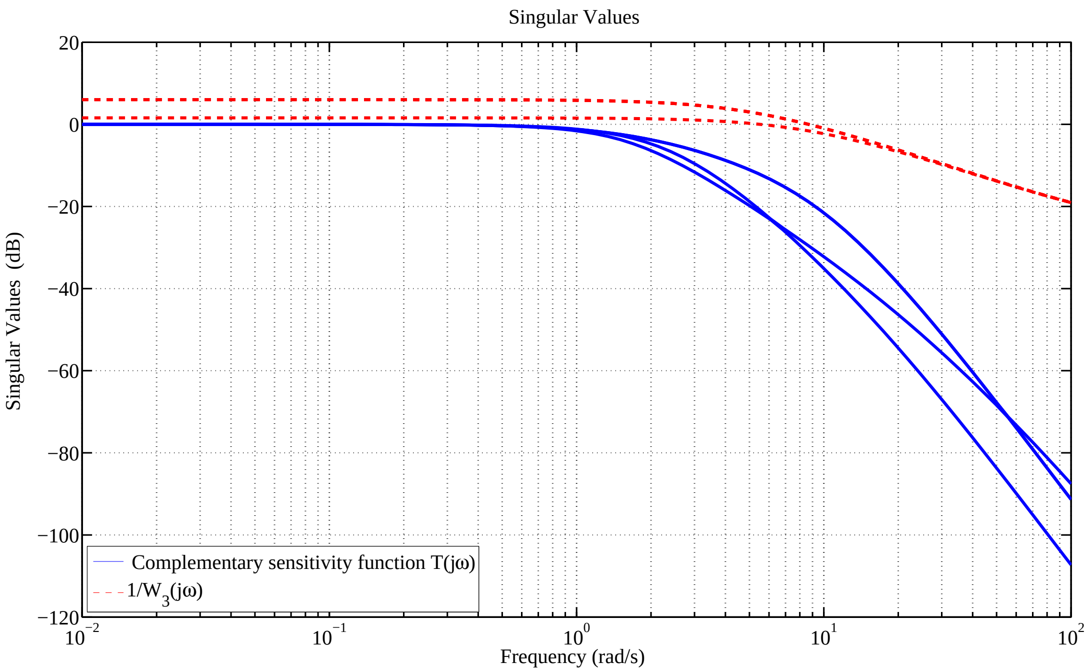

Figure 5.11: Singular value plots of the complementary sensitivity function and inverse of the stability weight with the Glover-Doyle.

5.5 Time Domain Simulation Results and Discussion

5.5.1 Time Domain Simulation Results

Linear and non-linear simulation models of the quadcopter have been developed in MATLAB/Simulink to evaluate the low- and full-order H_∞ controllers. White Guassian noise is added to outputs ($\phi,\ \theta,\ \psi,\ z_I$) for a realistic simulation. The noise power is chosen such that the signal to noise ratio is approximately 25 dB. Simulation results in Fig. 5.12 illustrate that the linear (green solid line) and non-linear (blue dashed line) models of the controlled quadcopter have similar responses. Fig. 5.12(a)-(d) (right) shows the forces corresponding to the attitude and altitude tracking for the non-linear model. Tracking with the *hifoo* controller in terms of roll and pitch have 34% and 50% overshoots respectively. Altitude and yaw have about 6 seconds settling times, whilst roll has a 10 second settling time, where the settling times are higher in the pitch response. Steady-state errors of Euler angles are 1%, 2% and 1%, respectively, and the vertical position has a 1% tracking error.

Closed-loop responses with the *hinfstruct* controller are shown in Fig. 5.13. Linear and non-linear models of the closed-loop system have similar responses. The roll, pitch, yaw angles and the altitude responses of the non-linear model have 2.5%, 1%, 3% and 1% steady-state errors, respectively. Roll and pitch responses in Fig. 5.13 have 24% and 23% overshoots, which are smaller than the overshoots in the responses with the *hifoo* controller. The yaw response has a 2% overshoot that is higher than the response with the *hifoo* controller. As a result, the *hinfstruct* controller seems to show a better performance than the *hifoo* controller. It can also be seen in Fig. 5.13 that the settling times for the roll and pitch are approximately 5 seconds, whilst altitude has a 2 second settling time.

Linear and non-linear model responses for the LMI controller are given in Fig. 5.14. Performance of this control approach is analysed as: roll, pitch and yaw responses have 15%, 17% and 2% overshoots, respectively. Roll and pitch angles settle over a longer time than 10 seconds with smaller steady-state errors than 2%. Furthermore, roll angle settles in 35 seconds, which is outside the desired control objective. Closed-loop responses for the Glover-Doyle controller are shown in Fig. 5.15. This full-order control approach provides good tracking performance. Attitude responses with the full order controller settle in 5 seconds. Both yaw angle and vertical position have 2% steady-state errors, which are higher than the steady-state errors for the roll and pitch orientations. By comparing simulation results in Figs. 5.12, 5.13, 5.14 and 5.15, it can be observed that *hinfstruct* the controller outperforms other controllers in terms of simplicity of implementation and tracking performance.

5.5.2 Discussion

The results of the simulations confirm that the structured H_∞ optimisation implemented in *hinfstruct* is an effective design approach. The low-order H_∞ controller achieves a performance close to the performance of a full-order controller if the same weight functions are used. Due to the sensitivity of the *hifoo* algorithm to weight selection, (i.e., the *hifoo* algorithm can not compute a controller with any weight selection), we first had to use this algorithm to design a fixed-order H_∞ controller using a trail-and-error approach to selecting weight functions; the selections of these weights are time consuming with the *hifoo* algorithm. Some performance criteria such as overshoot and steady-state error are still sacrificed while synthesising a controller with the *hifoo* algorithm. This has resulted in the selection of weights that do not provide the best performance when used by the other algorithms. With those weights, the *hinfstruct* and the Glover-Doyle controllers provide better performance than the LMI controller. Furthermore, the algorithms, apart from the *hifoo* algorithm, could compute controllers within reasonable computational times, as given in Table 5.3.

The LMI-based function can reduce the order of the controller if the norms of the R and S matrices are reduced. This function is not able to reduce the controller order to the same extent as the non-smooth algorithms do. The LMI approach reduces the order of the controller to the eighth order, but this reduction has increasingly deteriorated the performance of the closed-loop system. Therefore, the best-performing eleventh order controller computed by the LMI algorithm has the longest settling time for the roll and pitch orientations. The Glover-Doyle algorithm computed a controller with the best performance value, γ whilst the worst performance index was obtained by the *hifoo* algorithm. In terms of the response of the output sensitivity functions, the Glover-Doyle and LMI-based controllers show less waterbed effect; that is, making sensitivity functions smaller over a range frequencies slightly increases sensitivity somewhere.

In the case of the same input penalizing weights $W_2(s)$, the *hinfstruct* and the *hifoo* algorithms produced high control outputs to enable the quadcopter to reach desired height

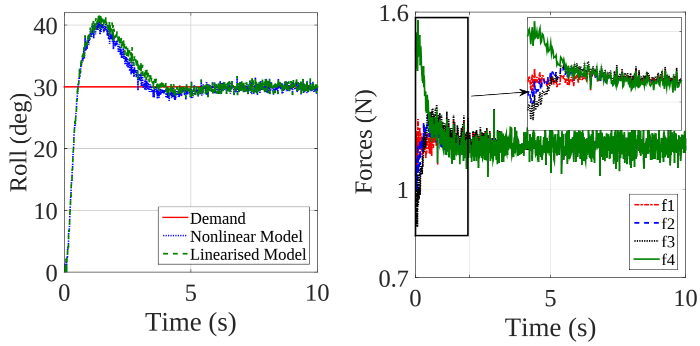

(a) Roll angle and corresponding motor forces.

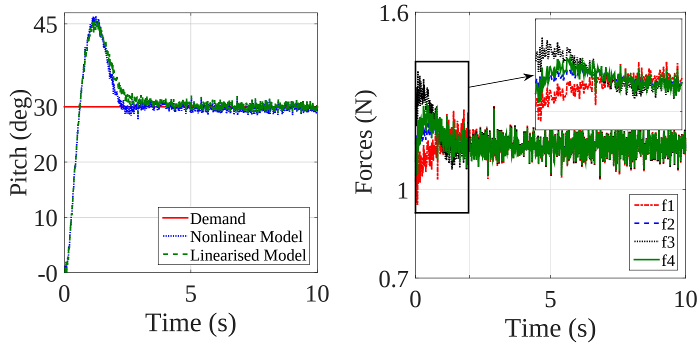

(b) Pitch angle and corresponding motor forces.

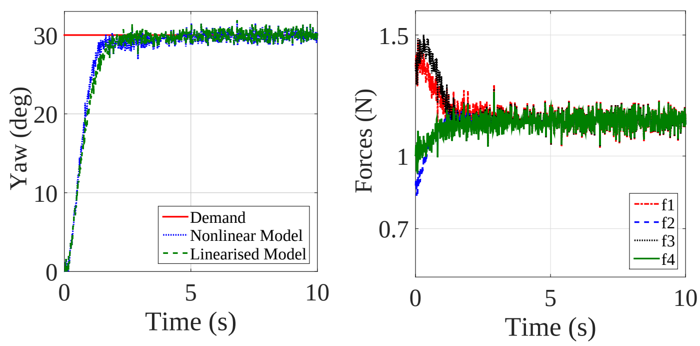

(c) Yaw angle and corresponding motor forces.

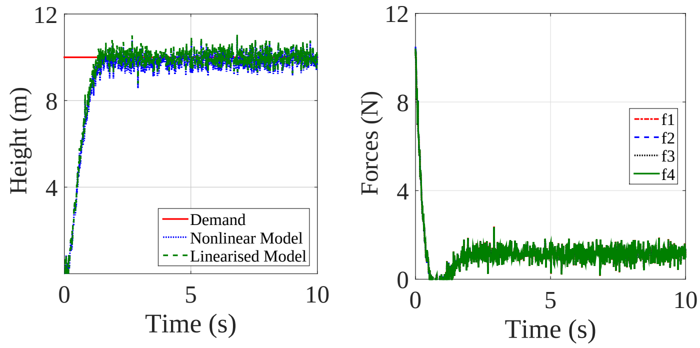

(d) Height position and corresponding motor forces.

Figure 5.12: Closed-loop step responses obtained with the *hifoo* controller and rotor forces with the non-linear model.

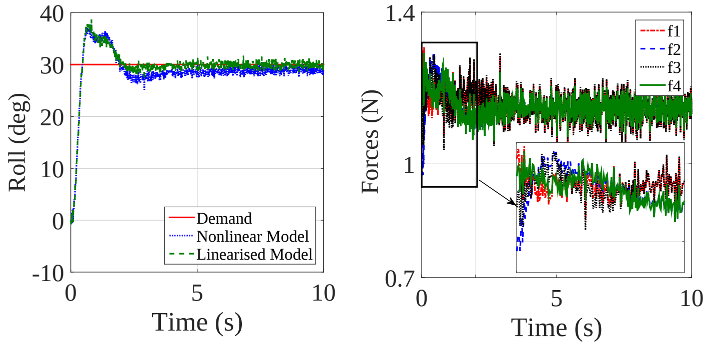

(a) Roll angle and corresponding motor forces.

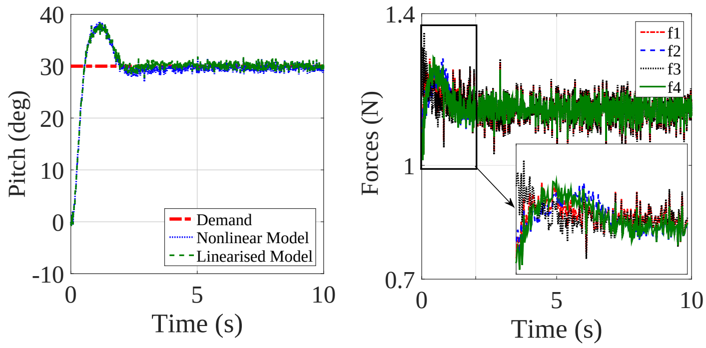

(b) Pitch angle and corresponding motor forces.

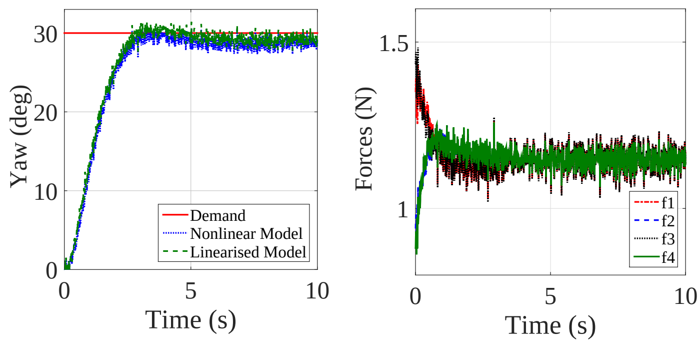

(c) Yaw angle and corresponding motor forces.

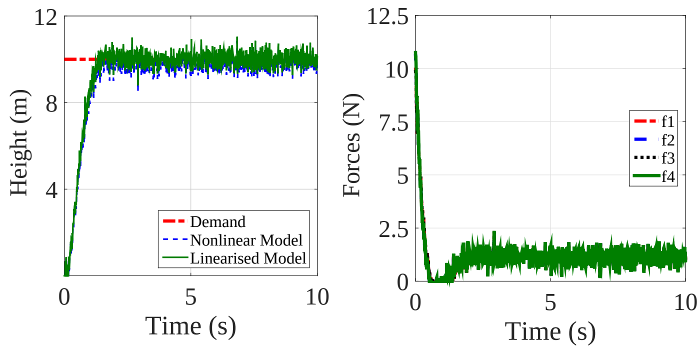

(d) Height position and corresponding motor forces.

Figure 5.13: Closed-loop step responses obtained with the *hinfstruct* controller and rotor forces with the non-linear model.

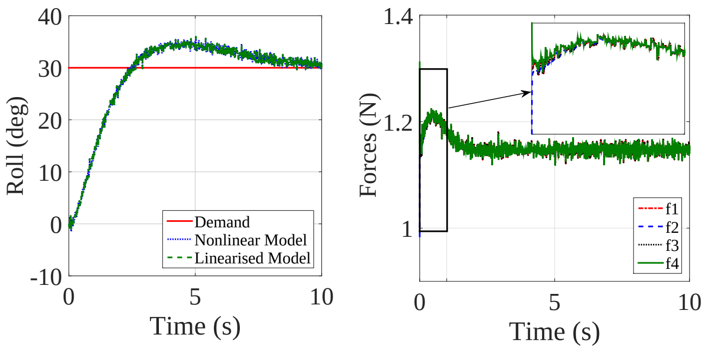

(a) Roll angle and corresponding motor forces.

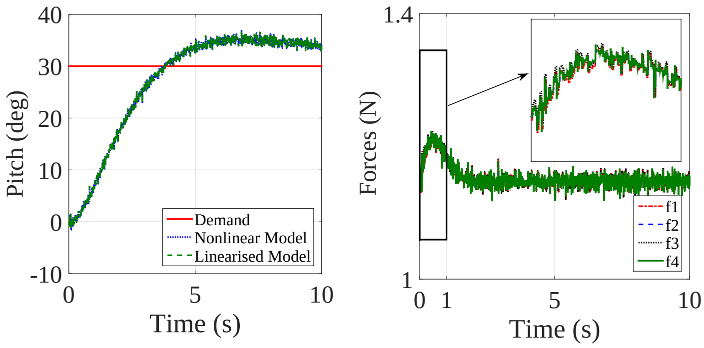

(b) Pitch angle and corresponding motor forces.

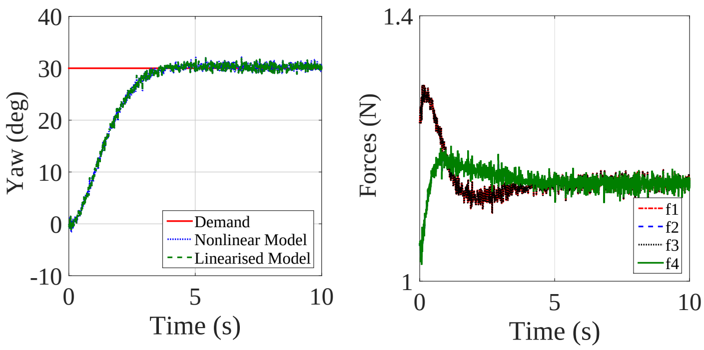

(c) Yaw angle and corresponding motor forces.

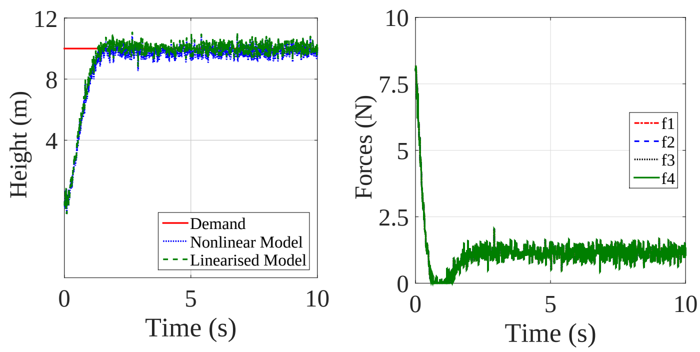

(d) Height position and corresponding motor forces.

Figure 5.14: Closed-loop step responses obtained with the LMI controller and rotor forces with the non-linear model.

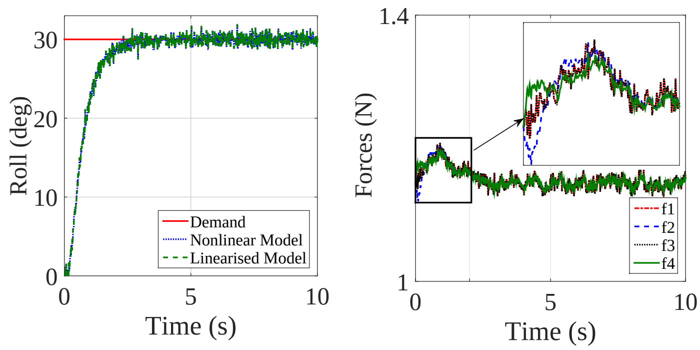

(a) Roll angle and corresponding motor forces.

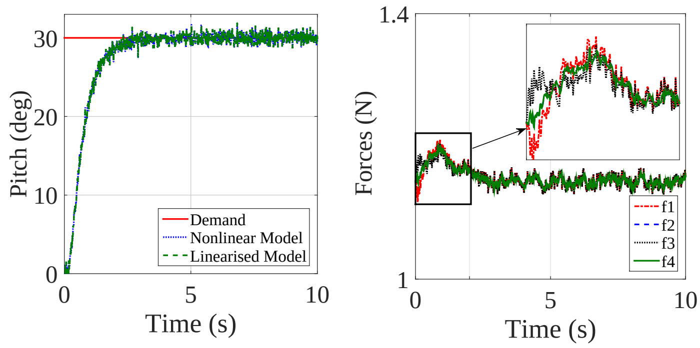

(b) Pitch angle and corresponding motor forces.

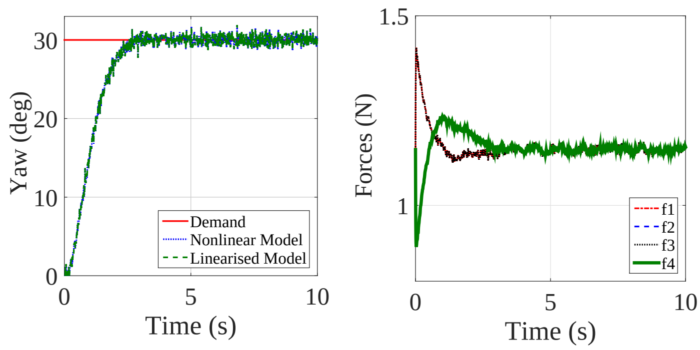

(c) Yaw angle and corresponding motor forces.

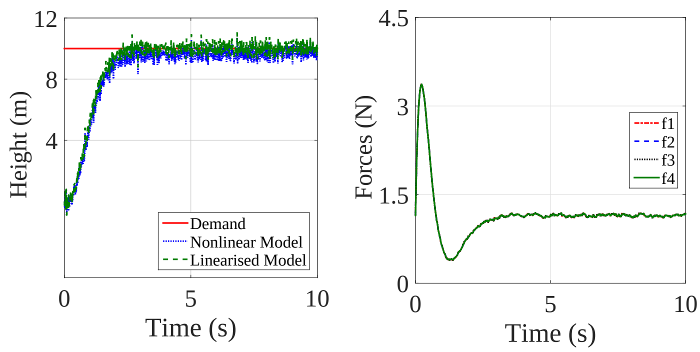

(d) Height position and corresponding motor forces.

Figure 5.15: Closed-loop step responses obtained with the Glover-Doyle controller and rotor forces with the non-linear model.

position. It was observed that the Glover-Doyle controller produced less control outputs. However, it is necessary to select a new penalising control input weight for the *hinfstruct*, the *hifoo* and the LMI algorithms. The sensitivity of the initial weight selection and computation time are important restrictions in the design of more than one local controller. Hence, the *hinfstruct* algorithm is a good choice for the design of local controllers for a switched control system.

5.6 Conclusions

This chapter has investigated four different H_∞ control synthesis algorithms: (i) fixed-order H_∞ optimisation; (ii) structured H_∞ optimisation; (iii) linear matrix inequities approach to H_∞ control; and (iv) mixed sensitivity H_∞ optimisation. The comparison of the above four algorithms has been undertaken in terms of performance and computational efficiency. The simulation results illustrated that the H_∞ controller approaches have achieved satisfactory performances. The *hinfstruct* and the *hifoo* controllers produced high control forces when the quadcopter tracks the desired height position. However, the *hifoo* controller has proven to be slightly worse in terms of its performance compared to the others. The sensitivity of the *hifoo* algorithm to initial weight selection and the long computational time associated with this algorithm are not desirable properties in practice. Hence, *hinfstruct* seems to be a better alternative to design low-order robust controllers.

The next chapter will use the *hinfstruct* algorithm because of its insensitivity to initial weight selection and computational efficiency. The control structure shown in this chapter will be modified to achieve full autonomous flight. For this reason, a double-loop control structure will be proposed. The inner loop will stabilise the attitude of the quadcopter. In addition, the inner loop will be switched between controllers corresponding to healthy and a faulty modes of operational conditions to enhance the reliability of the quadcopter in the instance of severe actuator faults. The outer loop will regulate the desired transitional velocities in the x, y and z axes.

CHAPTER 6

SWITCHING RECOVERY CONTROL SCHEMES IN THE CASE OF INTERMITTENT FAULTS

6.1 Introduction

This chapter develops new switched recovery schemes to improve system reliability and performance of a quadcopter UAV under conditions of intermittent loss of control (ILOC) and intermittent loss of motor (ILOM). Aircraft accident analysis in [15] has shown that loss of control is one of the common causes of accidents across all vehicle classes. Quadcopter UAVs might experience motor problems such as a loss of control or rotor faults due to their extended missions. As previously mentioned in Chapter 2, an intermittent fault is a time-dependent fault. This fault is active only over a certain period of time, which might cause a system malfunction, or may be inactive over another other period time that does not have any effect, and so allows the system to continue to operate normally (discontinuity in delivered action). Intermittent faults are not easily found and are not necessarily repeatable during tests of operational capability. Therefore, faults of this nature will clearly raise many concerns in aerospace systems [125, 148]. As given in the literature review section in Chapter 2, a number of approaches have been proposed regarding the reliability and the safety of a vehicle on the occurrence of different faults without considering either intermittent fault effects or stability of the system. This chapter deals with the relatively new problem of intermittent faults, which can be seen as the switch between a faulty and a fault-free quadcopter system. Characterising control effects in abnormal conditions enhances the ability of quadcopters to operate under intermittent rotor faults. It is assumed that integrated onboard systems can evaluate vehicle health and flight safety in real-time and provide any necessary information to the effective recovery scheme with only a small delay.

This chapter is organised as follows: Section 6.2 describes the problems of intermittent loss of control and loss of motor. Section 6.3 presents control structures and controller designs. Here, fixed-order H_∞ controllers corresponding to the healthy and the fault modes are designed. A switching control scheme is proposed to ensure that the desired translational velocity tracking is preserved when intermittent faults occur. Section 6.4 analyses the stability of the corresponding switched loop between the two modes of operation. Here, stability analysis uses dwell-time theory and the concept of average dwell-time based on multiple Lyapunov functions. These guarantee stability even if a time delay exists in the detection of the faults. Section 6.5 proposes a controller state initialisation method to reduce control discontinuity due to the switching between controllers. Time domain simulation results are given in Section 6.6. Finally, Section 6.7 gives some concluding remarks to the chapter.

6.2 Problem Description

This section states two different problems, namely intermittent loss of control and loss of motor, that might be experienced by quadcopter vehicles.

6.2.1 Case A: Problem of an Intermittent Loss of Control (ILOC) Effectiveness

This subsection will consider the loss of control problem that arises across all classes of aircraft systems. Once the quadcopter vehicle completely loses the control signal for motor M_i, then the vehicle has a constant input imposed that cannot be manipulated by the control systems. This fault can be generated in motors by multiplying its control inputs by a gain smaller than one, simulating a loss in control effectiveness. Now, linear models corresponding to quadcopter systems in different operational modes are presented as follows below. The non-linear dynamics of the vehicle can be written in a state-space form as

$$\begin{aligned} \dot{x}(t) = & \quad f(x(t), u(t)) \\ y(t) = & \quad h(x(t)) \end{aligned} \tag{6.1}$$

with state vector

$$x = [\phi \quad \theta \quad \psi \quad p \quad q \quad r \quad \dot{x}_I \quad \dot{y}_I \quad \dot{z}_I]' \tag{6.2}$$

and input vector

$$u = [f_1 \quad f_2 \quad f_3 \quad f_4]'. \tag{6.3}$$

The quadcopter model is separated into rotational and the translational dynamics to allow for the design of a nested control loop scheme. The system equations are linearised at hover ($\bar{x}_{1,eq} = 0$), for which the input is

$$u_{eq} = \frac{mg}{4}[1 \quad 1 \quad 1 \quad 1]'. \tag{6.4}$$

The rotational linear model of the quadcopter is given by

$$\begin{aligned} \dot{\bar{x}}_1 = & \quad A_{g_1}\bar{x}_1 + B_{g_1}\delta u \\ y = & \quad C\bar{x}_1 = [\phi \quad \theta \quad \psi]' \end{aligned} \tag{6.5}$$

where $\bar{x}_1 = [\phi \quad \theta \quad \psi \quad p \quad q \quad r]'$ is the attitude state vector.

When the quadcopter experiences a loss of control authority then the linear model becomes

$$\begin{aligned} \dot{\bar{x}}_1 = & \quad A_{g_2}\bar{x}_1 + B_{g_2}\delta u \\ y = & \quad C\bar{x}_1 \end{aligned} \tag{6.6}$$

where

$$A_{g_1} = A_{g_2} \quad = \quad \begin{bmatrix} 0 & 0 & 0 & 1 & 0 & 0 \\ 0 & 0 & 0 & 0 & 1 & 0 \\ 0 & 0 & 0 & 0 & 0 & 1 \\ 0 & 0 & 0 & -\frac{k_r}{I_{xx}} & 0 & 0 \\ 0 & 0 & 0 & 0 & -\frac{k_r}{I_{yy}} & 0 \\ 0 & 0 & 0 & 0 & 0 & -\frac{k_r}{I_{zz}} \end{bmatrix}$$

$$B_{g_1} = \begin{bmatrix} 0 & 0 & 0 & 0 \\ 0 & 0 & 0 & 0 \\ 0 & 0 & 0 & 0 \\ 0 & -\frac{L}{I_{xx}} & 0 & \frac{L}{I_{xx}} \\ -\frac{L}{I_{yy}} & 0 & \frac{L}{I_{yy}} & 0 \\ \frac{d}{I_{zz}} & -\frac{d}{I_{zz}} & \frac{d}{I_{zz}} & -\frac{d}{I_{zz}} \end{bmatrix}, \tag{6.7}$$

and where $B_{g_2} = B_{g_1}\lambda_f$, $\lambda_f = diag(k_1, ..., k_i)$, $i = 1, ..., 4$, $0 \leq k_i \leq 1$ and k_i give the percentage of loss of control effectiveness for the i^{th} motor. If $k_i = 0$, the speed of i^{th} rotor is no longer controllable, as given in [4], and in our case, $k_i = 0$ will be considered in the sense of discrete intervals.

6.2.2 Case B: Problem of an Intermittent Loss of Motor (ILOM)

In this subsection, the problem of intermittent switching between faulty and healthy quadcopter systems is considered. The term *faulty quadcopter* is used to refer to the quadcopter system in the presence of rotor failure, whereas *healthy quadcopter* refers to the vehicle under proper operational capability. Turning off a motor, as well as turning on a motor, will lead to instability of the vehicle at hover. In other words, the intermittent fault contributes to stability degradation during discrete intervals. When the quadcopter experiences a rotor failure (e.g. M_3), only two opposite motors will produce equal thrust to compensate for the quadcopter weight. This new equilibrium differs from that of the healthy case. If one removes M_3, then the system is nominally no longer controllable; however, controllability can be preserved if the vehicle is allowed to rotate around the vertical axis near the new equilibrium with a rate $r_{eq} = -\frac{mgd}{k_r}$.

The classical controllability tests are not sufficient to verify the controllability of the vehicle when experiencing rotor failure (because lifting forces are constrained to be positive). Discarding the rotational axis of attitude dynamics, a reduced attitude expression can be described and then the controllability of the faulty model quadcopter can be deduced [102].

Now, let us compute the corresponding linearised models for the quadcopter vehicle. Note that the heading angle, ψ, is no longer controllable in the case of loss of one motor, and hence the rotational dynamics of the linearised healthy quadcopter model at hover

($\bar{x}_{2eq} = 0$ and u_{eq}) are given by:

$$\begin{aligned} \dot{\bar{x}}_2 = &\quad A_{g_1}\bar{x}_2 + B_{g_1}\delta u \\ y = &\quad C_g\bar{x}_2 = [\phi \;\; \theta \;\; r]' \end{aligned} \tag{6.8}$$

where the attitude state vector, $\bar{x}_2 = [\phi \;\; \theta \;\; p \;\; q \;\; r]'$ and matrices are

$$A_{g_1} = \begin{bmatrix} 0 & 0 & 1 & 0 & 0 \\ 0 & 0 & 0 & 1 & 0 \\ 0 & 0 & -\frac{k_r}{I_{xx}} & 0 & 0 \\ 0 & 0 & 0 & -\frac{k_r}{I_{yy}} & 0 \\ 0 & 0 & 0 & 0 & -\frac{k_r}{I_{zz}} \end{bmatrix}$$

$$B_{g_1} = \begin{bmatrix} 0 & 0 & 0 & 0 \\ 0 & 0 & 0 & 0 \\ 0 & -\frac{L}{I_{xx}} & 0 & \frac{L}{I_{xx}} \\ -\frac{L}{I_{yy}} & 0 & \frac{L}{I_{yy}} & 0 \\ \frac{d}{I_{zz}} & -\frac{d}{I_{zz}} & \frac{d}{I_{zz}} & -\frac{d}{I_{zz}} \end{bmatrix}, \tag{6.9}$$

such that stability analysis can be conducted without losing the closed-loop structure. Control of ψ in the healthy case can be achieved through controlling the yaw rate.

For the faulty case, the linear system approximation corresponding to rotational dynamics about $\bar{x}_{2eq} = [0 \;\; 0 \;\; 0 \;\; 0 \;\; r_{eq}]$ and $u_{eq} = 0$ is given by

$$\begin{aligned} \dot{\bar{x}}_2 = &\quad A_{g_2}\bar{x}_2 + B_{g_2}\delta u \\ y = &\quad C_g\bar{x}_2 \end{aligned} \tag{6.10}$$

where A_{g_2} and B_{g_2} are

$$A_{g_2} = \begin{bmatrix} 0 & r_{eq} & 1 & 0 & 0 \\ -r_{eq} & 0 & 0 & 1 & 0 \\ 0 & 0 & -\frac{k_r}{I_{xx}} & -r_{eq}\frac{(I_{zz}-I_{yy})}{I_{xx}} & 0 \\ 0 & 0 & -r_{eq}\frac{(I_{xx}-I_{zz})}{I_{yy}} & -\frac{k_r}{I_{yy}} & 0 \\ 0 & 0 & 0 & 0 & -\frac{k_r}{I_{zz}} \end{bmatrix},$$

$$B_{g_2} = \begin{bmatrix} 0 & 0 & 0 & 0 \\ 0 & 0 & 0 & 0 \\ 0 & -\frac{L}{I_{xx}} & 0 & \frac{L}{I_{xx}} \\ -\frac{L}{I_{yy}} & 0 & 0 & 0 \\ \frac{d}{I_{zz}} & -\frac{d}{I_{zz}} & 0 & -\frac{d}{I_{zz}} \end{bmatrix}. \tag{6.11}$$

6.2.3 Linear Model of Translational Dynamics

The translational dynamics of the quadcopter (Eqs.4.42-4.44) depend on the Euler angles. The dependence of the translational components can be eliminated by defining the virtual inputs ($\hat{u}_x$, $\hat{u}_y$, $\hat{u}_z$) [18] as:

$$\hat{u}_x = u_f\left(\cos(\phi)\cos(\psi)\sin(\theta) + \sin(\phi)\sin(\psi)\right) \tag{6.12}$$

$$\hat{u}_y = u_f(\cos(\phi)\sin(\theta)\sin(\psi) - \cos(\psi)\sin(\phi)) \tag{6.13}$$

$$\hat{u}_z = u_f\cos(\theta)\cos(\phi) - mg \tag{6.14}$$

then the corresponding translational dynamic becomes

$$\dot{x}_{trans} = A_t x_{trans} + B_t \hat{u} \tag{6.15}$$

where

$$\begin{aligned} A_t &= \text{diag}[-k_t/m, -k_t/m, -k_t/m] \\ B_t &= \text{diag}[1/m, 1/m, 1/m] \end{aligned} \tag{6.16}$$

with the state vector $x_{trans} = [\dot{x}_I \quad \dot{y}_I \quad \dot{z}_I]'$, and input vector $\hat{u} = [\hat{u}_x \quad \hat{u}_y \quad \hat{u}_z]'$. A translational velocity controller will be designed for the linear system described in (6.15) in Section 6.3.3.

Next, we will describe designs of switching linear control laws for rotational dynamics under two different problems and a linear control law for translational dynamics.

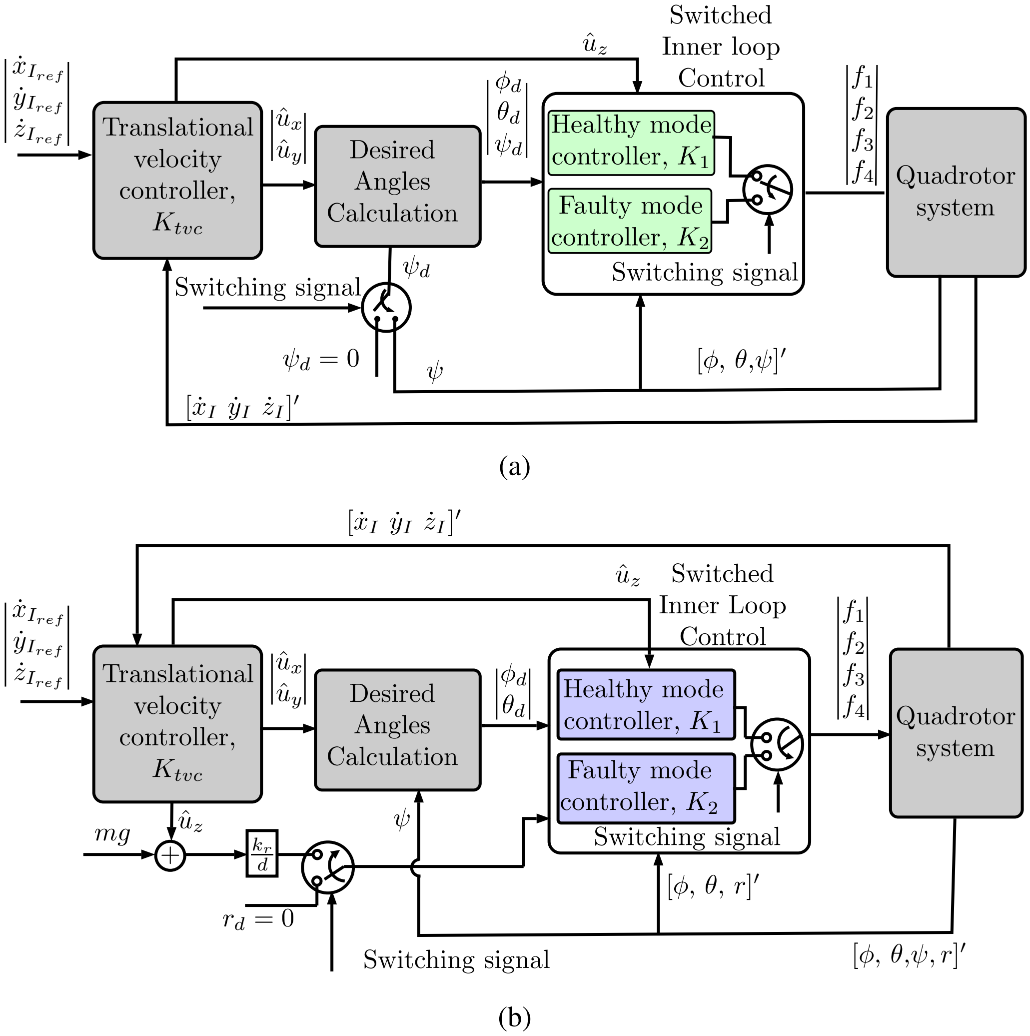

Figure 6.1: The double-loop control structure for translational tracking (a) in the case of ILOC, (b) in the case of ILOM.

6.3 Control Structures

Double-loop control structures have been implemented on real platforms by e.g., [20, 100, 102]. The rationale behind such double-loop schemes is that inner/ outer loop decoupling is practical because an inner loop stabilises a non-linear attitude, and translational velocity is regulated in an outer-loop. In this chapter, double-loop control architectures are developed as shown in Fig. 6.1. Here, event-based switching associated with the healthy and the faulty modes of operation are to be considered because of the introduction of a fault. The control structure shown in Fig. 6.1(a) is proposed to tackle the problem of ILOC. The switched inner-loop controller has the duty of stabilising the attitude angles controlling the coupled thrust forces. The outer-loop controller has the task to modify the desired roll and pitch angles to track the translational velocities. Here, the inner-loop controller is switched between healthy and faulty mode controllers based on the information from a FDD. On the other hand, the control structure shown in Fig. 6.1(b) is developed to overcome the problem of ILOM, where two inner-loop controllers and a translational velocity controller are also designed to achieve full stabilisation of the quadcopter. The main difference between the second control structure and the first is that the yaw angular speed is regulated instead of the yaw angle.

The control objective is to achieve a good tracking performance with a fast response time and a small steady state error for healthy and faulty flight modes of operation. The key control objective is to design a recovery scheme that enables the quadcopter to track given inertial velocities when experiencing intermittent loss of control or motor, ensuring stability in both healthy and faulty modes of operation. Inertial translational velocities with set points $\dot{x}_{I,ref}$, $\dot{y}_{I,ref}$ and $\dot{z}_{I,ref}$ are regulated by a translational velocity controller. Flowcharts in Figs. 6.2 and 6.3 show design procedures of the developed control structures exhibited in Fig. 6.1.

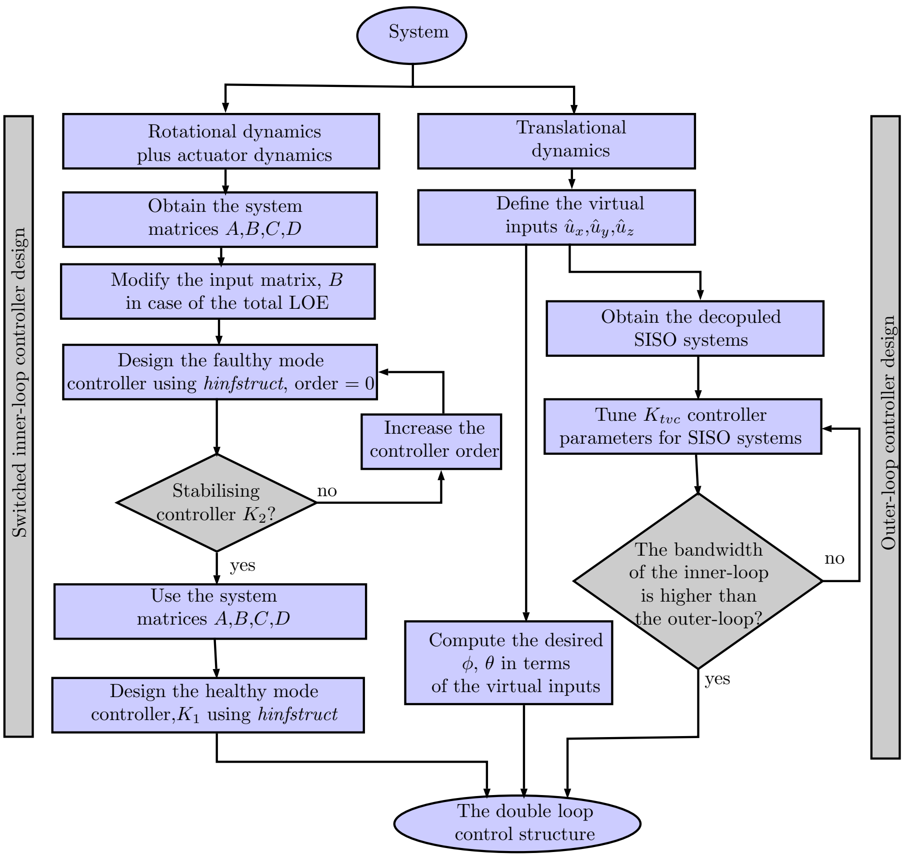

Figure 6.2: Flow diagram of the developed control structure of Fig. 6.1(a).

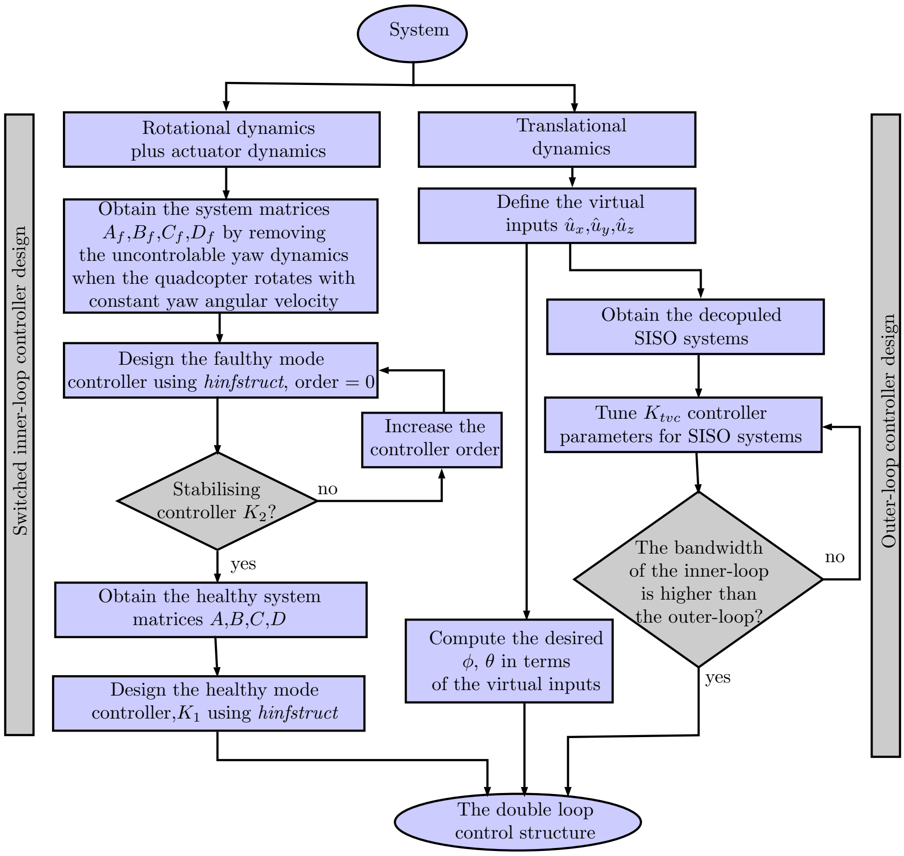

Figure 6.3: Flow diagram of the developed control structure of Fig. 6.1(b).

6.3.1 Switched Inner-loop Controller Designs

In this section, a pair of inner-loop controllers will be designed to address the problems of intermittent loss of control effectiveness and loss of motor, respectively. The controllers are computed using the procedure of the weight selection given in Section 5.2.1 of Chapter 5. Weighting functions are chosen to achieve robustness and performance objectives. Sensitivity and complementary sensitivity functions are used to reduce the effects of disturbance on the outputs and to attain robustness to modelling errors, respectively. A constant input penalty weight is chosen to limit the control effort. The controllers corresponding to the healthy and the faulty modes of operation are computed using *hinfstruct* [43, 45] to keep controller orders low (details of this algorithm has been given in Chapter 4) as follows:

Case A: Intermittent Loss of Control Effectiveness

For the problem of ILOC, the appropriate inner-loop control structure is illustrated in Fig. 6.4, where K_1 is the inner healthy controller for the plant (6.5) and K_2 is the inner faulty mode controller for the plant (6.6); ψ_d is switched between values of zero and measured value based on a fault-detection mechanism. The inner faulty mode controller will regulate only three control signals to achieve desired roll and pitch angles.

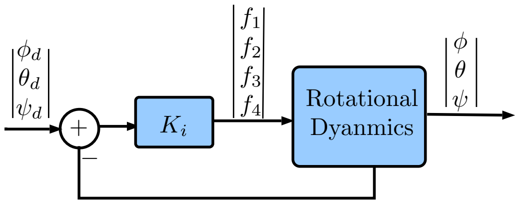

Figure 6.4: Inner-loop control structure in the case of ILOC, where $K_i \in \{K_1, K_2\}$.

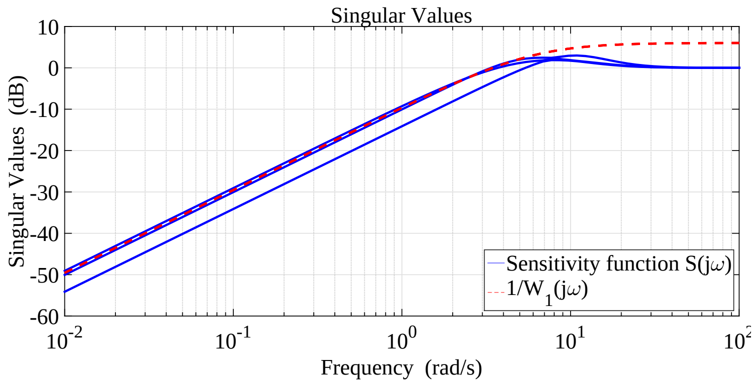

(a)

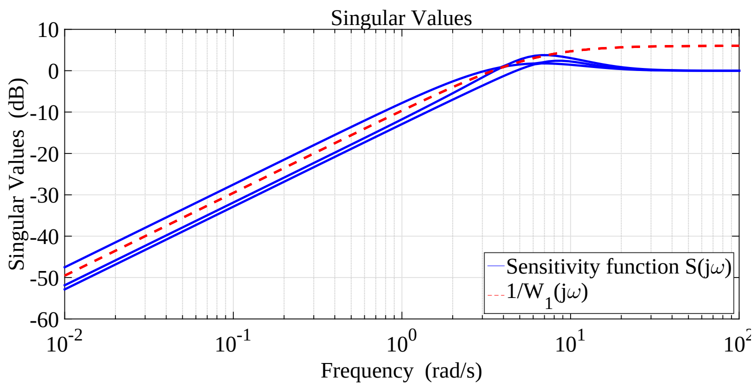

(b)

Figure 6.5: Singular value plots of the $S(j\omega)$ and inverse of the performance weight in the case of ILOC (a) for the healthy mode, and (b) for the faulty mode of operation.

With first-order weighting functions, the stabilising 4^{th} order healthy and fault mode inner-loop controllers have been designed. Closed-loop frequency responses for the healthy and the faulty plants are shown in Fig. 6.5(a)-(b). Analysing the frequency responses, the peak gains of the closed-loop sensitivity function are 2.96 dB at 11 rad/s and 3.76 dB at 6.7 rad/s for the healthy and faulty modes of operation, respectively. There is a considerable disturbance rejection over the low frequency range for both the healthy and faulty mode controllers. The disturbance is amplified between about 3.5 rad/s and 40 rad/s over the frequency range for the healthy and faulty modes of operation.

***Remark* 2:** It is assumed that an FDD exists and provides the required information for the switching recovery scheme. Several researchers have already proposed FDD schemes for actuator fault detection problems e.g., see [6, 24, 39, 128]. A model-based algorithm can be applied to the quadcopter to obtain an FDD scheme. The Luenberger state estimator is developed for estimating the outputs of actuators in the FDD scheme. The actuator dynamics are included in the linearised model of the quadcopter so as to estimate the outputs of actuators as the states of the system. The observer estimates the output of each actuator and the FDD scheme compares these outputs with the desired controller outputs. If the error between these two values is greater than a set threshold for a longer than some minimum time, the corresponding actuator is deemed to be faulty.

Case B: Intermittent Loss of Motor

For the ILOM problem, the inner-loop control structure is illustrated in Fig. 6.6, where K_1 is the inner healthy controller for the plant (6.8) and K_2 is the inner faulty mode controller for the plant (6.10); r_{ref} is switched between values of zero and $-(mg+\hat{u}_z)\frac{d}{k_r}$ based on a switching rule. First, we design the faulty mode controller whose task to

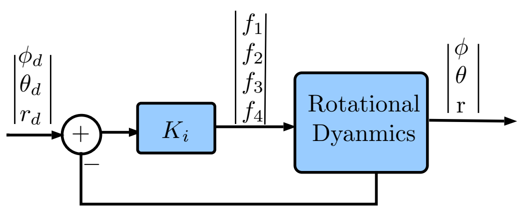

Figure 6.6: Inner-loop control structures (a) in the case of ILOC and (b) in the case of ILOM, where $K_i \in \{K_1, K_2\}$.

control roll and pitch angles and yaw angular velocity. The desired vertical velocity is obtained by modifying the yaw angular speed in the equilibrium neighbourhood. The healthy mode controller regulates the yaw angular velocity to maintain at 0 rad/s. In this case, the desired vertical velocity is achieved by entire forces f_i.

Similar to case A, with first-order weighting functions, the lowest-order-stabilising healthy and faulty mode inner-loop controllers obtained are of the 8^{th} order. Frequency responses are depicted in Fig. 6.7. The disturbance attenuation is more than 50 dB in the desired low frequency range for both cases. The disturbance is amplified between about 7 rad/s and 60 rad/s over the frequency range for the healthy mode of operation. The minimum closed-loop bandwidth is about 5 rad/s, which is sufficient to obtain a fast-tracking response during the faulty mode of operation. A faster time response for the yaw rate during the faulty mode of operation is anticipated.

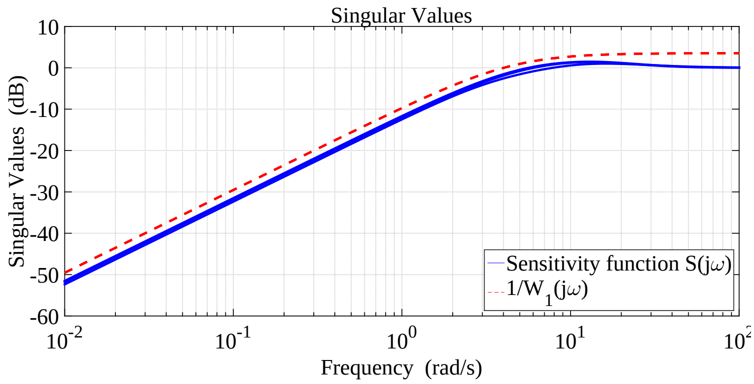

(a)

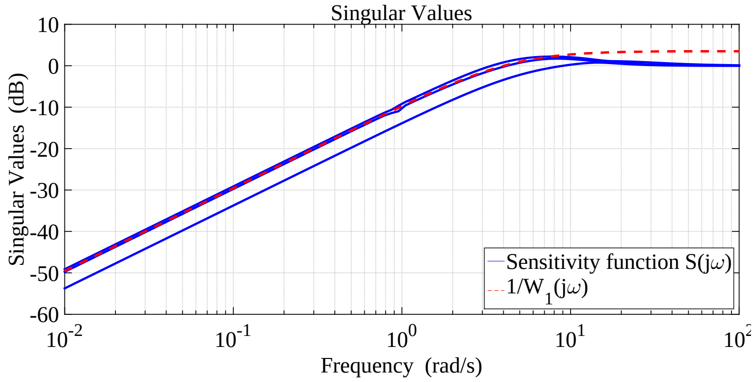

(b)

Figure 6.7: Singular value plots of the $S(j\omega)$ and inverse of the performance weight in the case of ILOM (a) for the healthy mode, (b) for the faulty mode of operation.

Remark 3: The switching rule might be state dependent for the loss of rotor problem. Assume that the effects of disturbance can be omitted. The yaw rate, r, of the quadcopter varies significantly between the two modes of operation. Consider the thresholds J_{th1},

J_{th2} and a small time delay t_d are given such that if $|r_m| > J_{th1}$ then the system is faulty or if $|r_m(t - t_d) - r_m| > J_{th2}$, then the system is healthy.

6.3.2 Desired Angles Calculation

The desired roll and pitch angles are computed in terms of the virtual control inputs. Expanding (6.12) and (6.13) and multiplying both sides by $\sin(\psi)$ and $\cos(\psi)$, respectively, sets up the term $\sin(\psi)\cos(\phi)\cos(\psi)\sin(\theta)$ to cancel

$$\frac{\hat{u}_x}{u_f}\sin(\psi) = \sin(\psi)\cos(\phi)\cos(\psi)\sin(\theta) + \sin(\phi)\sin^2(\psi) \tag{6.17}$$

$$\frac{\hat{u}_y}{u_f}\cos(\psi) = \cos(\psi)\cos(\phi)\sin(\theta)\sin(\psi) - \cos^2(\psi)\sin(\phi). \tag{6.18}$$

Subtracting (6.17) from (6.18) results in

$$\frac{\hat{u}_x}{u_f}\sin(\psi) - \frac{\hat{u}_y}{u_f}\cos(\psi) = \sin(\phi). \tag{6.19}$$

The upward lifting force can be found as $u_f = (\hat{u}_z + mg)/\cos(\phi)\cos(\theta)$ from (6.14). Substituting u_f in (6.19) yields

$$\frac{\cos(\theta)}{\hat{u}_z + mg}[\hat{u}_x\sin(\psi) - \hat{u}_y\cos(\psi)] = \tan(\phi). \tag{6.20}$$

The arctangent function is applied to both sides of (6.20), which yields the desired roll orientation as:

$$\phi_d = \arctan\left(\frac{\cos(\theta_d)}{\hat{u}_z + mg}[\hat{u}_x\sin(\psi) - \hat{u}_y\cos(\psi)]\right). \tag{6.21}$$

Following the similar procedure, the desired pitch orientation can be expressed as

$$\theta_d = \arctan\left(\frac{1}{\hat{u}_z + mg}(\hat{u}_x\cos(\psi) + \hat{u}_y sin(\psi))\right). \tag{6.22}$$

The periodic cyclic time-varying roll and pitch angles are evaluated based on (6.21) and (6.22), when the quadcopter spins around yaw axis due to rotor faults. The roll and pitch set points must be periodically generated by the outer loop controller to enable the quadrotor to reach the desired translational velocities. This is achievable if the measurement of yaw angle is provided [82].

6.3.3 Translational Velocity Controller

To design a translational velocity controller, the translational dynamics are considered to be an independent subsystem forced by x-, y- and z-axis components of the lifting thrust vector (i.e., $\hat{u}_x$, $\hat{u}_y$, $\hat{u}_z$). In Figs. 6.1(a)-(b), the outer-loop controller K_{tvc} is a standard controller gain (i.e., PI control gain). The PI controller parameters are chosen so that the outer closed-loop transfer function has a bandwidth sufficiently smaller than the bandwidth of inner-loop subsystem. The singular value frequency response plot of the closed-loop translational subsystem is shown in Fig. 6.8.

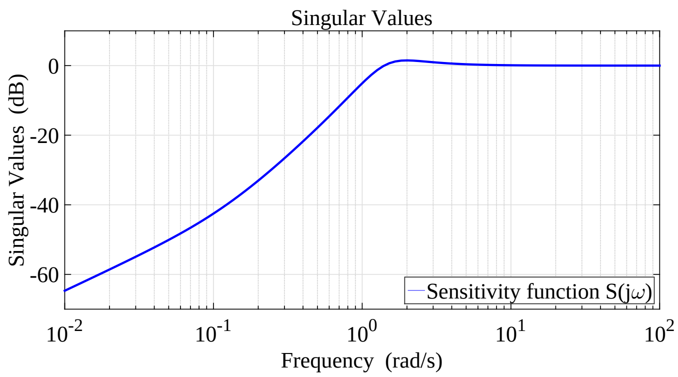

Figure 6.8: Singular value plot of the $S(j\omega)$ for the closed-loop outer subsystem

The translational velocity controller produces virtual inputs involving the calculation of the desired ϕ and θ orientations for the inner-loop controllers. The desired velocities $\dot{x}_I$ and $\dot{y}_I$ are then achieved by changing the pitch and roll angles. The vertical velocity demand will result in an increasing/ deceasing yaw angular velocity about the steady state, $-\frac{mgd}{k_r}$.

6.4 Stability Analysis of Switched Systems

In this section, our main concern is the stability of the inner loop under event-based switching. Each closed-loop system is locally stable over a particular range of operating conditions. As discussed in Schinkel et al.[123], unstable trajectories can occur by switching between stable systems. Therefore, the stability of the vehicle transitioning from a nominal to a faulty operation mode must be preserved. Now let us consider the output feedback configuration depicted in Fig. 6.9.

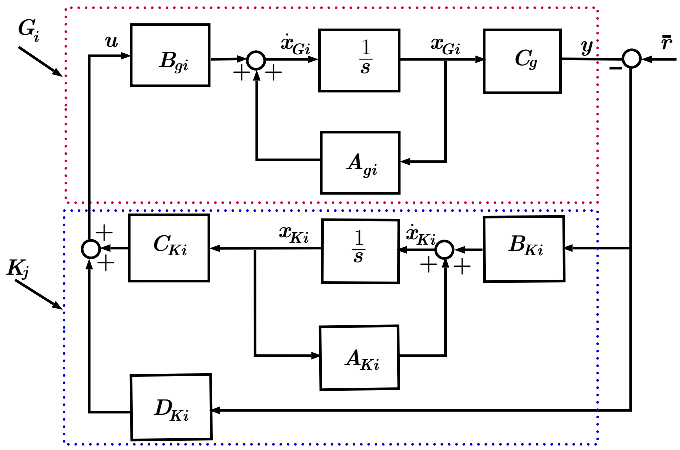

Figure 6.9: A state-space realisation of the closed-loop system.

In Fig. 6.9, the open loop plant is denoted by G_i and controllers by K_j with the state-space realisations:

$$G_i = \left[\begin{array}{c|c} A_{g_i} & B_{g_i} \\ \hline C_g & 0 \end{array}\right], \quad K_j = \left[\begin{array}{c|c} A_{Kj} & B_{Kj} \\ \hline C_{Kj} & D_{Kj} \end{array}\right]. \tag{6.23}$$

Denote that plant G_i has a state x_{G_i} and controller K_j has a state x_{K_j}, then the closed-loop state-space equations can be written as

$$\begin{bmatrix} \dot{x}_{G_i} \\ \dot{x}_{K_j} \end{bmatrix} = \underbrace{\begin{bmatrix} A_{gi} - B_{gi}D_{Kj}C_g & B_{gi}C_{Kj} \\ -B_{Kj}C_g & A_{Kj} \end{bmatrix}}_{\bar{A}_{i,j}} \underbrace{\begin{bmatrix} x_{G_i} \\ x_{K_j} \end{bmatrix}}_{x_{cl}} + \begin{bmatrix} BD_{Kj} \\ B_{Kj} \end{bmatrix} \bar{r} \tag{6.24}$$

$$\begin{bmatrix} u \\ y \end{bmatrix} = \begin{bmatrix} -D_{KjC_g} & C_{Kj} \\ C_g & 0 \end{bmatrix} \begin{bmatrix} x_{G_i} \\ x_{K_j} \end{bmatrix} + \begin{bmatrix} D_{Kj} \\ 0 \end{bmatrix} \bar{r} \tag{6.25}$$

where $\bar{A}_{i,j}$ is the evolution matrix of the closed-loop system. The following two sections use this result to prove the stability of the system under switching.

6.4.1 Dwell-time

As previously explained in Chapter 3, it is possible to ensure the stability of a switched system on the condition that switching is sufficiently slow. That is to say, a time T_d is determined such that if the system dwells at each stabilising controller for at least time T_d, then stability is guaranteed. This approach is referred to as minimum dwell-time stability theory. When the plant and controller are switched together, the closed-loop dynamics can be written as:

$$\dot{x}_{cl}(t) = \bar{A}_{\sigma(t)} x_{cl}(t) \quad \forall t \geqslant 0, \;\; i = 1, \ldots, N \tag{6.26}$$

where $\sigma(t)$ is the switching rule. $\bar{A}_{\sigma(t)}$ belongs to the set of closed-loop matrices $\bar{A}_i := \bar{A}_{i,i}$ (when $i = j$ in (6.24)), $i = 1, \ldots, N$, which are assumed to be stable.

Theorem* 6.4.1** ([49]):*** If there exist positive definite matrices $\{S_1, ..., S_N\}$ of compatible dimensions such that for a given scalar $T_d > 0$, the following conditions hold:

$$A_i' S_i + S_i A_i < 0 \quad \forall i = 1, ..., N \tag{6.27}$$

$$e^{A_i' T_d} S_j e^{A_i T_d} - S_i < 0 \quad \forall i \neq j = 1, ..., N, \tag{6.28}$$

then the system (6.26) is globally asymptotically stable for a dwell-time greater than or equal to T_d.

For completeness, the proof of Theorem 6.4.1 is also given as follows.

Proof. Consider the switching rule that $\sigma(t) = i \in \{1, ..., N\}$ for all $t \in [t_k, t_{k+1})$, where $t_{k+1} = t_k + T_{dk}$ with $T_{dk} \geq T_d > 0$ and that at $t = t_{k+1}$ the time switching control jumps to $\sigma(t) = j \in [t_k, t_{k+1})$. One can see from (6.27) that for all $t \in [t_k, t_{k+1})$, the time derivative of the Lyapunov function $V(x(t)) = x(t)' S_{\sigma(t)} x(t)$ along an arbitrary trajectory of (6.26) satisfies

$$\dot{V}(t) = x(t)'(A_i' S_i + S_i A_i) x(t) < 0 \tag{6.29}$$

from which one can deduce that there exists scalars $\alpha > 0$ and $\beta > 0$ such that

$$\| \, x(t) \, \|^2 \leq \beta e^{-\alpha(t - t_k)} V(x(t_k)) \quad \forall t \in [t_k, t_{k+1}). \tag{6.30}$$

On the other side, using the inequalities (6.28), one can obtain

$$\begin{aligned}
\dot{V}(t) &= x(t_{k+1})'S_j x(t_{k+1}) && (6.31)\\
&= x(t_k)'e^{A_i'T_{dk}}S_j e^{A_iT_{dk}}x(t_k) && (6.32)\\
&< x(t_k)'e^{A_i'(T_{dk}-T_d)}S_i e^{A_i(T_{dk}-T_d)}x(t_k) && (6.33)\\
&< x(t_k)'S_i x(t_k) && (6.34)\\
&< V(x(t_k)) && (6.35)
\end{aligned}$$

in which the second inequality is satisfied from the fact that for any $\tau = T_{dk} - T_d \geq 0$ it is true that $e^{A_i'\tau}S_i e^{A_i\tau} \leq S_i$. Consequently, the existence of $\bar{\mu} \in (0,1)$ makes $V(x(t_k)) \leq \bar{\mu}^k V(x_0) \quad \forall k \in \mathbb{N}$, which with the aid of (6.30) implies that the equilibrium solution $x = 0$ of (6.26) is globally asymptotically stable.

Remark* 4*: Theorem 6.4.1 requires both healthy and faulty control loops to be stable and also assumes that controllers retain the same states.

Theorem 6.4.1 is used to guarantee the stability of the closed-loop system in the cases of ILOC and/ or ILOM problems. First, the LMI constraints of Theorem 6.4.1 are feasible for a minimum dwell-time $T_d = 0.63\,\text{s}$, which was found by bisection for the loss of control problem. Second, this theorem also provides a dwell-time, T_d, for (6.26) that guarantees the stability of the switching between the inner closed-loop for the healthy case $(i = 1)$ and the faulty case $(i = 2)$ (that is, when the quadcopter experiences failure on motor 3), respectively. The LMI constraints of Theorem 6.4.1 are feasible for a minimum dwell-time $T_d = 0.85\,\text{s}$, which was found by bisection. The result of Theorem 6.4.1 guarantees the stability of the inner loop under intermittent faults at a rate of less than $0.54\,\text{Hz}$ between two local equilibrium points.

6.4.2 Multiple Lyapunov-like Functions with a Time Delay in Fault Detection

Now, it is assumed that the detection of the fault is not instantaneous and so a time delay must be taken into account in our analysis. Ignoring the fault detection delay may result in closed-loop instability and/ or degraded performance. Dwell-time theory does not work in this case because closed-loop may be unstable for certain periods. If the time delay is referred to as T_D, then the continuous time dynamics of the switched linear system (6.24) can be written as:

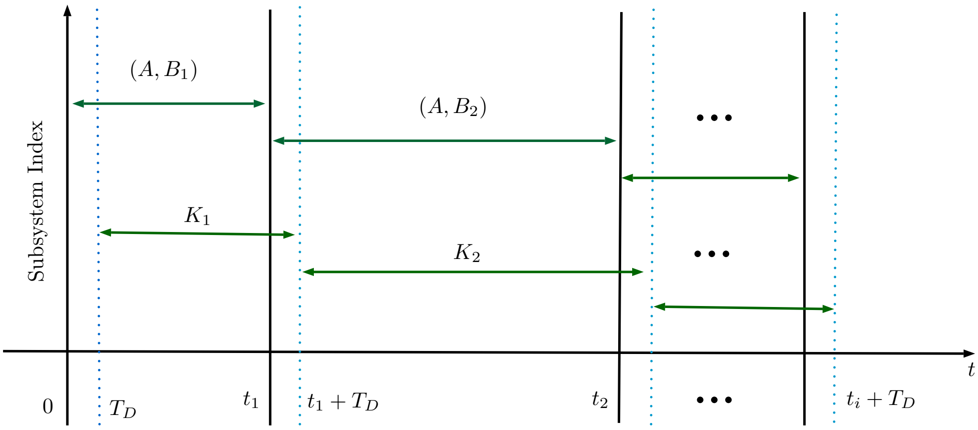

Figure 6.10: Evolution of the closed-loop system.

$$\dot{x}_{cl}(t) \quad = \quad \bar{A}_{\sigma(t-T_D)} x_{cl}(t) \tag{6.36}$$

where $\bar{A}_{\sigma(t-T_D)}$ is such that $\forall (i,j) \in 1 \dots N$:

$$\bar{A}_{\sigma(t-T_D)} = \begin{cases} \bar{A}_{i,j}\,, & \forall t \in [t_k, t_k + T_D), \qquad i \neq j \\ \bar{A}_i\,, & \forall t \in [t_k + T_D, t_{k+1}), \qquad i = j \end{cases} \tag{6.37}$$

where t_k are switching instants, $k \in 1 \dots N$. For instance, in (6.37) $\bar{A}_{2,1}$ represents the evolution matrix of the closed loop of the faulty plant with the healthy controller. This type of switching is called asynchronous switching where T_D is the asynchronous time delay, which in our case will be the time delay required to detect the fault on motor 3.

The multiple Lyapunov-like function is an effective tool for stability analysis, especially for a slowly switched system of an average dwell-time. The mode-unmatched controller will be applied in a closed-loop for a given period time in the case of asynchronous switching. The energy function of the system might be increased. In this case, the Lyapunov-like function is allowed to increase with a bounded rate [157].

An extended Lyapunov-like function is shown in Fig. 6.11, where t_k and t_{k+1} denotes the start and end times of an active subsystem. Let $T_\downarrow(t_k, t_{k+1})$, $T_\uparrow(t_k, t_{k+1})$ be unions of distributed intervals while Lyapunov function is increasing and decreasing

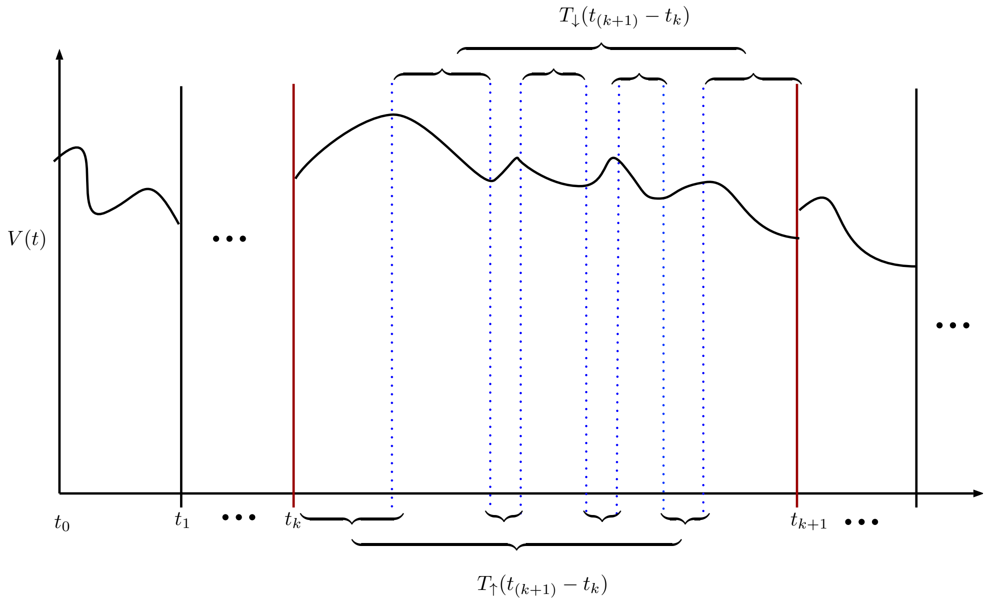

Figure 6.11: Extended Lyapunov-like function.

within the intervals $[t_k, t_{k+1})$. The separation gives $[t_k, t_{k+1}) = T_{\downarrow}(t_k, t_{k+1}) \cup T_{\uparrow}(t_k, t_{k+1})$. $T_{\uparrow}(t_{k+1} - t_k)$ and $T_{\downarrow}(t_{k+1} - t_k)$ gives the length of $T_{\uparrow}(t_k, t_{k+1})$ and $T_{\downarrow}(t_k, t_{k+1})$, respectively, in this figure. $T_{\uparrow}(t_k, t_{k+1})$ includes all the randomly distributed intervals where the Lyapunov function rises. However, $T_{\uparrow}(t_k, t_{k+1})$ will only be the interval close to the switching instants of subsystems for the asynchronously switching problem, and which depends on the running time of the unmatched controller. Here, we assume asynchronous switching time is known *a priori*. The following lemma gives the extended stability results with an average dwell-time when considering an asynchronously switching signal.

***Lemma* 6.4.1** ([157])*:* Consider the continuous time switched system of (6.36) $\sigma \in \mathbb{K}$ and $\alpha > 0$, $\beta > 0$ and $\mu > 1$ be given constants. Assuming that there exists $\mathcal{C}^1$ a function $V_{\sigma}(t) : \mathbb{R}^n \to \mathbb{R}$, $\sigma(t) \in \mathbb{K}$ and two class $\mathcal{K}_{\infty}$, functions k_1 and k_2, such that $\forall \sigma(t) = i \in \mathbb{K}$,

$$k_1(\|x(t)\|) \leq V_i(x_t) \leq k_2(\|x(t)\|) \tag{6.38}$$

$$\dot{V}_i(x_t) \leq \quad -\alpha V_i(x_t), \forall \in T_{\downarrow}(t_k, t_{k+1}) \tag{6.39}$$

$$\dot{V}_i(x_t) \leq \quad \beta V_i(x_t), \forall \in T_{\uparrow}(t_k, t_{k+1}) \tag{6.40}$$

and $\forall(\sigma(t_k) = i, \sigma(t_k^-) = j) \in \mathbb{K} \times \mathbb{K}, i \neq j$,

$$V_i(x_{t_k}) \leq \mu V_j(x_{t_k}) \tag{6.41}$$

then the system is globally uniformly asymptomatically stable for any switching signal with an average dwell-time,

$$T_a > T_a^* = (T_D(\alpha + \beta) + \ln \mu)/\alpha \tag{6.42}$$

where $T_D := \max_k T_\uparrow(t_k + 1 - t_k), \quad \forall k \in \mathbb{K}$.

Proof. Eqs. (6.39)-(6.40) are integrated for $t \in [t_k, t_{k+1})$, satisfying

$$\begin{aligned} V_{\sigma(t)} &\leq e^{-\alpha T_\downarrow(t_k,t)+\beta T_\uparrow(t_k,t)} V_{\sigma(t_k)}(x_{t_k}) \\ &\leq e^{-\alpha[T_\downarrow(t_k,t)+T_\uparrow(t_k,t)]} \frac{e^{\beta T_\uparrow(t_k,t)}}{e^{-\alpha T_\uparrow(t_k,t)}} V_{\sigma(t_k)}(x_{t_k}) \\ &= e^{-\alpha(t-t_k)}(e^{(\beta+\alpha)T_\uparrow(t_k,t)}) V_{\sigma(t_k)}(x_{t_k}) \end{aligned} \tag{6.43}$$

and using eqs.(6.41) ,(6.43), and where $N_\sigma(t_0, t)$ are the switching numbers of $\sigma(t)$ over the interval $[t_0, t)$ and given as $N_\sigma(t_0, t) \leqslant N_0 + (t - t_0)/T_a$, where N_0 is the chatter bound, one can obtain

$$\begin{aligned} V_{\sigma(t_k)}(x_{t_k}) &\leq e^{-\alpha(t-t_k)}(e^{(\beta+\alpha)T_\uparrow(t_k,t)})\mu V_{\sigma(t_k^-)}(x_{t_k}) \\ &\leq e^{-\alpha(t-t_k)}(e^{(\beta+\alpha)T_D})\mu V_{\sigma(t_k^-)}(x_{t_k}) \\ &\leq e^{-\alpha(t-t_k)-\alpha(t_k-t_{k-1})}(e^{(\beta+\alpha)T_D})\mu V_{\sigma(t_{k-1})}(x_{t_{k-1}}) \leq \dots \\ &\leq e^{-\alpha(t-t_0)}(e^{(\beta+\alpha)T_D})^{N_\sigma(t_0,t)}\mu^{N_\sigma(t_0,t)} V_{\sigma(t_0)}(x_{t_0}) \\ &\leq e^{N_0[(\beta+\alpha)T_D+\ln\mu]}(e^{-\alpha} e^{\frac{1}{T_a}(\beta+\alpha)T_D} e^{\frac{1}{T_a}\ln\mu})^{(t-t_0)} V_{\sigma(t_0)}(x_{t_0}) \\ &\leq e^{N_0[(\beta+\alpha)T_D+\ln\mu]} e^{-(\alpha-\frac{1}{T_a}(\beta+\alpha)T_D-\frac{1}{T_a}\ln\mu)(t-t_0)} V_{\sigma(t_0)}(x_{t_0}). \end{aligned} \tag{6.44}$$

Hence, if the ADT holds (6.42), it can be deduced that $V_{\sigma(t_k)}(x_{t_k})$ converges to zero when time $\longmapsto \infty$; then the asymptotic stability is proved with the help of (6.38).

Theorem* 6.4.2** ([157]):*** Consider the switched linear system (6.36) and let $1 > \alpha > 0$, $\beta > 0$ and $\mu > 1$ be given constants. If there exist matrices $P_i > 0$ $i, j = 1, ..., N$ such that

$$\bar{A}_i' P_i + P_i \bar{A}_i + \alpha P_i \leq 0 \tag{6.45}$$

$$\bar{A}_{i,j}' P_i + P_i \bar{A}_{i,j} - \beta P_i \leq 0 \tag{6.46}$$

$$P_i - \mu P_j \leq 0 \quad \forall i \neq j \tag{6.47}$$

then the system (6.36) is asymptotically stable for any switching signal with a dwell time greater than or equal to the average dwell time, T_a^*.

Proof. Consider the asynchronous switching case when the subsystem i has been switched; the controller K_j $\forall i \neq j \in \mathbb{K}$ is still active instead of K_i for T_D. Therefore, we have the following closed-loop systems described by

$$\dot{x}_{cl} = \begin{cases} \bar{A}_{i,j} x_{cl} & \forall t \in [t_k, t_k + T_D) \\ \bar{A}_i x_{cl} & \forall t \in [t_k + T_D, t_{k+1}) \end{cases}, \tag{6.48}$$

where $\forall (i,j) \in \mathbb{K} \times \mathbb{K}, i \neq j$,

$$\bar{A}_{i,j} := \begin{bmatrix} A_{gi} - B_{gi} D_{Kj} C_g & B_{gi} C_{Kj} \\ -B_{Kj} C_g & A_{Kj} \end{bmatrix}, \ \bar{A}_i := \begin{bmatrix} A_{gi} - B_{gi} D_{Ki} C_g & B_{gi} C_{Ki} \\ -B_{Ki} C_g & A_{Ki} \end{bmatrix}$$

The extended Lyapunov-like function is given by the following quadratic form:

$$V_i(x) = x' P_i x, \forall \sigma(t) = i \in \mathbb{K}, \quad P_i > 0 \tag{6.49}$$

Using eqs. (6.39), (6.40), (6.48) and (6.49), one can get,$\forall (i,j) \in \mathbb{K} \times \mathbb{K}, i \neq j$,

$$\begin{aligned} \dot{V}_i(t) + \alpha V_i(t) &= x_t' [\bar{A}_i' P_i + P_i \bar{A}_i + \alpha P_i] x_t, & (6.50) \\ \dot{V}_i(t) - \beta V_i(t) &= x_t' [\bar{A}_i' P_i + P_i \bar{A}_i - \beta P_i] x_t, & (6.51) \\ V_i(t_k) - \mu V_j(t_k) &= x_{t_k}' [P_i + \mu P_i] x_{t_k} & (6.52) \end{aligned}$$

Thus if

$$\bar{A}_i' P_i + P_i \bar{A}_i + \alpha P_i \leq 0 \tag{6.53}$$

$$\bar{A}_{i,j}' P_i + P_i \bar{A}_{i,j} - \beta P_i \leq 0 \tag{6.54}$$

$$P_i - \mu P_j \leq 0 \quad \forall i \neq j, \tag{6.55}$$

according to Lemma 6.4.1, it can be deduced that the closed-loop system (6.36) is globally asymptomatically stable for any switching signal with an average dwell time (6.42).

Remark 5: The conditions given in the above theorem are LMIs for selected α , β and μ. Then, selecting minimum values of μ and β *a priori*, the optimum value for α can be estimated by the bisection method when the solutions of the LMIs are feasible.

Here, Theorem 6.4.2 is applied to ensure stability of the quadcopter in any situation of intermittent loss of control or loss of rotor problems. First, it is assumed that loss of control can be detected in $T_D = 500$ ms. Selecting parameters in Theorem 6.4.2 as $\alpha = 0.01$, $\mu = 1.04$, and $\beta = 0.21$, then the LMIs have a feasible solution which results in T_a^* = 0.7106 using the formula (6.42). Second, if it is assumed that T_D= 100 ms (because rotor failures dramatically affect closed-loop responses, hence detection time could be shorter than the first problem), with chosen parameters $\alpha = 0.01$, $\mu = 1.04$ and $\beta = 0.04$, the LMIs of Theorem 6.4.2 with the state-space matrices of the quadcopter (Section 6.2) and of the controllers (Section 6.3) are feasible. Therefore, the average dwell-time is computed as T_a^*= 1.1055 s using (6.42). This result ensures the stability of the inner loop under intermittent faults at a rate of less than 0.9046 Hz and 100 ms of the unmatched controller between two local equilibrium points.

6.5 Transient Improvement of the Switched Controllers

Switching between controllers may lead to transition deterioration during switching. In this section, a simple method is presented to reinitialise the off-line controller state at the switching instant. A switched controller diagram is shown in Fig. 6.12, where e and u_1, u_2 are the inputs and the outputs of the online and offline controllers, and $\bar{\boldsymbol{r}}$ and y are the reference signal and the plant output, respectively. One needs to determine a controller state at time t which will eliminate the discontinuity between the online control output, u_1

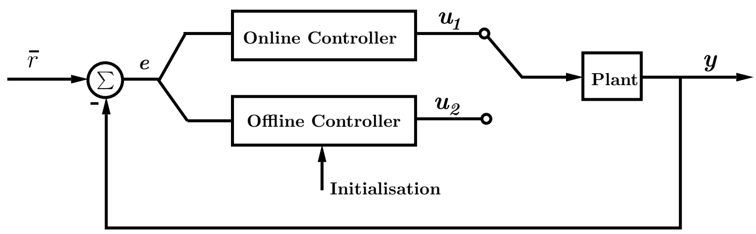

Figure 6.12: Switched controller diagram.

(the plant is driven initially by u_1 as shown in Fig. 6.12) and the off-line control output, u_2. Consider now the $n-$dimensional state space realisation of the online controller given by

$$\dot{x}_{K_i} = A_{Ki} x_{K_i} + B_{Ki} e \tag{6.56}$$

$$u_1 = C_{Ki} x_{K_i} + D_{Ki} e \tag{6.57}$$

and the offline controller as

$$\dot{x}_{K_j} = A_{Kj} x_{K_j} + B_{Kj} e \tag{6.58}$$

$$u_2 = C_{Kj} x_{K_j} + D_{Kj} e. \tag{6.59}$$

Let $u_1 = u_2$ to be at switching instant, t, then

$$C_{Kj} x_{K_j} + D_{Kj} e = C_{Ki} x_{K_i} + D_{Ki} e \tag{6.60}$$

and the off-line controller states at the switching time can determined as:

$$x_{K_j} = C_{Kj}^{\dagger} (C_{Ki} x_{K_i} + D_{Ki} e - D_{Kj} e) \tag{6.61}$$

where it is assumed that C_{Kj} is of full rank so that its pseudo-right inverse can be computed as ${C_{Kj}}^{\dagger}$= $C'_{Kj}(C_{Kj} C'_{Kj})^{-1}$.

Remark* 6*: The dwell-time stability conditions are based on the assumption that the plant and controller state-space matrices are switched but the controller state needs to stay the same for the dwell-time stability guarantees. Re-initialising the controller states before switching which will invalidate the stability guarantees. Strictly speaking, the stability guarantees are lost although the controller state initialisation improves switching transient in practice.

6.6 Time Simulation Results

Two different simulations have been run using the MATLAB and Simulink® software to validate the theoretical results with the non-linear dynamic model given in Chapter 4.

6.6.1 Case A: Intermittent Loss of Control Effectiveness

Simulation results are now presented when the quadcopter system is subject to intermittent loss due to control faults. The limit on each thrusting force f_i is 5 N. Assume that the intermittent fault starts acting at $t = 5$ s for motor 3 and fault information is available after $T_D = 500$ ms delay. Zero-mean Gaussian white noise with variances of 6.10^{-5} and 10^{-4} are added to the output channels $(\phi,\ \theta,\ \psi)$ and $(\dot{x},\ \dot{y},\ \dot{z})$ so that the measurement signal to noise ratio is approximately 25 dB.

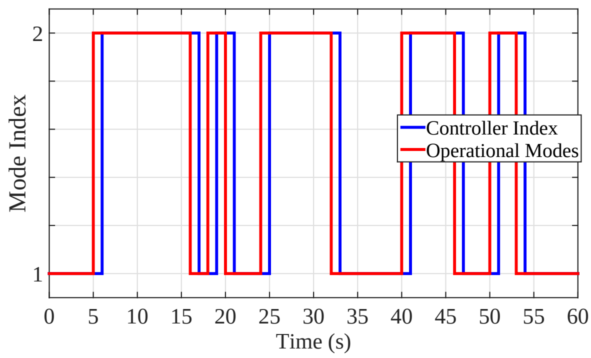

Figure 6.13: A random LOC profile and the corresponding controller with T_D delay: 2 indicates the loss of control mode and 1 indicates the fault-free mode.

A random loss of control authority profile is generated, as given in Fig. 6.13. It can be seen from this figure that the corresponding controller is following the mode with a fault detection delay, T_D. The simulation has been run to verify the effectiveness and advantages of the switching recovery control. Here, the quadcopter is required to track the heave velocity $\dot{z}_I$ according to the profile given in Fig. 6.14. Closed-loop responses for heave velocity trajectory tracking are given in Fig. 6.14 with the switching recovery control (blue dotted line) and the healthy mode controller (solid green line). In the landing situation, heave velocity reduces by -0.5 m/s, so all forces should be equally reduced to keep the vehicle stable and correspond to the command demand. One can see that the healthy mode controller fails to track the heave velocity between $t = 15$s and $t = 40$s, although the switched recovery control achieves perfect tracking performance. It can

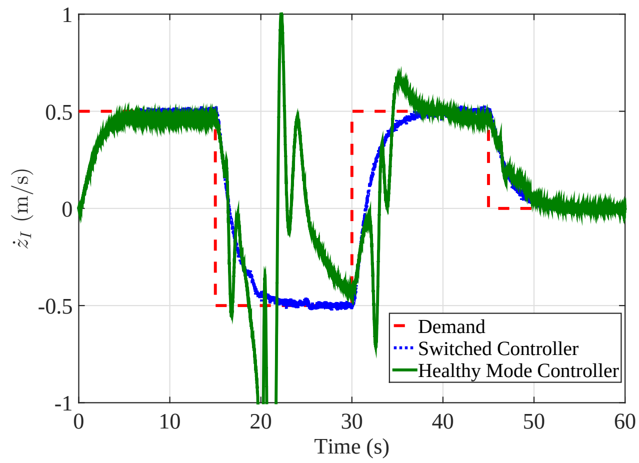

Figure 6.14: Heave velocity tracking response when the quadcopter vehicle experiences an intermittent LOC for motor 3.

be seen from Fig. 6.15, the vehicle increases its longitudinal velocity in the backwards direction at $t = 5$ s instead of a 0 m/s demand. The longitudinal velocity of the quadcopter reaches an undesirable $\dot{x}_I$ =-11 m/s at t =20 s. The switched recovery controller (blue lines) enables the quadcopter to track the $\dot{x}_I$ demand effectively. Fig. 6.16 is given to compare the $\dot{y}_I$ tracking performance of the switched recovery controller with the healthy mode controller. Loss of control in motor 3 also affects the lateral velocity because $\dot{y}_I$ reaches 1.1 m/s at $t = 17$s, 1 m/s at $t = 21$ s and -1.3 m/s at t =33, respectively.

The Euler angles are given in Fig. 6.17, which shows that the quadcopter rotates about the vertical axis as the heave velocity changes. It can be seen that ψ settles only when $\dot{z}_I$ is equal to zero. Figs. 6.17(a) and (b) show roll and pitch angles while the vehicle tracks vertical velocity under the loss of control problem. Pitch angle reaches -60^o at $t = 20$ when only the healthy mode controller is used. This results in an undesirable increase in $\dot{x}_I$ velocity. Longitudinal and lateral velocities are controlled by adjusting the roll and pitch angles. In this case, the roll and pitch angles remain small because of zero $\dot{x}_I$ and $\dot{y}_I$ demands when the switched controller is used. The healthy mode controller (green solid line) cannot stabilise the pitch and roll attitude of the quadcopter, which would obviously lead to a crash under loss of control conditions.

Fig.6.18 shows that the switched controller produces forces, f_i, which are proportional

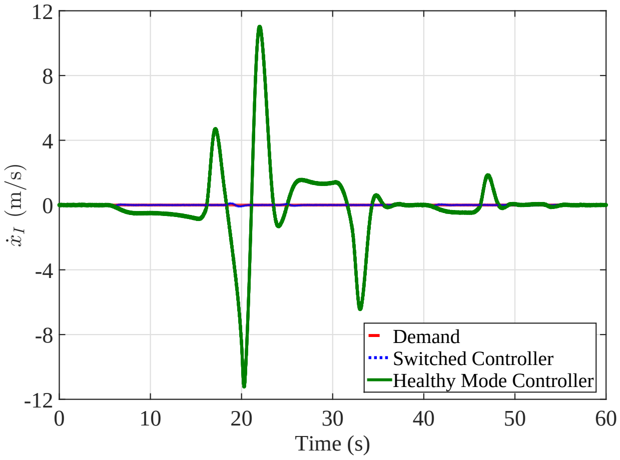

Figure 6.15: Velocity in the x-direction while performing vertical velocity tracking of LOC in motor 3.

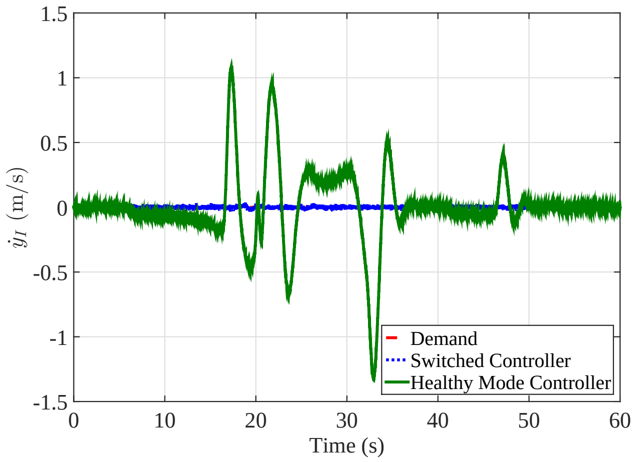

Figure 6.16: Velocity in y-direction while performing vertical velocity tracking of LOC in motor 3.

to the PWM (Pulse-Width Modulation) signals used to stabilise the quadcopter. When the quadcopter experiences LOC effectiveness for motor 3, one can see that f_2 and f_4 slightly increase or decrease such as to allow the vehicle to track the heave velocity demand. This shows that the heave velocity is controlled by the opposing motors M_2 and M_4 during loss of control authority for motor 3. For instance, f_2 and f_4 are increased (greater than 1.15 N) and f_1 is equalised to f_3 between t = 5 s and t = 16 s to achieve the vertical velocity demand. Similarly, f_2 and f_4 are decreased (less than 1.15 N) and f_1 is equalised to f_3 between t = 24 s and t =30 s such that the quadcopter can still land easily, despite the loss of control.

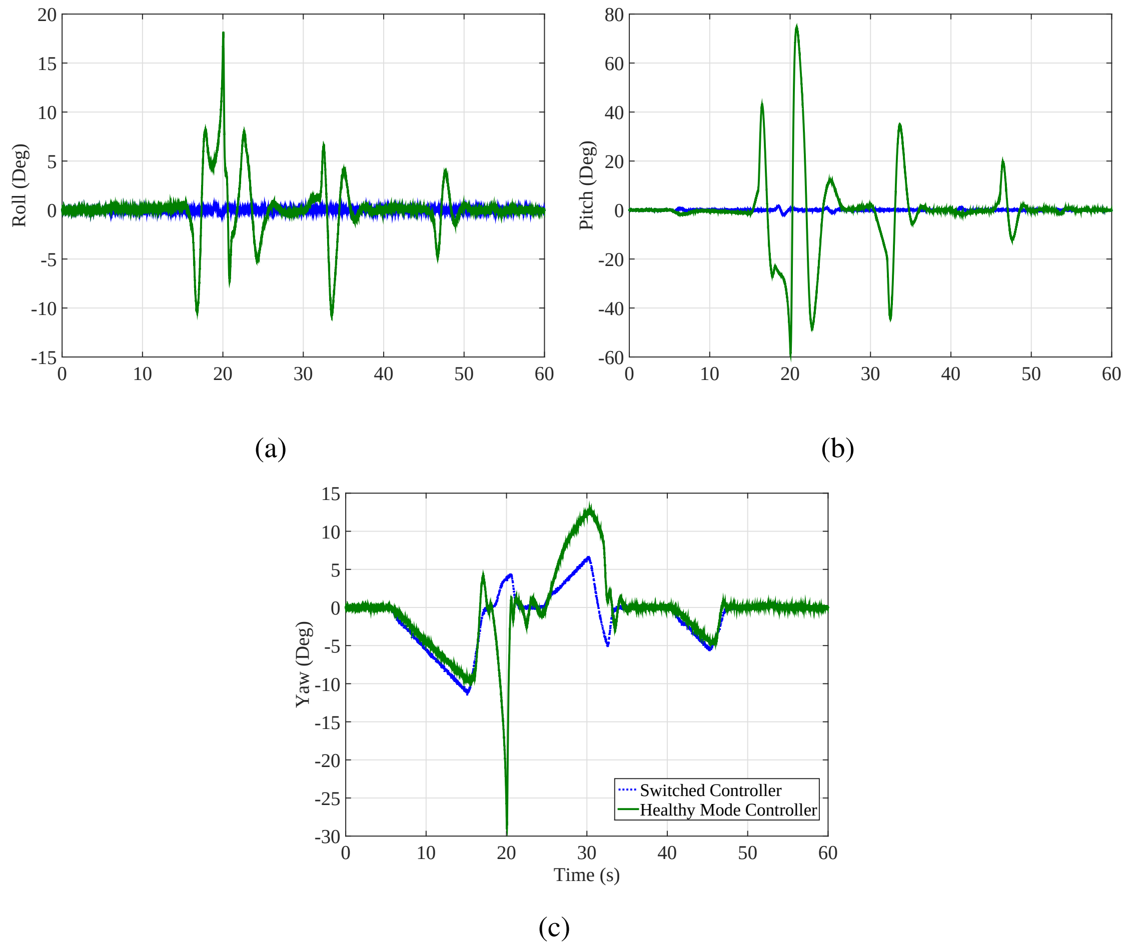

Figure 6.17: Euler angles corresponding to Fig. 6.14.

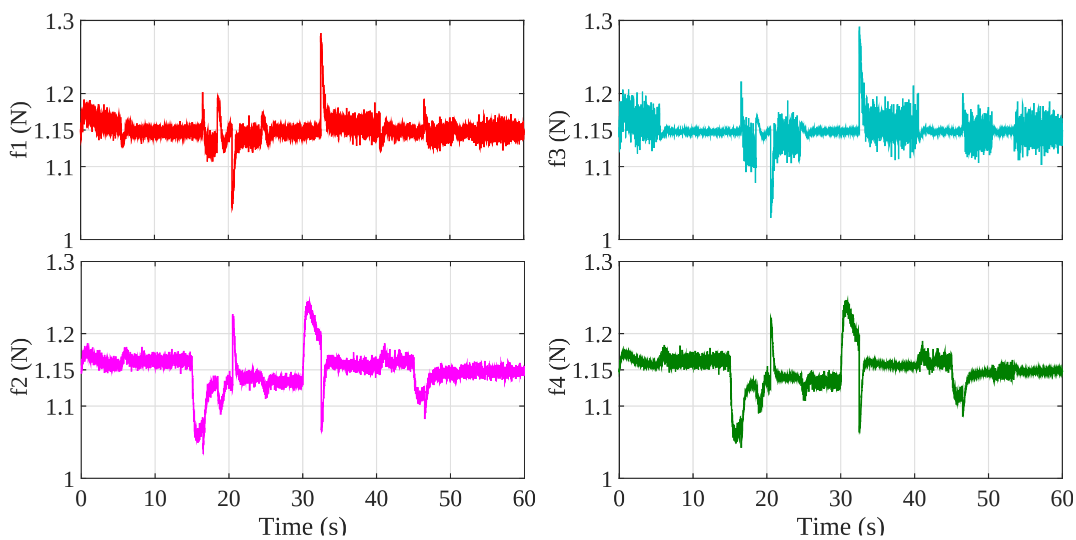

Figure 6.18: Control inputs when the switched controller is used under LOC conditions.

6.6.2 Case B: Intermittent Loss of Motor

This section presents the results obtained in the presence of an intermittent motor fault. As assumed in the previous section, the limit on each propeller force is 5 N. Fault detection time is assumed to be $T_D = 100$ ms, as mentioned in Section 6.4.2. To verify the effectiveness of the switching control, it is assumed that motor 3 is subject to a randomly intermittent fault (intervals satisfy the results obtained by using Theorems 6.4.1 and 6.4.2). Zero-mean Gaussian white noise with variances of 6.10^{-5} and 10^{-4} are added to the output channels (ϕ, θ, ψ, r) and $(\dot{x},\ \dot{y},\ \dot{z})$, respectively. To simulate an intermittent fault in motor 3, in the intermittent fault scenario this motor will be turned off between times $t = 20 - 39$ s, $t = 45 - 60$ s, $t = 75 - 85$ s, $t = 92 - 104$ s, $t = 107 - 110$ s and $t = 114 - 120$ s.

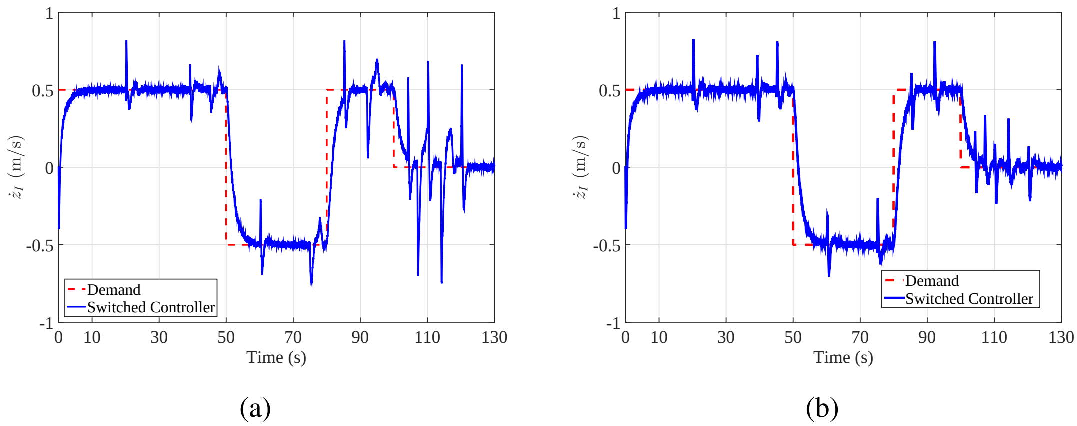

Figure 6.19: Heave velocity tracking responses (a) when there is no controller state initialisation, (b) when controller state initialisation is employed.

The quadcopter is required to track the heave velocity ($\dot{z}_I$) profile (red dashed line) shown in Fig. 6.19. It can be seen in Fig. 6.19(a) that switched recovery control preserves the stability of the vehicle, although the discontinuity between the controllers leads to transition degradation during intermittent switching. The switched recovery scheme given in Fig. 6.1(b) will include the controller state initialisation (Section 6.5) to reduce tracking deterioration during asynchronous switching. It can be seen that spikes are present in $\dot{z}_I$ due to the sudden change of control signal during the switching instants. Comparing Figs. 6.19(a-b), the response has been improved by 70% at $t = 110$, and similar improvements are observed during switching transients. The switched recovery scheme with state initialisation enables the quadcopter to track the desired heave velocity in the presence of an intermittent rotor fault. Intermittent loss of motor 3 influences the longitudinal

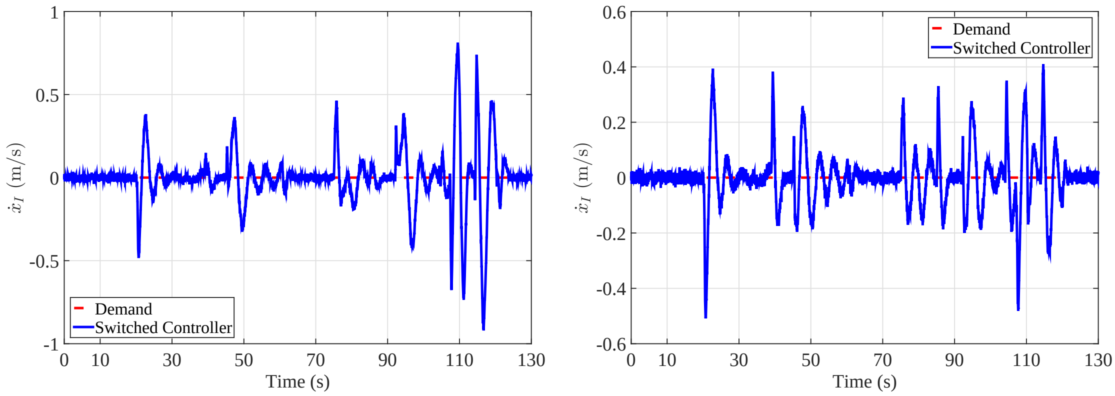

(a) (b)

Figure 6.20: Velocity in x-direction while the quadcopter tracks the vertical velocity demand of Fig. 6.21 with the intermittent fault (a) when there is no controller state initialisation, (b) when the controller state initialisation is employed.

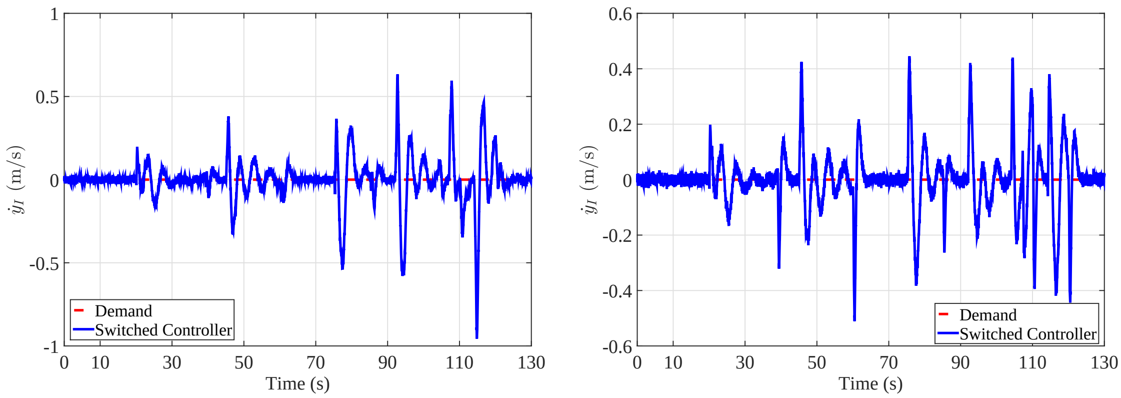

(a) (b)

Figure 6.21: Velocity in y-direction during the vertical velocity tracking demand with the intermittent fault (a) with no controller state initialisation, (b) when controller state initialisation is employed.

velocity of the vehicle shown in Fig. 6.20. Switching between controllers leads to large oscillations in $\dot{x}_I$ tracking without state initialisation (Fig. 6.20(a)). Improved longitudinal velocity tracking is given in 6.20(b). $\dot{x}_I$ reaches and undesirable -0.5 m/s at t =20.7 s due to loss of one motor and asynchronously switching; similar undesirable effects can be seen for the unmatched controller. Overall tracking is still possible, though with some degradation.

The lateral velocity $\dot{y}_I$ tracking is given in Fig. 6.21. When the quadcopter loses rotor 3 temporarily, this also effects the lateral velocity as the vehicle starts to rotate around vertical axis. Comparing Figs. 6.21(a-b), closed-loop lateral velocity tracking has been improved with the controller state initialisation; for instance, the velocity of the quadcopter reaches -0.4 m/s at t =114.7s instead of -0.96 m/s in the y-direction. The proposed recovery scheme enables the quadcopter to attain zero lateral velocity as possible as under the intermittent fault.

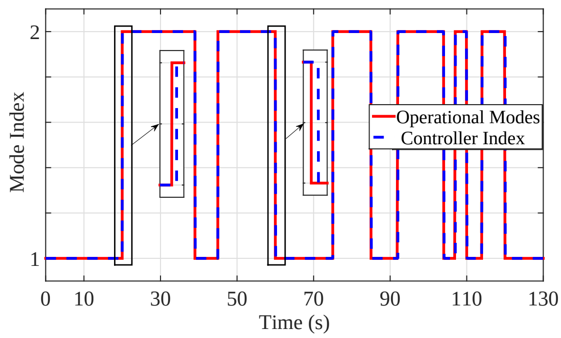

Figure 6.22: A random intermittent rotor fault profile: 2 is the rotor fault mode and 1 is the fault-free mode; the solid red line shows the operational modes and the blue dotted line shows the controller index.

The roll-pitch angles and yaw rate corresponding to Figs. 6.19, 6.20 and 6.21 are shown in Fig. 6.23. One can see from Fig. 6.23(a-b) that the roll and pitch angles are oscillatory about zero to preserve the stability of the vehicle. As can be seen from Fig. 6.23(c), the yaw angular velocity tracks the reference that switches between $r_{ref} = 0$ and $r_{ref} = 172^o$. This variation is not desired in the flight conditions; but in the case of the actuator fault, it is necessary to enable the quadcopter to return from missions. The angular yaw velocity increases when the quadcopter experiences the loss of rotor 3 due to an increase in the forces produced by M_2 and M_4 to compensate for the weight.

A random intermittent fault in motor 3 and the corresponding controller index is shown in Fig. 6.22. In the zoomed part of Fig. 6.22, it can be seen that the controllers exhibit a delayed response of $T_D = 40$ ms (switching from healthy mode to faulty mode controller) and $T_D = 90$ ms (switching from faulty to healthy mode controller). Control inputs in terms of forces ($f_1,\ f_2,\ f_3,\ f_4$) are given in Fig. 6.24. As expected, the effect of the fault is compensated by modifying the force generated by the pair of rotors M_2 and M_4. The controller initially produces an impulse force, f_1 and reduces f_1 to zero when rotor M_3 fails to produce the lifting force. Overall tracking performance is maintained thanks to the switching control with state controller initialisation.

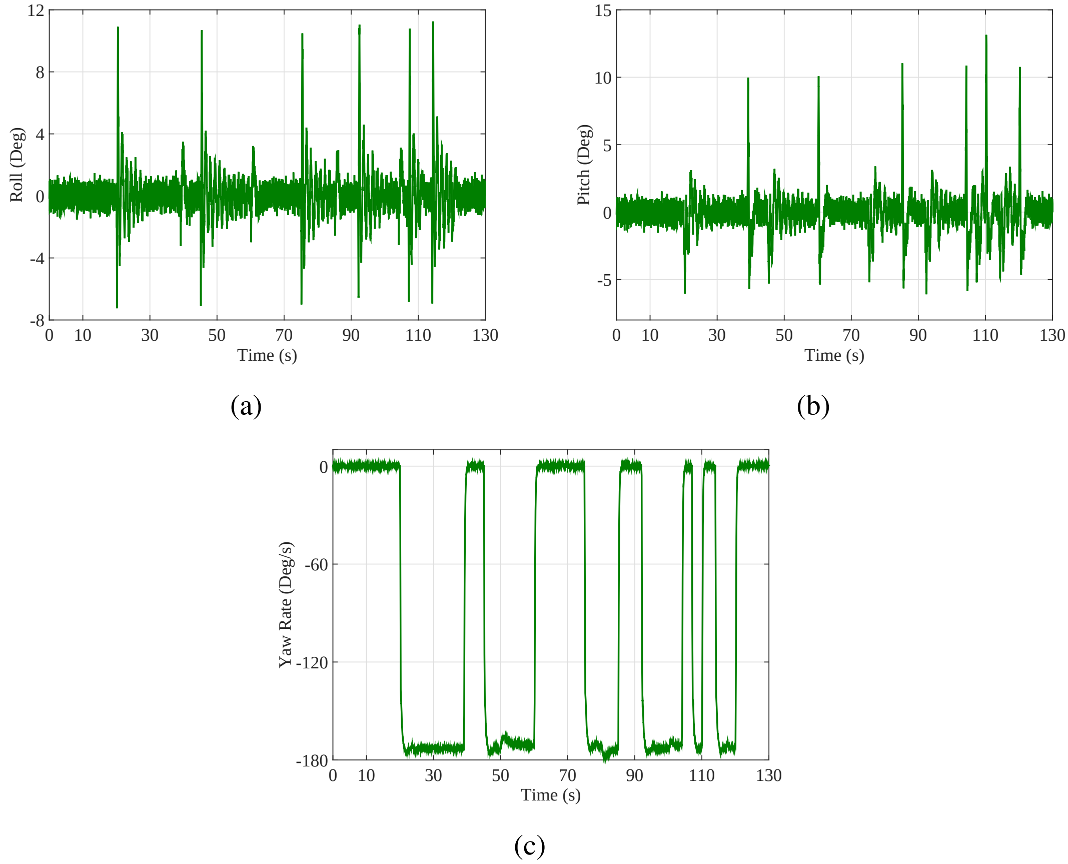

Figure 6.23: Roll and pitch angles, and yaw angular velocity, corresponding to Figs. 6.19-6.21 when the switched recovery controller with state initialisation is used.

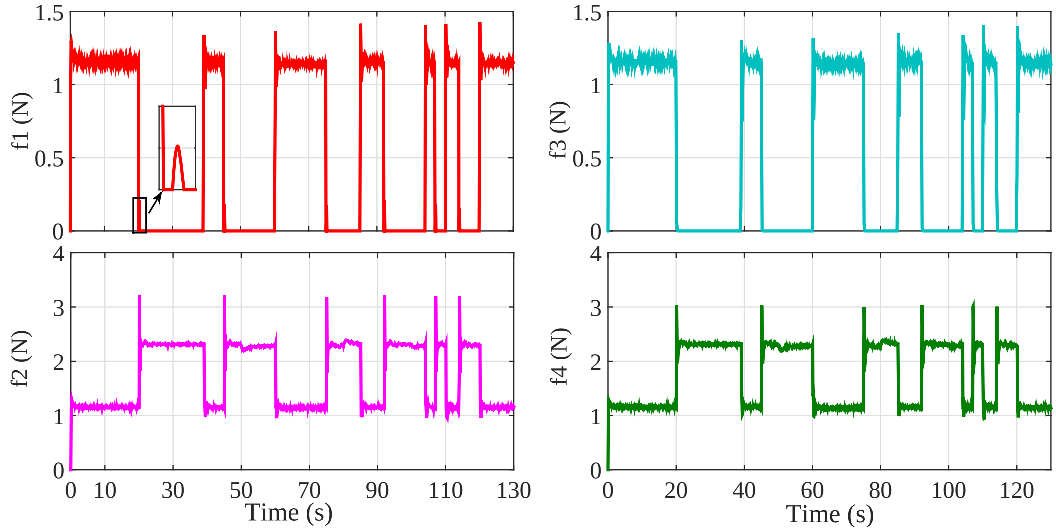

Figure 6.24: Control inputs when the switched controller with state initialisation is used.

6.7 Conclusions

This chapter has presented switched recovery control schemes for the problems of intermittent loss of control and motor, respectively. Two double-loop architectures have been developed to control the quadcopter UAV in healthy and faulty modes of operation by using fixed-order H_∞ feedback controllers. The first control structure permits the quadcopter to track a desired velocity trajectory using the remaining control signals when one motor became intermittently uncontrollable at equilibrium. The second control structure allows the quadcopter to track a desired velocity trajectory in the presence of an intermittent rotor fault. The stability of switching between healthy and faulty closed-loop systems was guaranteed using minimum dwell-time theory. Stability analysis was also conducted, as based on multiple Lyapunov functions that assure the stability of an asynchronously switched system. An initialisation scheme is considered to improve the switching transient when the quadcopter experiences intermittent rotor faults. These control schemes could also be employed when two opposite rotors lose control signals or thrusting forces intermittently.

CHAPTER 7

STATE-DEPENDENT SWITCHED CONTROL SCHEMES IN THE PRESENCE OF UNDETECTED FAULTS

7.1 Introduction

This chapter proposes a new passive fault tolerant control approach for stabilisation and to ensure the robust stability of the quadcopter UAV system involving time-varying motor faults. Fault detection and diagnosis has been assumed to be available in Chapter 6. Here, attention focusses on the time-varying loss of motor effectiveness that stems from a malfunctioning component or physical damage that has not been explicitly detected. The problem of the quadcopter subject to a time-varying LOE in one motor is treated as a polytopic-switched linear parameter varying control problem. A set of feedback controllers and a switching rule are determined such that the closed-loop system is globally asymptotically stable. The switching rule is a control variable to be determined from the available measurements to improve performance in the joint control law design. However, chattering is an undesired problem characterised by high switching frequencies [33, 132] that may cause equipment damage in real quadcopter systems. Hence, chattering on control outputs is also reduced by introducing a relaxed minimum switching rule in this chapter. The synthesis conditions of a fault tolerant control law is formulated in terms of linear matrix inequalities with coupled prechosen scalars. A switched dynamic output feedback H_∞ control is also proposed, considering that the switching strategy depends on only the measured output through the controller state variable. The developed self-recovery approach preserves the stability of the quadcopter system and improves its operational performance in the presence of time-varying faults without an explicit detection mechanism. This chapter is organised as follows. Section 7.2 describes the problem of time-varying motor faults in a quadcopter system. Switched H_2 and H_∞ stability and stabilisation conditions are given in Sections 7.3 and 7.4, respectively. Furthermore, a dynamic output feedback switched control scheme is proposed in Section 7.3.3. Fault tolerant control based on the minimum and relaxed minimum switching rules is designed in Section 7.5 and simulation results are illustrated in Section 7.6. Finally, conclusions are given in Section 7.7.

7.2 Problem Statement

A linearised model of the rotational dynamics of the quadcopter given in Chapter 4 is computed about the hover; this results in matrices A and B. Then, the continuous time-linearised rotational dynamics of the quadcopter system are subject to a time-varying motor fault is treated as a continuous time-varying switched polytopic system defined by

$$\begin{aligned} \dot{x}(t) &= Ax(t) + B\Omega_{\lambda(t)}u(t) + Hw(t), \quad x(0) = x_0 \\ z(t) &= E_{\sigma(t)}x(t) + F_{\sigma(t)}u(t) + G_{\sigma(t)}w(t) \\ y(t) &= Cx(t) + Dw(t) \end{aligned} \tag{7.1}$$

where $x \in \mathbb{R}^n$ is the state, $u \in \mathbb{R}^m$ is control input, $w \in \mathbb{R}^q$ is the external disturbance such that $w \in \mathcal{L}_2$, $y(t) \in \mathbb{R}^r$ is the measured output and $z \in \mathbb{R}^p$ is controlled output which depends on the minimum switching strategy $\sigma(t)$ to be designed. For $t \geq 0$ at each instant of time, the parameter varying matrix $\Omega_{\lambda(t)}$ is such that

$$\Omega_{\lambda(t)} = \sum_{j=1}^{N} \lambda_j(t)\Omega_j \tag{7.2}$$

where the parameter vector $\lambda(t) = [\lambda_1(t), \ldots, \lambda_N(t)]' \in \mathbb{R}^N$ is assumed to belong to the unitary simplex $\wedge$ given by

$$\wedge = \left\{ \lambda \in \mathbb{R}^N : \lambda_j \geq 0, \sum_{j=1}^{N} \lambda_j = 1 \right\} \tag{7.3}$$

and Ω_j are determined by assuming that the maximum LEO is known, for all $j \in \mathbb{K}$. More precisely, Ω_j =diag$\{k_{1,j}, k_{2,j}, \ldots, k_{i,j}\}$ that are known and describes the LEO faults, where each $k_{i,j}$ represents the LEO of the i^{th} actuator, i.e. its degree of degradation. For instance, $k_{i,j} = 0.6$ would present that the i^{th} actuator is degraded by 40$\%$ (the delivered action is 60% of the nominal one). On the contrary, $k_{i,j} = 1$ indicates the fault-free case, while $k_{i,j}$ = 0 would denote a 100% degradation, which corresponds to a total loss. Here, for the fault-free case, $k_{3,1} = 1$, and for the partial LOE, $k_{3,2} = 0.5$.

7.3 Switched H_∞ Control

Assume that the time-varying parameter $\lambda(t) \in \wedge$ is not estimated or measured. Hence, it is proposed to apply a state-dependent switched control scheme for time-varying polytopic systems ensuring a minimal H_∞ performance. Fig. 7.1 shows the control scheme with $u(t) = K_{\sigma(x(t))}$ where $\sigma(.)$ is the switching function and $K_1, \ldots, K_N$ are state feedback gains. This control structure does not depend on $\lambda(t) \in \wedge$, avoiding online measurements of the time-varying parameter.

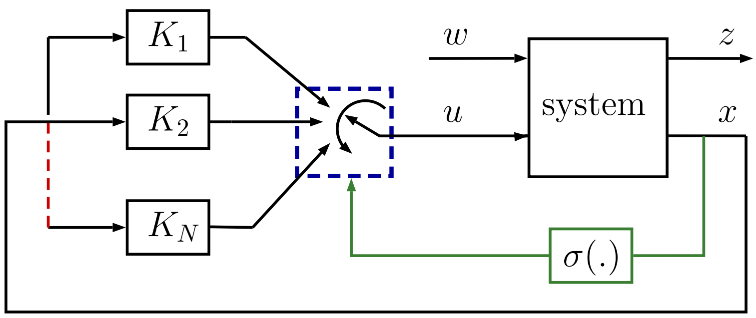

Figure 7.1: A state-dependent switched control scheme.

Here, the system (7.1) can be given as:

$$\dot{x}(t) = Ax(t) + B_\lambda u(t) + Hw(t) \tag{7.4}$$

$$z(t) = E_\sigma x(t) + F_\sigma u(t) + G_\sigma w(t) \tag{7.5}$$

with $x(0) = 0$, where $x \in \mathbb{R}^n$ is the state, $u \in \mathbb{R}^m$ is control input, $w \in \mathbb{R}^q$ is the external disturbance such that $w \in L_2$ and $z \in \mathbb{R}^p$ is the controlled output which depends on the N triples of matrices (E_i, F_i, G_i), $i \in \mathbb{K}$ used to define possibly conflicting N different criteria since $\sigma(t) \in \mathbb{K}$. It is assumed that the entire set of state variables are available for feedback, yielding $u = K_{\sigma(x(t))}x$ where K_σ for all $\sigma \in \mathbb{K}$ are state feedback gain matrices of compatible dimensions to the design.

The purpose here is to design the K_σ and the switching rule $\sigma(x(t))$ in order to make the origin $x = 0$ of the closed-loop system globally asymptotically stable and to achieve a minimal worst case H_∞ norm given by [27], [28]

$$\sup_{w \in L_2} \|z\|_2^2 - \rho\|w\|_2^2 < 0 \tag{7.6}$$

which are satisfied for $\rho > 0$. Whenever the switching rule is constant ($\sigma \in \mathbb{K}$ for all $t \geqslant 0$), the quantity ρ is equal to the H_∞ squared norm with respect to $\lambda \in \wedge$ of the closed-loop subsystem transfer function w to z.

Now, it will be useful to give the following lemmas before proceeding.

Lemma* 7.3.1** ([30]):*** A parameter-dependent matrix $\Pi(\lambda)$ with elements given by

$$\pi_{ij}(\lambda) := \begin{cases} \gamma_i\lambda_j, & j \neq i, \\ \gamma_i(\lambda_i - 1), & j = i \end{cases} \tag{7.7}$$

is Metzler and $\Pi(\lambda) \in \mathcal{M}$ is for all $\lambda \in \wedge$, where γ_i is for all $i \in \mathbb{K}$.

Proof. A result of (7.7) implies that $\gamma_i\lambda_j \geqslant 0$ and

$$\sum_{j=1}^{N} \pi_{ji}(\lambda) = \sum_{j \neq i=1}^{N} \gamma_i\lambda_j + \gamma_i(\lambda_i - 1) \tag{7.8}$$

$$= \gamma_i(\sum_{j=1}^{N} \lambda_j - 1) \tag{7.9}$$

$$= 0 \tag{7.10}$$

for each $i \in \mathbb{K}$ and all $\lambda \in \wedge$.

The adopted piecewise quadratic Lyapunov function given in Chapter 3 that does not depend explicitly on $\lambda(t) \in \wedge$ is

$$V(x) = \min_{i \in N} x' P_i x \tag{7.11}$$

where $P_i > 0$ for all $i \in \mathbb{K}$. If there are positive definite matrices P_i satisfying certain conditions, then the min-switching strategy:

$$\sigma(t) = \arg\min_{i \in N} x(t)' P_i x(t) \tag{7.12}$$

is globally stabilising. The current active controller index i is determined by the min-switching strategy shown in Fig.7.2.

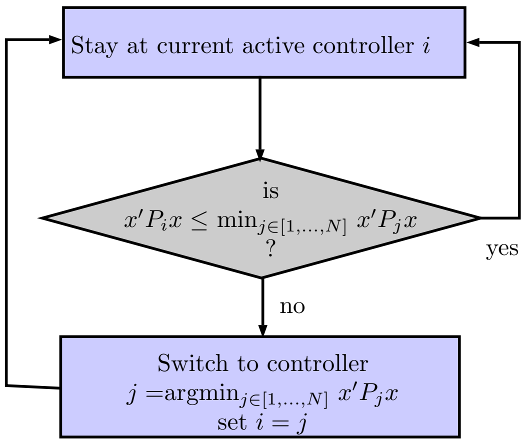

Figure 7.2: Min-switching strategy.

Lemma* 7.3.2** ([49]):*** Let $Q \geq 0$ be given. Consider a set of positive matrices $\{P_1, ..., P_N\}$ and a scalar $\gamma > 0$ holds the modified Lyapunov-Metzler inequalities

$$A_i' P_i + P_i A_i + \gamma(P_j - P_i) + Q < 0, i = 1, ..., N \tag{7.13}$$

Then the state-dependent switching function (7.12) with $u(t) = K_{\sigma(x(t))} x(t)$ makes the equilibrium solution $x = 0$ of $\dot{x}(t) = A_{\sigma(x(t))} x(t)$ globally asymptotically stable and

$$\int_0^\infty x(t)' Q x(t) dt < \min_{i=1,\ldots,N} x_0' P_i x_0. \tag{7.14}$$

7.3.1 Stability Analysis

This subsection presents the stability analysis conditions for a time-varying switched polytopic system that minimises the worst-case H_∞ performance. Consider the time-varying closed-loop switched polytopic system obtained from (7.4)- (7.5) by setting $u = 0$, as:

$$\dot{x}(t) = A_{\lambda(t)\sigma(x)}x(t) + Hw(t), \;\; x(0) = 0 \tag{7.15}$$

$$z(t) = E_{\sigma(x)}x(t) + G_{\sigma(x)}w(t) \tag{7.16}$$

where $\sigma(x)$ represents the switching rule between matrices $A_{\lambda(t)i}$, E_i and G_i for all $i \in \mathbb{K}$. The system matrices of (7.15)-(7.16) reside within following polytope:

$$\begin{bmatrix} A_{\lambda i} & H \\ E_i & G_i \end{bmatrix} = \sum_{j \in \mathbb{K}} \lambda_j \begin{bmatrix} A_{ji} & H \\ E_i & G_i \end{bmatrix} \tag{7.17}$$

for $\lambda(t) \in \wedge$. Notice that the first sub-index denotes the polytopic vertex, whilst the second refers to the switching rule.

Based on the results of Lemma 7.3.2 and on the special subclass of parameter-dependent Metzler matrices given in Lemma 7.3.1, the following theorem gives the stability conditions and a performance criterion for the time-varying closed-loop switched polytopic system (7.15)-(7.16).

Theorem* 7.3.1*: Consider that there exist the symmetric positive definite matrices P_i, $i \in \mathbb{K}$ and positive scalars γ_i for all $i \in \mathbb{K}$ and ρ satisfying the following modified Lyapunov-Metzler inequalities

$$\begin{bmatrix} He\{A'_{ji}P_i\} + \gamma_i(P_j - P_i) & * & * \\ H'P_i & -\rho I & * \\ E_i & G_i & -I \end{bmatrix} < 0, \;\; i, j \in \mathbb{K} \times \mathbb{K} \tag{7.18}$$

for all $i,\ j \in \mathbb{K}$, then the min-switching strategy (7.12) is globally stabilising and the time-varying switched polytopic system (7.15)-(7.16) satisfies the constraint (7.6).

Proof. Using (7.7) implies that the equality

$$\begin{aligned}\sum_{j=1}^{N}\pi_{ji}(\lambda)P_j &= \gamma_i\sum_{j\neq i=1}^{N}\lambda_jP_j+\gamma_i(\lambda_i-1)P_i\\ &= \gamma_i\sum_{j=1}^{N}\lambda_jP_j-\gamma_iP_i\\ &= \gamma_i\sum_{j=1}^{N}\lambda_j(P_j-P_i)\end{aligned}\tag{7.19}$$

holds for each $i \in \mathbb{K}$ and $\lambda \in \wedge$. The feasibility of (7.18) requires the first diagonal block to be negative definite for the switched polytopic system to be asymptotically stable. Applying the Schur Complement to the inequality (7.18) with respect to the third row and column, by rearranging the terms one obtains

$$\begin{bmatrix} He\{A'_{ji}P_i\} & * \\ H'P_i & 0\end{bmatrix} < -\begin{bmatrix} E'_i \\ G'_i\end{bmatrix}\begin{bmatrix} E_i & G_i\end{bmatrix} - \begin{bmatrix}\gamma_i(P_j-P_i) & * \\ 0 & -\rho I\end{bmatrix}. \tag{7.20}$$

Multiplying the result by $\lambda_j \geq 0$ and summing up terms, this yields

$$\begin{bmatrix} He\{A'_{\lambda i}P_i\} & * \\ H'P_i & 0\end{bmatrix} < -\begin{bmatrix} E'_i \\ G'_i\end{bmatrix}\begin{bmatrix} E_i & G_i\end{bmatrix} - \begin{bmatrix}\gamma_i\sum_{j=1}^{N}\lambda_j(P_j-P_i) & * \\ 0 & -\rho I\end{bmatrix} \tag{7.21}$$

For the system (7.15)-(7.16), consider that at some time $t \geqslant 0$ the switching rule $\sigma(t) = i \in \mathcal{I}(x(t))$, where $\mathcal{I}(x) = \{i \in \mathbb{K} : V(x) = x'P_ix\}$, that is, $\mathcal{I}(x)$ is the active subsystem index.

Multiplying to the left of (7.21) by $[x' \;\; w']$ and to the right by its transpose, the Dini derivative (similar to that of Theorem 1 in [27]) along a trajectory of system (7.15)-(7.16) satisfies

$$D^+v(x) \;=\; \min_{l\in I(x)}\begin{bmatrix} x \\ w\end{bmatrix}'\begin{bmatrix} He\{A'_{\lambda i}P_l\} & * \\ H'P_l & 0\end{bmatrix}\begin{bmatrix} x \\ w\end{bmatrix}$$

$$\begin{aligned}
&\leq \begin{bmatrix} x \\ w \end{bmatrix}' \begin{bmatrix} He\{A'_{\lambda i}P_i\} & * \\ H'P_i & 0 \end{bmatrix} \begin{bmatrix} x \\ w \end{bmatrix} \\
&< -z'z + \rho w'w - \sum_{j=1}^{N} \lambda_j (P_j - P_i) \\
&< -z'z + \rho w'w - \sum_{j=1}^{N} \pi_{ji}(\lambda) x' P_j x \\
&< -z'z + \rho w'w
\end{aligned} \tag{7.22}$$

where $\sum_{j=1}^{N} \pi_{ji}(\lambda)x'P_jx \geq \sum_{j=1}^{N} \pi_{ji}(\lambda)x'P_ix = 0$ since $\Pi(\lambda) \in \mathcal{M}$ and $i \in \mathcal{I}(x(t))$, so that the last inequality is satisfied. Both sides of (7.22) are integrated from 0 to $+\infty$ considering that $V(x(0)) = 0$, the asymptotic stability of the origin requires that for $V(x(\infty)) \geq 0$, the following inequality is verified

$$\int_0^\infty z(t)'z(t)dt < \rho \int_0^\infty w(t)'w(t)dt \tag{7.23}$$

for all $w \in \mathcal{L}_2$. As a result, (7.6) satisfies and the proof is completed.

7.3.2 Switched H_∞ State Feedback Control

The system (7.4)- (7.5) is defined by the convex combination:

$$\begin{bmatrix} A & B_\lambda & H \\ E_\sigma & F_\sigma & G_\sigma \end{bmatrix} = \sum_{j \in \mathbb{K}} \lambda_j \begin{bmatrix} A & B_j & H \\ E_i & F_i & G_i \end{bmatrix}, i, j \in \mathbb{K} \times \mathbb{K} \tag{7.24}$$

where the matrices A, B_j, H, E_i, F_i, G_i for $i, j \in \mathbb{K} \times \mathbb{K}$ at the polytope vertex are known for the control law design and λ belongs to the unitary simplex $\wedge$. Now the conditions provided in Theorem 7.3.1 can be generalised to compute a number of state feedback gains $K_i \in \mathbb{R}^{m \times n}$, $\forall i \in \mathbb{K}$ and a min-switching strategy $\sigma(x) = i, \ \ i \in \mathbb{K}$ such that the closed-loop switched polytopic system is globally asymptotically stable and satisfies performance constraint (7.6).

Theorem* 7.3.2*: If there exist symmetric positive definite matrices S_i, $i \in \mathbb{K}$, matrices Y_i, positive scalars ρ and γ_i holding in the following modified Metzler inequalities:

$$\begin{bmatrix} He\{S_iA' + Y_i'B_j'\} - \gamma_i S_i & * & * & * \\ H' & -\rho I & * & * \\ E_iS_i + F_iY_i & G_i & -I & * \\ \gamma_i S_i & 0 & 0 & -\gamma_i S_j \end{bmatrix} < 0, \;\; i, j \in \mathbb{K} \times \mathbb{K} \tag{7.25}$$

then the min-switching strategy (7.12) with $P_i = S_i^{-1}$ $i \in \mathbb{K}$ and the state feedback gains $K_i = Y_iS_i^{-1}$ for all $i \in \mathbb{K}$ make the closed-loop polytopic system asymptotically stable, satisfying (7.6).

Proof. Performing the Schur Complement on the inequality (7.25) with respect to the third row and column, multiplying both sides of the result by diag$\{S_i^{-1}, I, I\}$ and then replacing the closed-loop matrices $(A + B_jK_i$, $E_i + F_iK_i)$ by (A_{ji}, E_i), one obtains

$$\begin{bmatrix} He\{A_{ji}'P_i\} + \gamma_i(P_j - P_i) & * & * \\ H'P_i & -\rho I & * \\ E_i & G_i & -I \end{bmatrix} < 0 \tag{7.26}$$

The inequality (7.26) reduces to (7.18). Therefore, the claim follows from Theorem 7.3.1. As a result (7.6) satisfies and the proof is concluded.

The feasibility of inequalities (7.25) requires that there exist state feedback gains $K_1, \ldots, K_N$ such that matrices $A_{ii} = A_i + B_iK_i$ are asymptotically stable for all $i \in \mathbb{K}$. This is an expected condition due to robust stability.

***Remark* 7:** The Lyapunov function (7.11) is not based on the uncertain parameter $\lambda \in \wedge$, the results of Theorem 7.3.2 can cope with time-varying systems without estimation of an uncertain reduction in an actuator's effectiveness.

***Remark* 8:** The inequalities (7.25) are difficult to solve due to the product of variables $\{\gamma_1, ..., \gamma_N\}$, $\{S_1, ..., S_N\}$ if the number of subsystems are greater than two. To overcome this difficulty, only one scalar variable, $\gamma = \gamma_i > 0$ is considered as the expense of a conservative solution. Therefore, the result of Theorem 7.3.2 remains valid whenever scalars γ_i are replaced by scalar $\gamma > 0$.

One potential disadvantage of the minimum switching strategy is chattering, which is an undesirable phenomenon stemming from infinitely fast switching. A tunable parameter, $\mu > 1$ will additionally be introduced to the results of Theorem 7.3.2 in order to reduce chattering. The stabilisation of switched systems using a relaxed min-switching strategy is illustrated in Fig. 7.3, where the solid line indicates the active system and dotted line denotes the inactive system. The switch occurs at point *a* using the min-switching strategy. However, the relaxed min-switching strategy allows the switch to occur at point b, where the difference is given by $x(t)'(\mu-1)P_jx(t)$. The current active controller index i is determined by the relaxed min-switching strategy shown in Fig.7.4. The following theorem is given using the relaxed minimum switching strategy so that the proposed approach is more attractive for implementation.

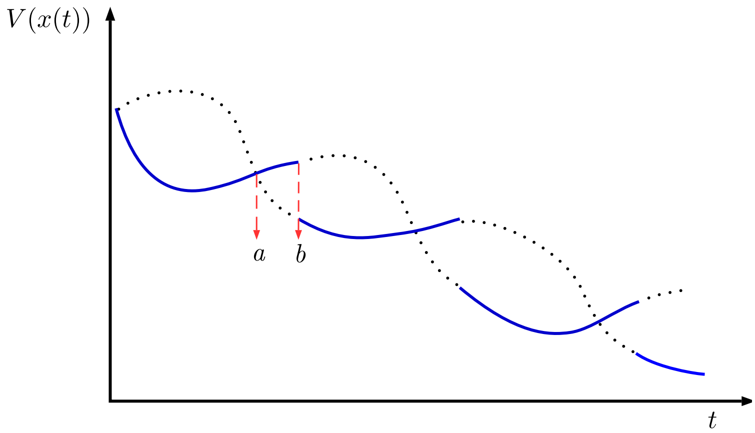

Figure 7.3: Lyapunov function values with the relaxed min-switching strategy, $N = 2$.

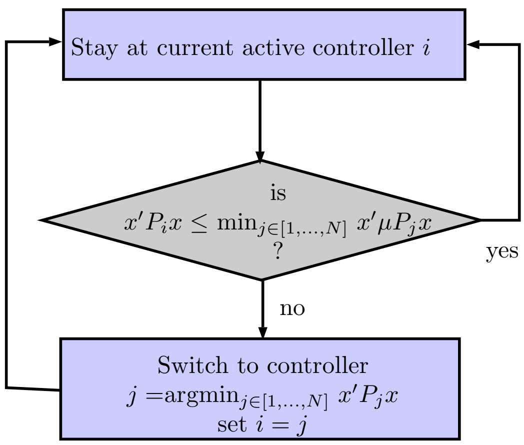

Figure 7.4: Relaxed min-switching strategy.

***Theorem* 7.3.3:** If there are symmetric positive definite matrices S_i for $i \in \mathbb{K}$, matrices Y_i, $i \in \mathbb{K}$ and positive scalars ρ, γ_i and $\mu > 1$ satisfying the modified Lyapunov-Metzler inequalities

$$\begin{bmatrix} He\{S_i A_q' + Y_i' B_q'\} - \gamma_i S_i & * & * & * \\ H_q' & -\rho I & * & * \\ E_i S_i + F_i Y_i & G_i & -I & * \\ \gamma_i \mu S_i & 0 & 0 & -\gamma_i \mu S_j \end{bmatrix} < 0, \;\; i \neq j \in \mathbb{K} \times \mathbb{K} \tag{7.27}$$

then the relaxed min-switching strategy,

$$\sigma(t) := \{i \in \mathbb{K} : x' S_i^{-1} x \leq \min_{j \in \mathbb{K}} \mu x' S_j^{-1} x\} \tag{7.28}$$

and the state feedback gains $K_i = Y_i S_i^{-1}$ for all $i \in \mathbb{K}$ make the closed-loop polytopic system globally asymptotically stable, satisfying (7.6).

Proof. The Schur complement is applied to (7.27) with respect to the last row and column. Multiplying both sides of the result by diag $\{S_i^{-1}, I, I\}$, denoted $P_i = S_i^{-1}$ and using the following associations $A_{ji} \longrightarrow (A + B_j K_i)$ and $E_i \longrightarrow (E_i + F_i K_i)$, we have

$$\begin{bmatrix} He\{A_{ji}' P_i\} + \gamma_i(\mu P_j - P_i) & * & * \\ H' P_i & -\rho I & * \\ E_i & G_i & -I \end{bmatrix} < 0, \;\; i, j \in \mathbb{K} \times \mathbb{K} \tag{7.29}$$

The feasibility of (7.29) requires the first diagonal block to be negative definite for the switched polytopic system to be asymptotic stable. Performing the Schur Complement to (7.29) with respect to the last row and column and rearranging the terms, we have

$$\begin{bmatrix} He\{A_{ji}' P_i\} & * \\ H' P_i & 0 \end{bmatrix} < - \begin{bmatrix} E_i' \\ G_i' \end{bmatrix} \begin{bmatrix} E_i & G_i \end{bmatrix} - \begin{bmatrix} \gamma_i(\mu P_j - P_i) & * \\ 0 & -\rho I \end{bmatrix}. \tag{7.30}$$

Multiplying by λ_j, and summing up for all terms, this yields

$$\begin{bmatrix} He\{A_{\lambda i}' P_i\} & * \\ H' P_i & 0 \end{bmatrix} < - \begin{bmatrix} E_i' \\ G_i' \end{bmatrix} \begin{bmatrix} E_i & G_i \end{bmatrix} - \begin{bmatrix} \gamma_i \sum_{j=1}^{N} \lambda_j (\mu P_j - P_i) & * \\ 0 & -\rho I \end{bmatrix} \tag{7.31}$$

Multiplying the left side of (7.31) by $[x' \quad w']$ and the right by its transpose, the Dini derivative along a trajectory of the system (7.15)-(7.16) satisfies

$$\begin{aligned}
D^+v(x) &\le \begin{bmatrix} x \\ w \end{bmatrix}' \begin{bmatrix} He\{A'_{\lambda i}P_i\} & * \\ H'P_i & 0 \end{bmatrix} \begin{bmatrix} x \\ w \end{bmatrix} \\
&< -z'z + \rho w'w - x' \left(\sum_{j=1}^{N} \lambda_j (\mu P_j - P_i) \right) x \\
&= -z'z + \rho w'w - x' \left(\gamma_i \sum_{j=1}^{N} \lambda_j (P_j - P_i) \right) x - x' \left(\gamma_i \sum_{j=1}^{N} \lambda_j (\mu - 1) P_j \right) x \\
&= -z'z + \rho w'w - x' \left(\sum_{j=1}^{N} \pi_{ji}(\lambda) P_j \right) x - x' \left(\gamma_i \sum_{j=1}^{N} \lambda_j (\mu - 1) P_j \right) x \\
&< -z'z + \rho w'w - x' \left(\sum_{j=1}^{N} \pi_{ji}(\lambda) P_j \right) x
\end{aligned}$$

$$\begin{aligned}
&< -z'z + \rho w'w - x' \left(\sum_{j=1}^{N} \pi_{ji}(\lambda) P_i \right) x \\
&= -z'z + \rho w'w
\end{aligned} \tag{7.32}$$

where $\sum_{j=1}^{N} \pi_{ji}(\lambda) x' P_j x \ge \sum_{j=1}^{N} \pi_{ji}(\lambda) x' P_i x$ since $\Pi(\lambda) \in \mathcal{M}$ and $i \in \mathcal{I}(x(t))$ so that the last inequality is satisfied. Integrating both sides of (7.32) from 0 to $+\infty$ and considering that $V(x(0)) = 0$, then the asymptotic stability of the origin requires that $V(x(\infty)) \ge 0$ and it can be concluded that

$$\int_0^\infty z(t)'z(t)dt < \rho \int_0^\infty w(t)'w(t)dt \tag{7.33}$$

for all $w \in \mathcal{L}_2$. As a result, (7.6) satisfies and the proof is concluded.

7.3.3 Switched H_∞ Dynamic Output Feedback Control

This section generalises the conditions of Theorem 7.3.1 to tackle the dynamic output feedback switched control design. The dynamic output feedback control design scheme consists of the determination of a switching rule, $\sigma(y(t))$, and a dynamic output feedback switching controller, $\mathbf{K}_\sigma$, given by the full-state space equations

$$\dot{x}_K(t) = A_{K\sigma(x_K)}x_K(t) + B_{K\sigma(x_K)}y(t) \tag{7.34}$$

$$u(t) = C_{K\sigma(x_K)}x_K(t) \tag{7.35}$$

such that for a given scalar $\rho > 0$, the equilibrium point of the closed-loop time-varying system is globally asymptotically stable with the initial condition $x(0) = 0$, and the inequality (7.6) holds. The difficulty here is to simultaneously compute the switched controller dynamics and the switching function that preserve stability and provide the desired performance.

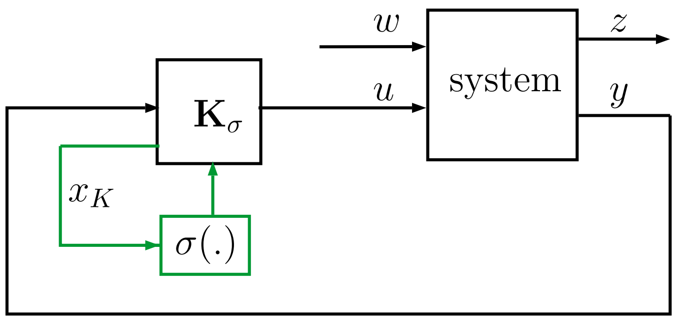

Figure 7.5: Closed-loop structure with the switched dynamic output control.

Connecting the system (7.1) and the switched controller (7.34)-(7.35) with $x(0) = 0$, as shown in Fig. 7.5, we have

$$\dot{x}_{cl}(t) = A_{cl,\lambda\sigma}x_{cl}(t) + H_{cl,\sigma}w(t)(t) \tag{7.36}$$

$$z(t) = E_{cl,\sigma}x_{cl}(t) + G_{cl,\sigma}w(t) \tag{7.37}$$

where $x_{cl} = [x(t)' \;\; x_K(t)']' \in \mathbb{R}^{2n}$, $G_{cl,\sigma} = G_\sigma$ and

$$A_{cl,\lambda\sigma} = \begin{bmatrix} A & B_\lambda C_{K\sigma} \\ B_{K\sigma}C & A_{K\sigma} \end{bmatrix}, \quad H_{cl,\sigma} = \begin{bmatrix} H \\ B_{K\sigma}D \end{bmatrix}, \quad E_{cl,\sigma} = \begin{bmatrix} E'_\sigma \\ C'_{K\sigma}F'_\sigma \end{bmatrix}' \tag{7.38}$$

where $\sigma = i \in \mathbb{K}$. The closed-loop system matrices reside within the following polytope:

$$\begin{bmatrix} A_{cl,\lambda\sigma} & H_{cl,\sigma} \\ E_{cl,\sigma} & G_{cl,\sigma} \end{bmatrix} = \sum_{j\in\mathbb{K}} \lambda_j \begin{bmatrix} A_{cl,j\,i} & H_{cl,i} \\ E_{cl,i} & G_{cl,i} \end{bmatrix}, i, j \in \mathbb{K} \times \mathbb{K} \tag{7.39}$$

where

$$A_{cl,j\,i} = \begin{bmatrix} A & B_j C_{Ki} \\ B_{Ki} C & A_{Ki} \end{bmatrix}, \quad H_{cl,\,i} = \begin{bmatrix} H \\ B_{Ki} D \end{bmatrix}, \quad E_{cl,\,i} = \begin{bmatrix} E_i' \\ C_{Ki}' F_i' \end{bmatrix}' \tag{7.40}$$

and $G_{cl,\,i} = G_i$ are defined for all $i, j, \in \mathbb{K} \times \mathbb{K}$. The aim here is to determine matrices (A_{Ki}, B_{Ki}, C_{Ki}) and the switching rule $\sigma(x_K)$ such that the closed-loop system holds for the conditions of Theorem 7.18. The inequalities (7.18) with ($A_{cl,\,j,\,i}$, $H_{cl,\,i}$,$E_{cl,i}$, $G_{cl,i}$) instead of (A_i, H_i, E_i, G_i) for all $i \in \mathbb{K}$ have to be satisfied for some augmented positive definite matrix $\tilde{P}_i \in \mathbb{R}^{2n \times 2n}$ with the structure

$$\tilde{P}_i = \begin{bmatrix} Y & V \\ V' & \hat{Y}_i \end{bmatrix}, \quad \det(V) \neq 0 \tag{7.41}$$

which makes the min-switching strategy dependent on the measured output. The min-switching strategy provided in Theorem 7.3.1 is such that

$$\arg\min_{i \in \mathbb{K}} x_{cl}'\, \tilde{P}\, x_{cl} = \arg\min_{i \in \mathbb{K}} x_K'\, \hat{Y}_i\, x_K = \sigma(x_K) \tag{7.42}$$

such that it depends only on the measured output $y(t)$ via the controller state variable $x_K(t)$. This structure is mandatory whenever a switching function is imposed, particularly when it is based on a controller state variable. Before giving the conditions to be used to synthesise a dynamic output feedback switching controller, we need the results presented in the next lemmas.

Lemma* 7.3.3** ([29]):*** Let a non-singular matrix V and symmetric matrices Y and X_i for all $i \in \mathbb{K}$ hold

$$\begin{bmatrix} Y & * \\ I & X_i \end{bmatrix} > 0, i \in \mathbb{K}. \tag{7.43}$$

It is possible to determine non-singular matrices U_i and symmetric matrices $\hat{Y}_i$ and $\hat{X}_i$ for all $i \in \mathbb{K}$ such that

$$\tilde{P}_i = \tilde{S}_i^{-1} = \begin{bmatrix} Y & * \\ V' & \hat{Y}_i \end{bmatrix} > 0, \tilde{S}_i = \begin{bmatrix} X_i & * \\ U_i' & \hat{X}_i \end{bmatrix} > 0, i \in \mathbb{K} \tag{7.44}$$

Proof. Using the above three conditions, $X_iY + U_iV' = I$, $X_iV + U_i\hat{Y}_i = 0$ and $U_i'Y + \hat{X}_iV' = 0$, one obtains $U_i = (I - X_iY)V'^{-1}$, $\hat{Y}_i = V'(Y - X_i^{-1})^{-1}V$, $\hat{X}_i = V^{-1}(YX_iY - Y)V'^{-1}$ and $U'V + \hat{X}_i\hat{Y}_i = I$. The full-rank matrix, Γ, is defined by

$$\Gamma = \begin{bmatrix} Y & I \\ V' & 0 \end{bmatrix} \tag{7.45}$$

that linearises the product $\Gamma'\tilde{S}_i\Gamma$, which is equal to (7.43).

Lemma* 7.3.4** ([162]):*** For any matrices X, Y with compatible dimensions and scalar $\epsilon > 0$, the following inequality satisfies:

$$X'Y + Y'X \leq \epsilon X'X + (1/\epsilon)Y'Y. \tag{7.46}$$

Lemmas 7.3.3 and 7.3.4 are essential to derive the following theorem.

Theorem* 7.3.4*: For the augmented closed-loop switched polytopic system (7.36)-(7.37) and given $\rho > 0$, there exist matrices A_{Ki}, B_{Ki} and C_{Ki} for all $i \in \mathbb{K}$ such that (7.18) holds for some positive definite matrices $\tilde{P}_i$ of the form (7.41) if there exist symmetric positive definite matrices Y, X_i for all $i \in \mathbb{K}$, symmetric matrices Z_{ij}, matrices N_i, L_i, W_i for all $i, j \in \mathbb{K} \times \mathbb{K}$, and if the chosen scalars γ_i and ϵ satisfy the inequalities

$$\begin{bmatrix} \Upsilon_{11i} + He\{(B_j - B_i)W_i\} - \epsilon I & * & * & * \\ A + N_i' & \Upsilon_{22ij} + \gamma_i Z_{ij} + 2Y - \epsilon^{-1}I & * & * \\ H'Y + D'L_i' & H' & -\rho I & * \\ E_i & E_iX_i + F_iW_i & G_i & -I \end{bmatrix} < 0 \tag{7.47}$$

with $\Upsilon_{11i} = He\{YA + L_iC\}$ and $\Upsilon_{22ij} = He\{AX_i + B_jW_i\}$

$$\begin{bmatrix} Z_{ij} + X_i & * & * \\ X_i & X_j & * \\ I & I & Y \end{bmatrix} > 0 \tag{7.48}$$

for all $i, j \in \mathbb{K} \times \mathbb{K}$.

When (7.47) and (7.48) are satisfied, the output feedback min-switching strategy given by $\sigma(x_K) = \arg\min_{i\in\mathbb{K}} x_K'V'(Y - X_i^{-1})^{-1}Vx_K$ and the full-order dynamic output feedback controller can be defined by

$$A_{Ki} = V^{-1}(N_i - YAX_i - YB_iW_i - L_iCX_i)(I - YX_i)^{-1}V \tag{7.49}$$
$$B_{Ki} = V^{-1}L_i \tag{7.50}$$
$$C_{Ki} = W_i(I - YX_i)^{-1}V \tag{7.51}$$

in which V is an arbitrary non-singular matrix that assures the closed-loop system is globally asymptotically stable and satisfies (7.6).

Proof. Performing a congruence transformation with matrices diag $\{\Gamma'\tilde{S}_i, I, I\}$ on condition (7.18), the following matrices are obtained for all $i, j \in \mathbb{K} \times \mathbb{K}$

$$\Gamma'\tilde{S}_i\Gamma = \begin{bmatrix} Y & * \\ I & X_i \end{bmatrix} \tag{7.52}$$
$$\Gamma' A_{cl,ji}\tilde{S}_i\Gamma = \begin{bmatrix} YA + L_iC & N_i + Y(B_j - B_i)W_i \\ A & AX_i + B_jW_i \end{bmatrix} \tag{7.53}$$
$$E_{cl,i}\tilde{S}_i\Gamma = \begin{bmatrix} E_i & E_iX_i + F_iW_i \end{bmatrix} \tag{7.54}$$
$$\Gamma' H_{cl,i} = \begin{bmatrix} YH + L_iD \\ H \end{bmatrix} \tag{7.55}$$

where we use the one-to-one change of variables, $N_i = VA_{Ki}U_i' + YAX_i + YB_iW_i + L_iCX_i$, $L_i = VB_{Ki}$ and $W_i = C_{Ki}V^{-1}(I - YX_i)$ from (7.49) -(7.51) and the equality $U_i' = V^{-1}(1 - YX_i)$ can be obtained from the fact that $\tilde{S}_i^{-1} = \tilde{P}_i$. Additionally, we have

$$\begin{aligned} \Gamma'\tilde{S}_i(\tilde{P}_j - \tilde{P}_i)\tilde{S}_i\Gamma &= \Gamma'(\tilde{S}_i\tilde{S}_j^{-1}\tilde{S}_i - \tilde{S}_i)\Gamma = \Gamma'((\tilde{S}_i - \tilde{S}_j)\tilde{S}_j^{-1}(\tilde{S}_i - \tilde{S}_j) + (\tilde{S}_i - \tilde{S}_j))\Gamma \\ &= \Gamma'(\tilde{S}_i - \tilde{S}_j)\Gamma(\Gamma\tilde{S}_j\Gamma')^{-1}\Gamma'(\tilde{S}_i - \tilde{S}_j)\Gamma + \Gamma'(\tilde{S}_i - \tilde{S}_j)\Gamma \\ &= \begin{bmatrix} 0 & 0 \\ 0 & \hat{Z}_{ij} \end{bmatrix} \end{aligned} \tag{7.56}$$

with $\hat{Z}_{ij} = (X_i - X_j) + (X_i - X_j)(X_j - Y^{-1})^{-1}(X_i - X_j)$, where $(\Gamma'\tilde{S}_j\Gamma)^{-1}$ is calculated by using the matrix inverse lemma as:

$$(\Gamma'\tilde{S}_j\Gamma)^{-1} = \begin{bmatrix} Y & * \\ I & X_j \end{bmatrix}^{-1} = \begin{bmatrix} (Y - X_j^{-1})^{-1} & -Y^{-1}(X_j - Y^{-1})^{-1} \\ -X_j^{-1}(Y - X_j^{-1})^{-1} & (X_j - Y^{-1})^{-1} \end{bmatrix} \quad (7.57)$$

On the other hand, if the Schur Complement is performed twice with respect to the last two block diagonal elements of (7.48), then the following inequality is obtained as:

$$\begin{aligned} Z_{ij} &> Y^{-1} - X_i + (X_i - Y^{-1})(X_j - Y^{-1})^{-1}(X_i - Y^{-1}) &(7.58)\\ &= (X_i - X_j) + (X_i - X_j)(X_j - Y^{-1})^{-1}(X_i - X_j) &(7.59)\end{aligned}$$

which implies that $Z_{ij} > \hat{Z}_{ij}$, where the equality (7.59) is obtained from the inequality (7.58) by writing $(X_i - Y^{-1}) = (X_i - X_j) + (X_j - Y^{-1})$ and performing the appropriate multiplications. By algebraic manipulation, conditions in (7.18) become

$$\begin{bmatrix} \Upsilon_{11i} & * & * & * \\ A + N_i' + Y(B_j - B_i)W_i & \Upsilon_{22ij} + \gamma_i Z_{ij} & * & * \\ H'Y + D'L_i' & H' & -\rho I & * \\ E_i & E_iX_i + F_iW_i & G_i & -I \end{bmatrix}$$

$$= \underbrace{\begin{bmatrix} \Upsilon_{11i} & * & * & * \\ A + N_i' & \Upsilon_{22ij} + \gamma_i Z_{ij} & * & * \\ H'Y + D'L_i' & H' & -\rho I & * \\ E_i & E_iX_i + F_iW_i & G_i & -I \end{bmatrix}}_{\Sigma_{ij}} + \begin{bmatrix} 0 & * & * & * \\ Y(B_j - B_i)W_i & 0 & * & * \\ 0 & 0 & 0 & * \\ 0 & 0 & 0 & 0 \end{bmatrix}$$

$$= \Sigma_{ij} + \begin{bmatrix} 0 \\ Y \\ 0 \\ 0 \end{bmatrix} \begin{bmatrix} (B_j - B_i)W_i & 0 & 0 & 0 \end{bmatrix} + \begin{bmatrix} W_i'(B_j' - B_i') \\ 0 \\ 0 \\ 0 \end{bmatrix} \begin{bmatrix} 0 & Y & 0 & 0 \end{bmatrix} \quad (7.60)$$

Recalling Lemma 7.3.4 and taking into account the fact that $T'R^{-1}T \geqslant T + T' - R$ for

$T \in \mathbb{R}^{n\times n}$ and $R' = R > 0$, see [50], then the equivalent condition to (7.60) becomes

$$\begin{aligned}
&\leq \quad \Sigma_{ij} + \epsilon \begin{bmatrix} 0 \\ Y \\ 0 \\ 0 \end{bmatrix} \begin{bmatrix} 0 & Y & 0 & 0 \end{bmatrix} + \epsilon^{-1} \begin{bmatrix} W_i'(B_j' - B_i') \\ 0 \\ 0 \\ 0 \end{bmatrix} \begin{bmatrix} (B_j - B_i)W_i & 0 & 0 & 0 \end{bmatrix} \\
&\geqslant \quad \Sigma_{ij} + \begin{bmatrix} 0 & * & * & * \\ 0 & 2Y - \epsilon^{-1}I & * & * \\ 0 & 0 & 0 & * \\ 0 & 0 & 0 & 0 \end{bmatrix} + \begin{bmatrix} W_i'(B_j' - B_i') + (B_j - B_i)W_i - \epsilon I & * & * & * \\ 0 & 0 & * & * \\ 0 & 0 & 0 & * \\ 0 & 0 & 0 & 0 \end{bmatrix}
\end{aligned} \tag{7.61}$$

The above inequality yields exactly to the condition (7.47). Furthermore, as given in [29], the switching function is given by (7.42), where $\hat{Y}_i = V'(Y - X_i^{-1})^{-1}V$ with non-singular matrix V due to fact that $\tilde{S}_i\tilde{S}_i^{-1} = I$ from Lemma 7.3.3. The proof of the proposed theorem is concluded.

The switched H_∞ controller was designed due to the requirement for robustness under time-varying actuator faults and model uncertainties. On the other hand, H_2 control theory is effective in coping with noise perturbations acting on each input channel and is appealing in terms of obtaining a better transient performance [32]. Therefore, in order to evaluate the performance of the switched H_∞ state feedback controller, in the following section we will represent a switched H_2 state feedback control from the work of [30].

7.4 Switched H_2 Control

In this section, a set of state feedback gains and a switching rule are determined to deal with time-varying polytopic systems and preserve the globally asymptomatic stability of the closed-loop system by minimising H_2 performance. A general model of the system (7.1) can be described by

$$\dot{x}(t) = Ax(t) + B_{\lambda(t)}u(t) + Hw(t), \quad x(0) = 0 \tag{7.62}$$

$$z_2(t) = E_{2\sigma(x)}x(t) + F_{2\sigma(x)}u(t) \tag{7.63}$$

In Fig. 7.1, the control law is connected to the system (7.62)-(7.63) and applying the external input $w(t) = e_k\delta(t)$ in which e_k is the k-th column of the $n \times n$ identity matrix, the output signal $z_k(t)$ for all $t \geq 0$ is found that generates the following worst case H_2 performance [30, 51]:

$$J(K_1, \ldots, K_N, \sigma) = \max_{\lambda(t)\in\wedge} \sum_{k=1}^{n} ||z_k(t)||_2^2 \tag{7.64}$$

The cost (7.64) is equal to the maximum H_2 squared norm with respect to $\lambda \in \wedge$ of the closed-loop transfer function from the input w to the output z. Therefore, the switching rule and a set of gains $\{K_1, \ldots, K_N\}$ are jointly computed to solve the optimal control problem

$$\min_{K_1,\ldots,K_N,\sigma} J(K_1, \ldots, K_N, \sigma). \tag{7.65}$$

An upper bound to $J(.)$ is considered here to define a guaranteed H_2 cost problem that can be solved by an available LMI solver.

7.4.1 Stability Analysis

In order to analyse stability of a time-varying switched polytopic system under the H_2 norm constraint, consider the time-varying switched polytopic system is

$$\begin{aligned} \dot{x}(t) &= A_{\lambda(t)\sigma(x)}x(t), \qquad x(0) = x_0 \\ z(t) &= E_{\sigma(x)}x(t) \end{aligned} \tag{7.66}$$

where

$$A_{\lambda(t)\sigma(x)} = \sum_{j=1}^{N} \lambda_j(t)A_{j\sigma(x)} \tag{7.67}$$

for some $\sigma(.) \in \mathbb{K}$, $\lambda(t) \in \wedge$ and $E_\sigma \in \{E_1, \ \ldots, \ E_N\}$. As mentioned before, the first sub-index refers to the polytope vertex, whilst the second denotes the switching rule.

As in the previous section, using the parameter-dependent Metzler matrices given in (7.7), the next theorem is given for the stability conditions and performance criterion for the system (7.66).

Theorem* 7.4.1** ([30]):*** Consider symmetric positive definite matrices P_i and scalar $\gamma_i > 0$ for all $i \in \mathbb{K}$ satisfying the modified Lyapunov-Metzler inequalities

$$\begin{bmatrix} A'_{ji}P_i + P_iA_{ji} + \gamma_i(P_j - P_i) & E'_{2i} \\ * & -I \end{bmatrix} < 0 \tag{7.68}$$

for all $i, j \in \mathbb{K} \times \mathbb{K}$, then the state-dependent switching function

$$\sigma(x) = \arg\min_{i\in\mathbb{K}} x'P_ix \tag{7.69}$$

makes the equilibrium solution $x = 0$ of the system (7.66) globally asymptotically stable and the inequality

$$\max_{\lambda\in\wedge} \int_0^\infty z(t)'z(t)dt < \min_{i\in\mathbb{K}} x'_oP_ix_0 \tag{7.70}$$

holds.

7.4.2 Switched H_2 State Feedback Control

Based on the analysis results in the previous subsection, it is now possible to give the following theorem to compute the gains for the switched H_2 state feedback control.

Theorem* 7.4.2** ([30]):*** Consider symmetric positive definite matrices X_i, matrices Y_i and positive scalars γ_i satisfying the following inequalities

$$\begin{bmatrix} He\{X_iA' + Y_i'B_j'\} - \gamma_iX_i & * & * \\ E_{2i}X_i + F_{2i}Y_i & -I & * \\ \gamma_iX_i & 0 & -\gamma_iX_j \end{bmatrix} < 0, \quad \forall\, i,\ j \in \mathbb{K}\times\mathbb{K}, \tag{7.71}$$

then the state feedback switched control with $K_i = Y_iX_i^{-1}$ for $i \in \mathbb{K}$ and the switching function (7.12) with $P_i = X_i^{-1}$ $i \in \mathbb{K}$ make the equilibrium solution $x = 0$ of system ((7.62)-(7.63)) globally asymptotically stable and

$$J(K_1, \ldots K_{N,\sigma}) < \min_{i\in\mathbb{K}} Tr(H'X_i^{-1}H) \tag{7.72}$$

The best guaranteed cost is obtained by solving the following optimisation problem:

$$\min_{i\in\mathbb{K}} \inf_{\gamma>0,\mathcal{X}\in\Upsilon} \left\{ Tr(W_i) : \begin{bmatrix} W_i & * \\ H & X_i \end{bmatrix} > 0 \quad \forall i \in \mathbb{K} \right\} \tag{7.73}$$

where $\mathcal{X} = \{X_1, Y_1, \ldots, X_N, Y_N\}$ contains the matrix variable and Υ is the set of all feasible solutions of inequalities (7.71).

***Remark* 9:** Theorem 7.4.2 is difficult to implement when the number of subsystems is greater than one. As mentioned before, considering $\gamma_i = \gamma > 0$ is reduced in complexity at the expense of conservatism. The result of Theorem 7.4.2 remains valid whenever scalars γ_i are replaced by scalar $\gamma > 0$.

Now, in order to reduce the chattering, the results of Theorem 7.4.2 can be modified including a tunable parameter as given in the following theorem.

***Theorem* 7.4.3:** If symmetric positive definite matrices X_i, matrices Y_i and positive scalars γ_i and $\mu > 1$ satisfy the following inequalities

$$\begin{bmatrix} He\{X_iA' + Y_i'B_j'\} - \gamma_i X_i & * & * \\ E_{2i}X_i + F_{2i}Y_i & -I & * \\ \gamma_i \mu X_i & 0 & -\gamma_i \mu X_j \end{bmatrix} < 0, \quad \forall\, i,\, j \in \mathbb{K}\times\mathbb{K}, \tag{7.74}$$

then the state feedback switched control with $K_i = Y_i X_i^{-1}$ for $i \in \mathbb{K}$ and the relaxed min-switching strategy,

$$\sigma(t) := \{i \in \mathbb{K} : x'X_i^{-1}x \le \min_{j\in\mathbb{K}} \mu x' X_j^{-1} x\} \tag{7.75}$$

make the equilibrium solution $x = 0$ of system (7.62)-(7.63) globally asymptotically stable and (7.72).

Proof. Apply the Schur Complement to inequality (7.74) with respect to the last row and column, denoting $P_i = X_i^{-1} > 0$ for all $i \in \mathbb{K}$. Multiplying both sides of the result by $\text{diag}\{X_i^{-1}, I\}$ and using the associations $A_{ji} \longrightarrow (A + B_jK_i)$ and $E_{2i} \longrightarrow (E_{2i} + F_{2i}K_i)$, we have

$$\begin{bmatrix} A'_{ji}P_i + P_iA_{ji} + \gamma_i(\mu P_j - P_i) & E'_{2i} \\ * & -I \end{bmatrix} \tag{7.76}$$

Applying the Schur Complement to the inequality (7.76) and denoting $Q_i \longrightarrow E'_{2i}E_{2i}$, Theorem 7.4.1 reduces to the following inequality

$$A'_{ji}P_i + P_iA_{ji} + Q_i + \gamma_i(\mu P_j - P_i) < 0 \tag{7.77}$$

Multiplying the result by $\lambda_j \geq 0$ and summing up over all terms, one obtains

$$A'_{\lambda i}P_i + P_iA_{\lambda i} + Q_i + \gamma_i \sum_{j=1}^{N} \lambda_j(\mu P_j - P_i) < 0 \tag{7.78}$$

and from the property of the *sum* operator and in light of the relaxed switching rule (7.75), it can be verified that

$$\begin{aligned} A'_{\lambda i}P_i + P_iA_{\lambda i} + Q_i &< -\gamma_i \sum_{j=1}^{N} \lambda_j(\mu P_j - P_i) \\ &= -\gamma_i \sum_{j=1}^{N} \lambda_j(P_j - P_i) - \gamma_i \sum_{j=1}^{N} \lambda_j(\mu - 1)P_j \\ &= -\sum_{j=1}^{N} \pi_{ji}(\lambda)P_j - \gamma_i \sum_{j=1}^{N} \lambda_j(\mu - 1)P_j \\ &< -\sum_{j=1}^{N} \pi_{ji}(\lambda)P_i = 0 \end{aligned} \tag{7.79}$$

Integrating both sides of 7.79 yields

$$\int_0^\infty \dot{V}(x(t)))dt = V(x(\infty)) - V(x(0) < \int_0^\infty x(t)'Q_ix(t)dt \tag{7.80}$$

The asymptotic stability of the origin implies that $V(x(\infty)) \geq 0$, which readily verifies the inequality

$$\int_0^\infty z(t)'z(t)dt = \int_0^\infty x(t)'Q_{\sigma(x(t)))}x(t)dt < \min_{i\in\mathbb{K}} x_0'P_ix_0 \tag{7.81}$$

holds for all $i \in \mathbb{K}$ with $\Pi(\lambda) \in \mathcal{M}$. Consequently, the proof can be completed by following that of Theorem 7.4.1.

The theorems represented above are valid if $\gamma_i = \gamma > 0$ for all $i \in \mathbb{K}$ at the expense of more conservative but easier to solve conditions. The problem of switched control in the presence of time-varying faults reduces to finding a solution to a finite number of LMIs under H_∞ or H_2 performance, which can be done efficiently using the YALMIP interface [90] with the solver SDPT3 [141].

7.5 Switched Fault Tolerant Control Designs

In this section, the main control objective is to enable the quadcopter to track given inertial velocities ensuring stability, despite the occurrence of an undetected motor fault. To achieve this, a double-loop control structure with an integral action is proposed, as shown in Fig. 7.6. For the design, the dynamics are linearised at hover. The inner loop (rotational dynamics) includes a switched H_∞ or H_2 controller, which is switched according to a min-switch strategy $\sigma(t)$. The outer loop, which includes the translational dynamics, is controlled with a proportional-integral controller and produces pitch and roll commands for the inner-loop control system. As a result, pitch and roll commands have to be tracked well. This can be achieved by extending the rotational dynamic with the integrated errors in the Euler angles.

A new state vector e_η is defined to represent the tracking errors for the reference commands given in Fig. 7.6, $e_\eta = [\phi_d \quad \theta_d \quad \psi_d]' - [I_{3\times3} \quad 0_{3\times3}]x$. The integral of this error vector is

$$\bar{e}_\eta = \int_0^\infty e_\eta dt. \tag{7.82}$$

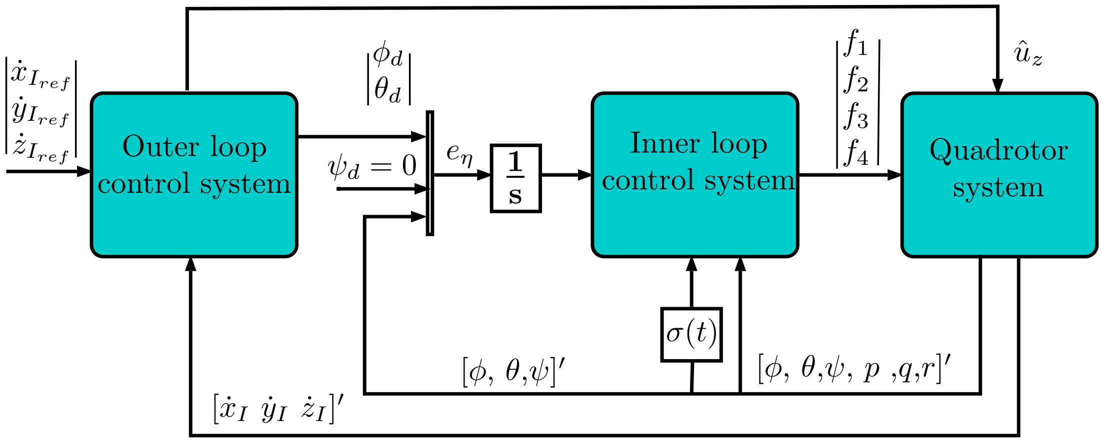

Figure 7.6: An overview of the control structure.

The original system is expanded to include the new states as follows:

$$\begin{bmatrix}\dot{x}\\ \dot{\bar{e}}_\eta\end{bmatrix} = \underbrace{\begin{bmatrix}A & 0_{6\times3}\\ -I_{3\times6} & 0_{3\times3}\end{bmatrix}}_{\tilde{A}} \begin{bmatrix}x\\ \bar{e}_\eta\end{bmatrix} + \underbrace{\begin{bmatrix}B_{\lambda(t)}\\ 0_{3\times4}\end{bmatrix}}_{\tilde{B}_{\lambda(t)}} u + \underbrace{\begin{bmatrix}H\\ 0_{3\times4}\end{bmatrix}}_{\tilde{H}} w + \begin{bmatrix}0_{6\times3}\\ I_{3\times3}\end{bmatrix} r_{ref} \tag{7.83}$$

Using the under-brace notations in (7.83) and setting $r_{ref} = [\phi_d\ \theta_d\ \psi_d]' = 0$, the augmented rotational model subject to time-varying motor faults can be simplified as

$$\dot{\tilde{x}} = \tilde{A}\tilde{x} + \tilde{B}_{\lambda(t)}u + \tilde{H}w \tag{7.84}$$

$$\tilde{z} = \tilde{E}_\sigma\tilde{x} + \tilde{F}_\sigma u + \tilde{G}_\sigma w \tag{7.85}$$

where $\tilde{H}$ is the disturbance matrix. The state vector is $\tilde{x} = [\phi\ \ \theta\ \ \psi\ \ p\ \ q\ \ r\ \ e_\eta]$, where e_η is the error vector between the reference and measured Euler angles and the input vector $u = [f_1\ \ f_2\ \ f_3\ \ f_4]'$. $\tilde{z}$ is the controlled output that depends on matrices $\tilde{E}_\sigma$, $\tilde{F}_\sigma$ and $\tilde{G}_\sigma$. The system (7.84)-(7.85) can be rewritten as

$$\begin{bmatrix}\tilde{A} & \tilde{B}_\lambda & \tilde{H}\\ \tilde{E}_\sigma & \tilde{F}_\sigma & \tilde{G}_\sigma\end{bmatrix} = \sum_{j\in\mathbb{K}} \lambda_j \begin{bmatrix}\tilde{A} & \tilde{B}_j & \tilde{H}\\ \tilde{E}_i & \tilde{F}_i & \tilde{G}_i\end{bmatrix}, i,j \in \mathbb{K}\times\mathbb{K}. \tag{7.86}$$

The switched inner loop controller designs are described in the following sections for the system of (7.86).

Design procedure of the outer-loop control system have already been shown in Chap-

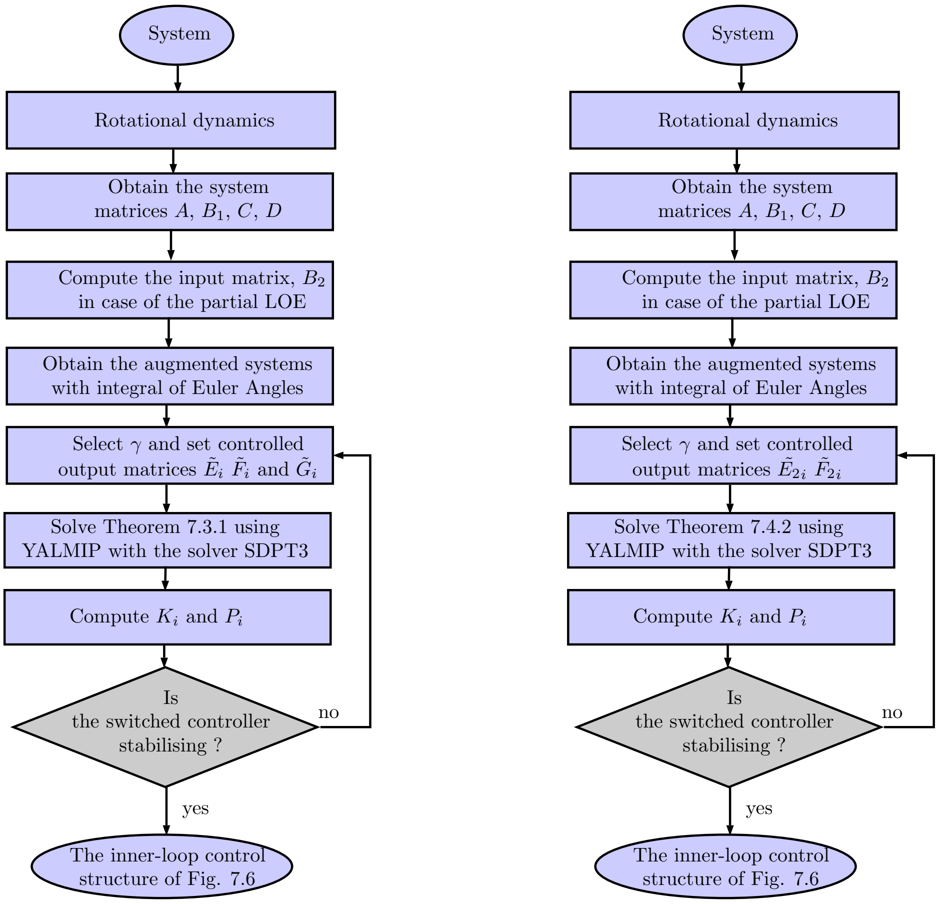

(a) Switched H_∞ Controller (b) Switched H_2 Controller

Figure 7.7: Flow diagrams of the switched state feedback controller designs.

ter 6. Therefore, design procedures of the switched H_∞ and H_2 state feedback controllers with the min-switching strategy are only shown in Figs. 7.7b and 7.7a. Flow digram of designing switched controllers with the relaxed min-switching strategy will flow a similar procedure by using Theorems 7.3.3 and 7.4.3 that require selection of parameter μ.

7.5.1 Switched H_∞ State Feedback Control

The LMIs of Theorem 7.3.2 are solved by considering the system (7.84)-(7.85). An input disturbance matrix is taken into consideration as $\tilde{H} = \tilde{B}_j$, for $j = 1$.

Using Bryson's rule [76], the maximum allowable deviations to the Euler angles, ϕ, θ, ψ, for a fault case are greater than those in a fault-free case. Therefore, the diagonal elements of $\tilde{E}_i$ corresponding to the Euler angles during a fault are allowed to be smaller than those in the fault-free case. Input weights $\tilde{F}_i$ are selected considering the effects of the control input forces; larger values of $\tilde{F}_i$ lead to a stricter limit on the control input signal.

The quadcopter system has an input coupling, i.e., f_1 and f_3 affect the pitch orientation while f_1, f_2, f_3 and f_4 influence the yaw orientation. Hence, the off-diagonal elements of matrices $\tilde{F}_i$ should be selected such that they impose a reduced penalty on the faulty motor. As a result, the controlled output matrices in (7.86) have been selected as follows:

$$\tilde{F}_{1_\infty} = 2\begin{bmatrix} 0 & -1 & 0 & 1 \\ -1 & 0 & 1 & 0 \\ 1 & 1 & 1 & 1 \\ 0 & -1 & 0 & 1 \\ -1 & 0 & 1 & 0 \\ 1 & 1 & 1 & 1 \\ 0 & -1 & 0 & 1 \\ -1 & 0 & 1 & 0 \\ 1 & 1 & 1 & 1 \end{bmatrix}, \quad \tilde{F}_{2_\infty} = 2\begin{bmatrix} 0 & -1 & 0 & 1 \\ -1 & 0 & 0.1 & 0 \\ 1 & 1 & 0 & 1 \\ 0 & -1 & 0 & 1 \\ -1 & 0 & 0.1 & 0 \\ 1 & 1 & 0.1 & 1 \\ 0 & -1 & 0 & 1 \\ -1 & 0 & 0.1 & 0 \\ 1 & 1 & 0.1 & 1 \end{bmatrix} \tag{7.87}$$

$$\begin{aligned} \tilde{E}_{1_\infty} &= \text{diag}\{6, 6, 6, 0.01, 0.01, 0.01, 5, 5, 5\}, \\ \tilde{E}_{2_\infty} &= \text{diag}\{1, 1, 1, 0.01, 0.01, 0.01, 5, 5, 5\} \end{aligned} \tag{7.88}$$

$$\tilde{G}_{1_\infty} = 0.05\tilde{F}_{1_\infty}, \;\; \tilde{G}_{2_\infty} = 0.0.5\tilde{F}_{1_\infty} \tag{7.89}$$

Solving the LMIs in (7.25) yields $\rho = 21.70$ with $\gamma = 400$ found by line search. Using the same controlled output matrices, the conditions of Theorem 7.3.3 are solved with $\mu = 1.09$ and $\gamma = 100$ found by line search. This results in a performance index of $\rho = 23.0568$. Notice that the performance index increases by a lower value of γ when the relaxed minimum strategy is used. The conditions of Theorem 7.3.3 can reduce the chattering on the control input signals at the expense of closed-loop tracking performance.

7.5.2 Switched H_2 State Feedback Control

As previously, Theorem 7.4.2 is valid if $\gamma_i = \gamma > 0$ for all $i \in \mathbb{K}$. The disturbance matrix is assumed to be $\tilde{H} = [0.1\ 0.1\ 0.5\ \ 0\ 0\ 0\ 0.1\ 0.1\ 0.5]$. Using Bryson's rule, the matrices in (7.86) are chosen as follows:

$$\tilde{E}_{1_2} = \tilde{E}_{1_\infty}, \quad \tilde{E}_{2_2} = \tilde{E}_{2_\infty} \tag{7.90}$$

and

$$\tilde{F}_{1_2} = 0.5\tilde{F}_{1_\infty}, \ \tilde{F}_{2_2} = 0.5\tilde{F}_{2_\infty} \tag{7.91}$$

Solving the LMIs in (7.71) yields the minimum guaranteed cost $J(K_1, K_2, \sigma) \leq 3.05$ with $\gamma = 200$ found by line search. Now, using those controlled output matrices once again, the conditions of Theorem 7.4.3 are solved with the tunable parameters $\mu = 1.1$ and $\gamma = 20$ found by line search. This results in a performance index of 10.8578. Theorem 7.4.3 can also reduce chattering at the expense of increasing the performance index. The associated simulation results are given in Section 7.6.

7.5.3 Constant H_2 State Feedback Control

Now, for comparison purposes, a constant state feedback H_2 controller is designed using the function *msfsyn* in MATLAB. This computes multi-objective H_2 state-feedback controllers that robustly enforce the specifications over the entire polytope of the plants. For simplicity, the prescribed LMI region $\mathcal{D}$ is chosen as a half-plane pole placement constraint $x_c < -4$, and it is included in the design to provide a fast transient response. With suitable weighting matrices, the LMI optimisation gives an H_2 performance index of 2.82.

7.5.4 Switched H_∞ Dynamic Output Feedback Control

This section presents a switched H_∞ dynamic output feedback control design. This control scheme depends on the measured output $y(t) = [\phi \ \ \theta \ \ \psi]$. The double-loop control structure of Fig. 7.6 is modified as given in Fig. 7.8. Design procedure of the switched H_∞ dynamic output feedback controller with the min-switching strategy is shown in Fig. 7.9. Here, we assume that only the Euler angles (ϕ, θ, ψ) and inertial translational velocities (x_I, y_I, z_I) are accessible, as considered in Chapter 6.

The input disturbance matrix, $H = B_j$, for $j = 1$ is considered as before. It is assumed that roll, pitch and yaw angles are measurable and the effects of any input disturbances

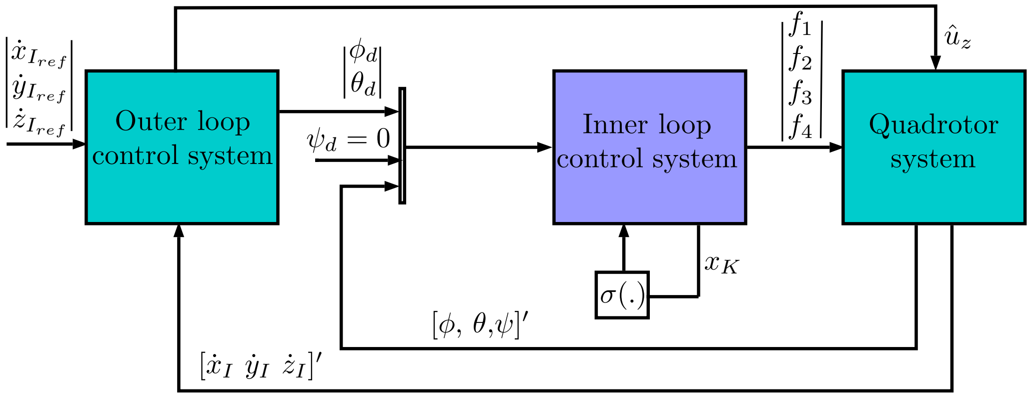

Figure 7.8: Modified structure for switched dynamic output feedback control.

are proportional to some constant value. Then output matrix and disturbance matrices are

$$C = \begin{bmatrix} 1 & 0 & 0 & 0 & 0 & 0 \\ 0 & 1 & 0 & 0 & 0 & 0 \\ 0 & 0 & 1 & 0 & 0 & 0 \end{bmatrix}, \quad D = 0.1 \begin{bmatrix} 0 & -1 & 0 & 1 \\ -1 & 0 & 1 & 0 \\ 1 & 1 & 1 & 1 \end{bmatrix}. \tag{7.92}$$

Again, we use Bryson's rule [76] such that smaller values of F_i result in a reduced limit on the control input. In addition to this, conflict criteria are chosen to obtain the switching that improves the closed-loop performance. As a result, weighting matrices are chosen for the conditions of Theorem 7.3.4 as follows

$$\begin{aligned} E_1 &= \text{diag}\{8.3, 8.3, 8.3, 0.01, 0.01, 0.01\}, \\ E_2 &= \text{diag}\{8, 8, 8, 0.01, 0.01, 0.01\}, \end{aligned}$$

$$F_1 = 0.6 \begin{bmatrix} 0 & -1 & 0 & 1 \\ -1 & 0 & 1 & 0 \\ 1 & 1 & 1 & 1 \\ 0 & -1 & 0 & 1 \\ -1 & 0 & 1 & 0 \\ 1 & 1 & 1 & 1 \end{bmatrix}, \quad F_2 = 0.5 \begin{bmatrix} 0 & -1 & 0 & 1 \\ -1 & 0 & 0.1 & 0 \\ 1 & 1 & 0.1 & 1 \\ 0 & -1 & 0 & 1 \\ -1 & 0 & 0.1 & 0 \\ 1 & 1 & 0.1 & 1 \end{bmatrix},$$

$$G_1 = 0.85 F_1, \quad G_2 = 0.65 F_1. \tag{7.93}$$

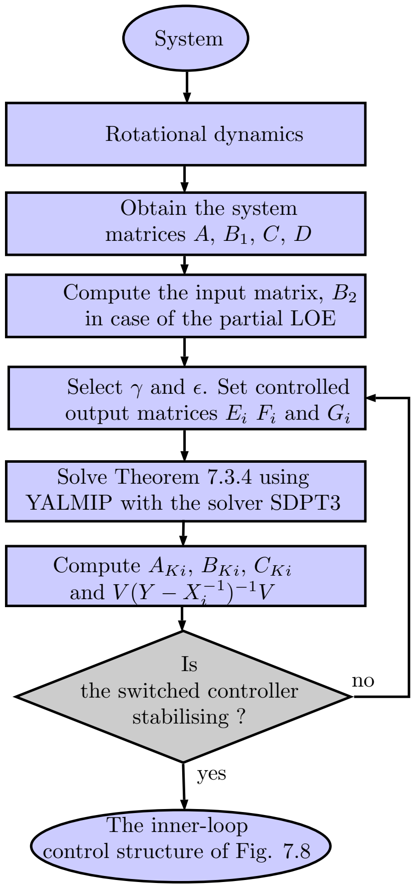

Figure 7.9: Flow diagram of the switched H_∞ dynamic output feedback control design.

Solving the LMIs in (7.47) and (7.48) results in $\rho = 2$ with a choice of $\epsilon = 0.063$ and $\gamma = 700$ found by line search.

7.6 Simulation Results

This section presents the results of simulations of the proposed FTC described in Section 7.5 for a fault in motor 3 with the model of the quadcopter dynamics given in Chapter 4. The fault profile is shown in Fig. 7.10. Here, the quadcopter is required to track the vertical velocity $\dot{z}_I$ command shown in Fig. 7.11(a).

The responses with the constant H_2 controller and with the switched FTC approaches are given in Fig 7.11. It can be seen that even a small fault, e.g., LOE = 0.1 at $t = 32$s (Fig. 7.10), can degrade the system performance by 4% if the constant H_2 control is used. Both switched-state feedback controllers show tolerance capability because the tracking performance is preserved with zero deterioration at t=10s for an LOE = 0.4. Similarly,

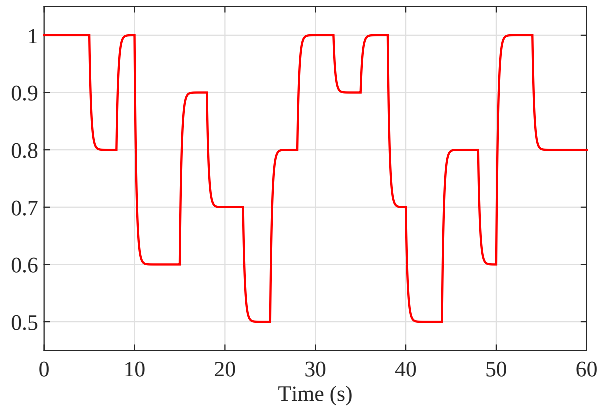

Figure 7.10: Profile for the loss of effectiveness in motor 3.

when the LOE is equal to 0.5, the switched controller exhibits a very small performance degradation. Overall, one can also see from Fig. 7.11(a) that vertical tracking with the switched H_∞ control is very satisfactory, as is the switched H_2 controller under different LOEs in motor 3.

The responses in terms of inertial velocity tracking in the x-direction are given in Fig. 7.11(b). The reference is set to zero; the quadcopter with the constant H_2 controller reaches an inertial longitudinal velocity $\dot{x}_I$ of 0.2 m/s, while with the switched H_∞ state feedback control reaches 0.01 m/s at $t = 44$s, respectively, showing that regulation is better when the switched H_∞ controller is used. It can be seen from Fig. 7.11(c) that the switched H_2 control loop exhibits small oscillations in terms of lateral velocity $\dot{y}_I$, which reaches 0.03 m/s with the constant H_2 controller at $t =$10s. The switched H_∞ controller performs better than the switched H_2 controller in terms of lateral velocity tracking as its tracking error is almost zero.

Figs. 7.12 and 7.13 show the switched H_∞ and H_2 state feedback control outputs, respectively. Switched-state feedback controllers do not produce much chattering in the fault-free case. When faults do occur, the switched-state feedback control output for motor 3 shows increased chattering and at a higher magnitude than for other outputs. Fig. 7.14 shows the translational velocity tracking when the relaxed minimum switching strategy is employed. It can be seen from Fig. 7.14(a) that vertical velocity tracking deteriorates by $\%10$ at $t = 10$ for LOE=0.4, and at $t = 40$ for LOE=0.5 when the switched H_∞ state feedback controller is used. The switched H_2 state feedback controller, however, exhibits a better vertical tracking response as deterioration is less than $\%6$ at both

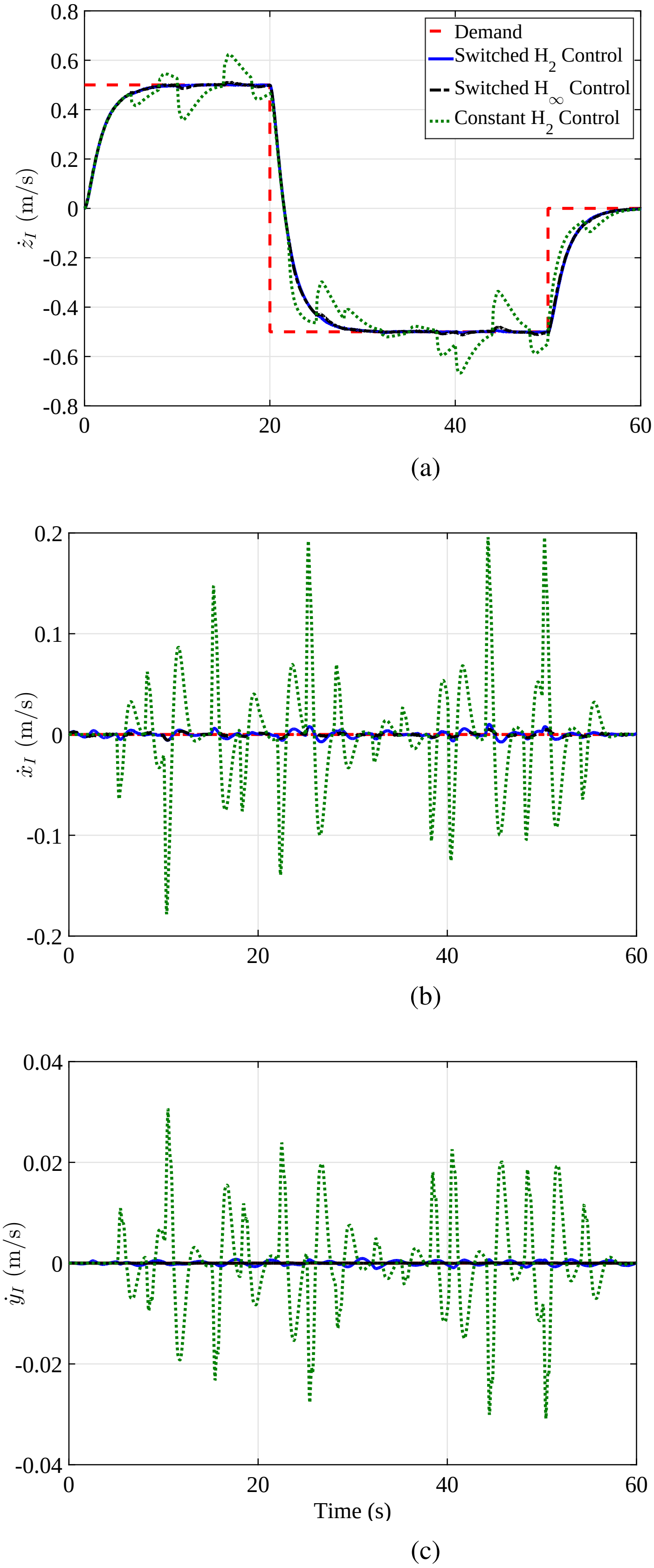

Figure 7.11: Translational velocities in the presence of time-varying LOE in motor 3: comparison of closed-loop responses of the constant H_2 control, the switched state feedback H_2 and H_∞ controllers.

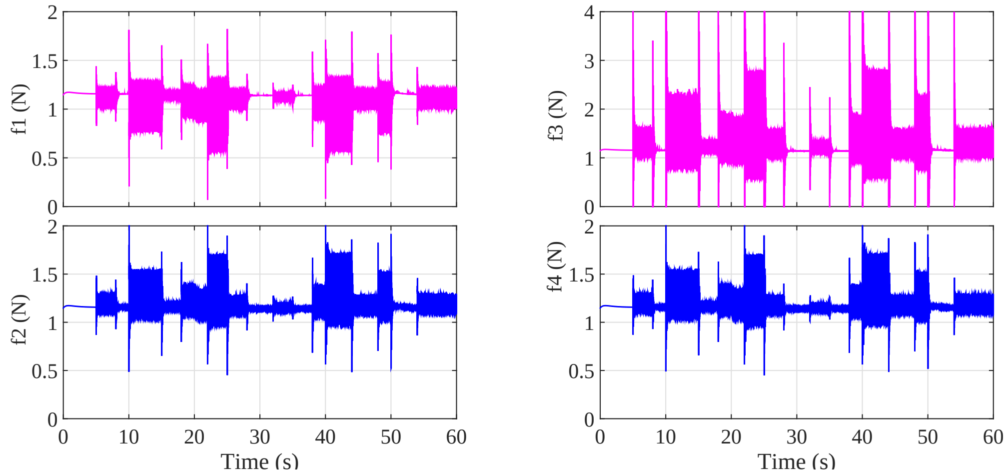

Figure 7.12: Switched H_∞ state feedback control output.

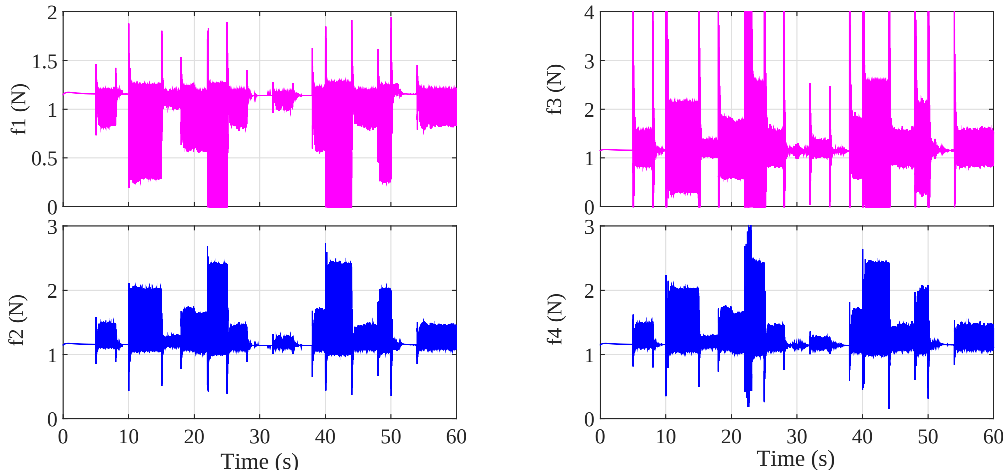

Figure 7.13: Switched H_2 state feedback control output.

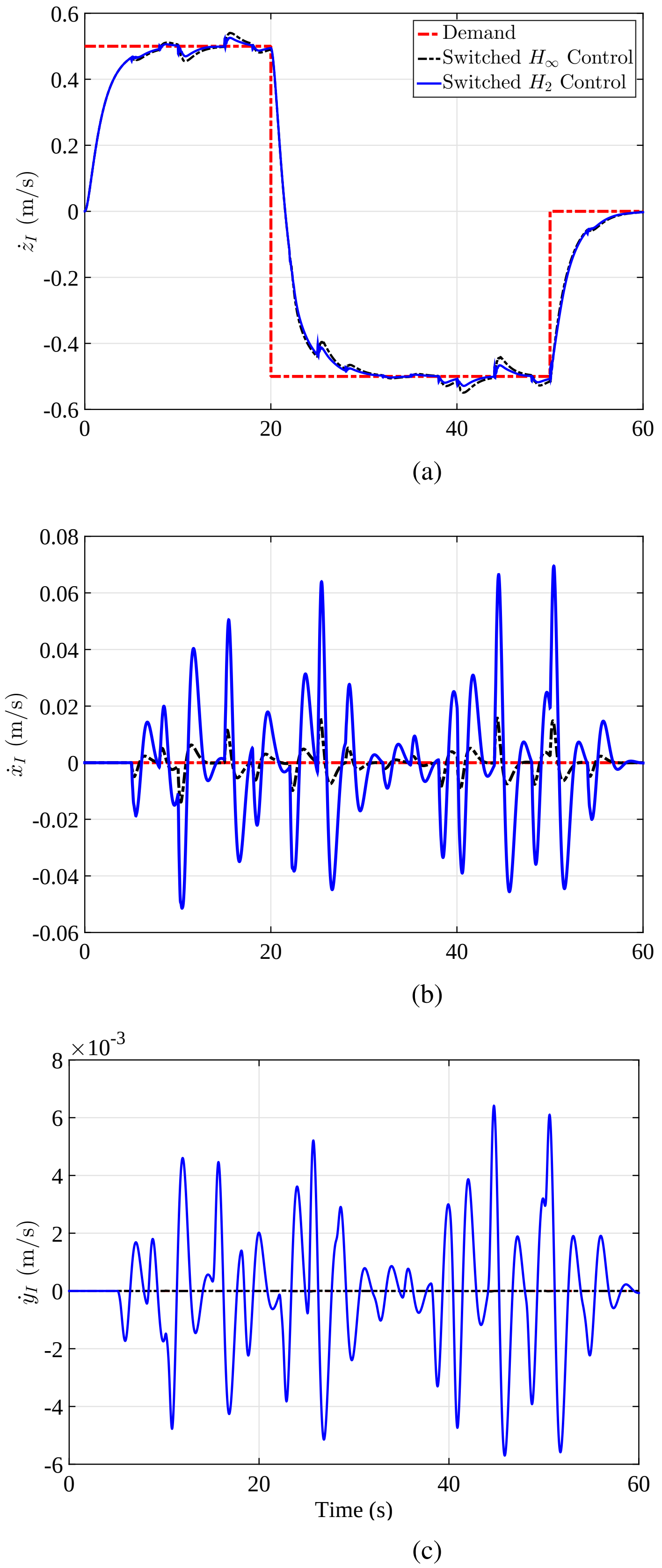

Figure 7.14: Translational velocities in the presence of time-varying LOE in motor 3: comparison of closed-loop responses of the switched state feedback H_2 and H_∞ controllers under the relaxed minimum switching strategy.

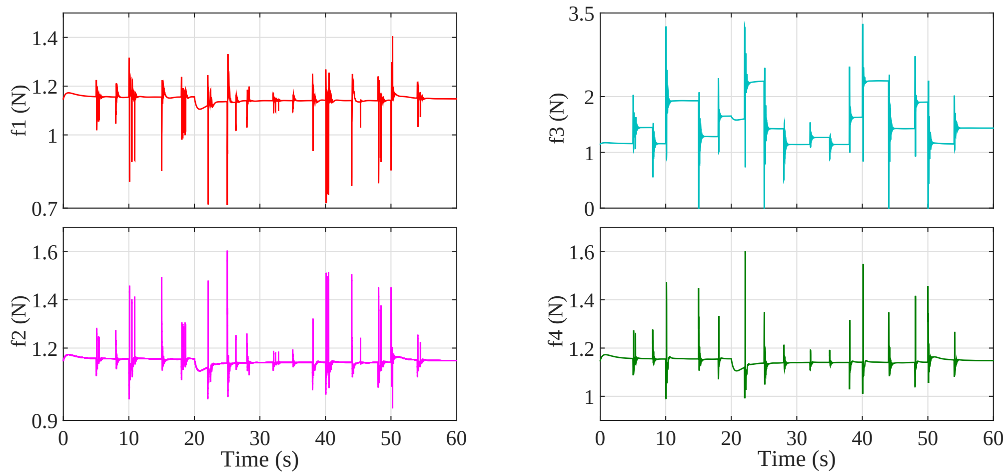

Figure 7.15: Switched H_∞ state feedback control output when using the relaxed minimum switching strategy.

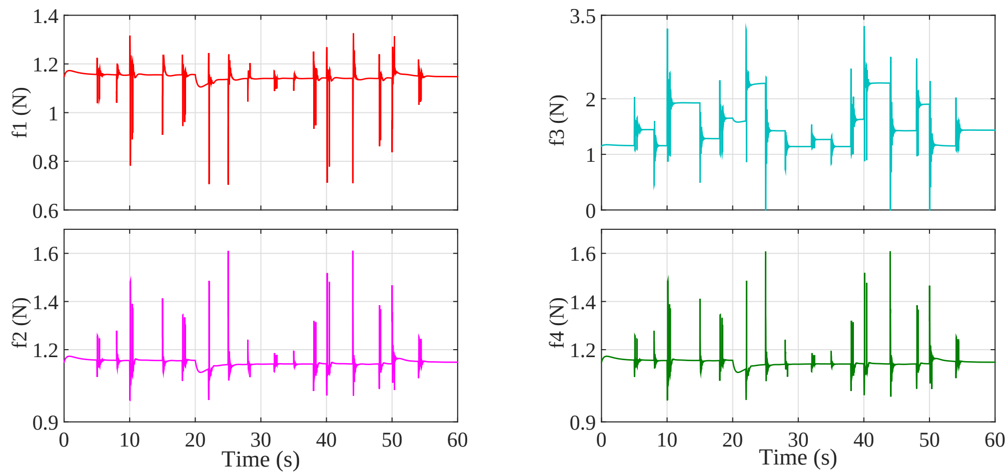

Figure 7.16: Switched H_2 state feedback control output when using the relaxed minimum switching strategy.

fault occurrence times. Fig. 7.14(b) shows that $\dot{x}_I$ tracking with the switched H_2 state feedback controllers is oscillatory around 0.05 m/s, and this oscillation is higher than that of the switched H_∞ state feedback controller. It can be said that the switched H_∞ controller is better than the switched H_2 controller in terms of longitudinal velocity tracking. One can also see from Fig. 7.14(c), that $\dot{y}_I$ tracking with the switched H_∞ state feedback controller is excellent.

Figs. 7.15 and 7.16 are given to illustrate that the relaxed min-switching strategy significantly reduces the chattering on control forces - at the expense of degraded performance - compared to the min-switching strategy. There is a trade-off between chattering and performance. All in all, the fault-tolerant controllers exhibit an acceptable performance when the quadcopter experiences a time-varying motor fault without the need for fault information. We show the closed-loop responses of the switched H_∞ dynamic

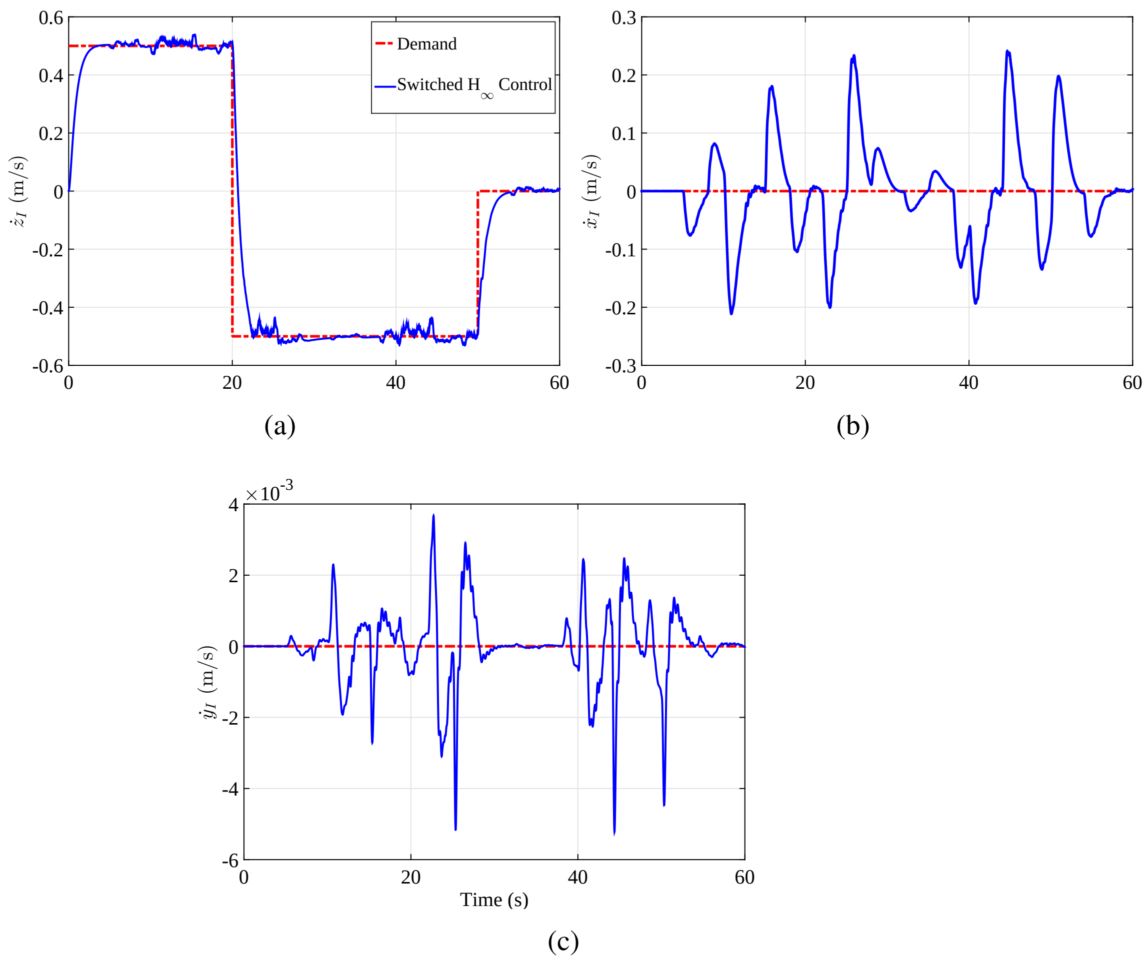

Figure 7.17: Translational velocities in the presence of a time-varying LOE in motor 3 when the switched H_∞ dynamic output controller is used.

output feedback controller in Fig. 7.17(a-c). Here, the tracking of the heave velocity is achieved well; on the other hand, longitudinal velocity tracking is somewhat worse than that of the state feedback switched control scheme. Furthermore, the vehicle is able to track the $\dot{y}_I$ demand well. Lastly, Fig. 7.18 is given to show the existence of chattering on forces that could be eliminated by considering the relaxed minimum strategy, as discussed in the case of the full-state feedback.

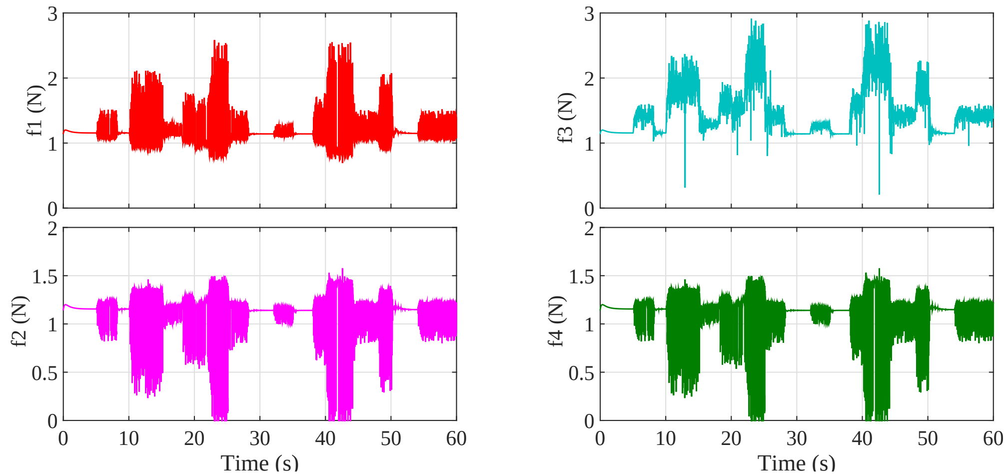

Figure 7.18: Switched dynamic output feedback H_∞ control outputs.

7.7 Conclusions

This chapter has presented a state-dependent switched recovery control scheme for a quadcopter. First of all, related stability and stabilising conditions are given in terms of LMIs satisfying pre-specified H_∞ performance. Here, a state feedback switched control scheme has been given, which consists of state feedback gains that are switched according to a minimum switching rule. The proposed controller compensates for the faults and allows the quadcopter to track the desired velocity commands accurately. The proposed approach exhibits good tolerance to faults without requiring explicit detection. However, chattering on control outputs is a drawback of the proposed approach if implemented on a real platform. To overcome the chattering problem, this chapter has also proposed a relaxed minimum strategy that gives the designer a degree of flexibility to reduce the chattering. Furthermore, a dynamic output feedback switched control scheme has been developed by assuming that the switching strategy depends only on the measured output through the controller state variable. Fault-tolerant performance of the switched H_∞ state feedback controller has been compared with the switched and constant H_2 state feedback controllers. Simulation results of the associated non-linear dynamics have shown the effectiveness of the proposed fault recovery control schemes based on the min-switching and relaxed min-switching strategies.

CHAPTER 8

CONCLUSIONS AND FUTURE RESEARCH

8.1 Conclusions

Quadcopter unmanned aerial vehicles require some form of advanced control system to maintain stability about all axes, even in the case of the malfunction of the actuation system. Such UAV systems can be modelled as a switched linear system. Due to the fact that the introduction of a switching mechanism may lead to closed-loop instability, it is practically important to analyse and synthesise the resulting switched system. For this purpose, we have focused on recoverability and stability of a quadcopter UAV by exploiting the stability and stabilisation of a switched system. This thesis has revealed that switched feedback controllers can maintain acceptable performance and stability for a quadcopter in the presence of severe motor faults using two different switched recovery strategies. First, a switching recovery control scheme was employed to cope with an imperfect actuation system under pre-determined dwell time constraints. Second, a state-dependent switched control approach has been proposed to overcome assumptions such as the existence of a fault detection mechanism, the continuity of the motor fault and its time variation rate, ensuring stability and a prescribed H_2 or H_∞ performance.

The main contributions of this thesis are summarised as follows.

- Chapter 5 investigates various methods including fixed-order, structured H_∞ synthesis, the LMI approach and mixed sensitivity H_∞ optimisation. In the literature, fixed-order [58] and structured H_∞ optimisation [44] algorithms are described as having the potential to overcome the practical limitation of full-order, unstructured H_∞ controllers. Hence, we present a comparative analysis of the flight performances of low-order robust controllers. The analysis presented here identifies the computational efficiency and tracking performance of each low-order robust control technique, comparing with a full-order H_∞ controller obtained using the Glover-Doyle algorithm. Simulation results have shown that the non-convex optimisation approach, *hinfstruct*, is more efficient than *hifoo* in computing low-order controllers for quadcopter UAVs.

- Chapter 6 presents switching recovery control schemes for a quadcopter UAV. Here, we have developed control schemes for two different problems: intermittent loss of a control signal, and loss of a motor. In order to design model-based control laws that are switched under dwell-time constraints, first the whole UAV system is divided into inner and outer loop subsystems, coupled with a non-linear interconnection term. The proposed recovery strategy consists of switching between the inner loop feedback controllers designed for the nominal and faulty modes of operation. By contrast, when new controllers were introduced into feedback loop, transient signals due to the initial states of the controllers occurred at each transition. These transient signals degraded the performance of the resulting closed loop in the presence of intermittent loss of the motor. A simple method has been introduced to initialise the controller states during switching instants. Closed-loop stability is guaranteed thanks to the standard and more advanced asynchronous dwell-time theories. Intermittent loss of control for a motor/ loss of a motor is simulated with a full non-linear model of the quadcopter. Two different simulation results have been reported. In the first simulation, developed switching control scheme permitted the quadcopter to track a desired velocity trajectory using the remaining control signals when one motor became uncontrollable. The second simulation was run for when a motor produces an intermittent thrust force. It has been demonstrated that fixed-order H_∞ output feedback controllers can stabilise the attitudes of the vehicle in the case of intermittent motor faults for the tracking of the translational velocities.

- In Chapter 7, a switched control scheme has been proposed for the problem of time varying loss of motor effectiveness. This control scheme consists of state feedback gains which are switched according to a min-switching rule. The proposed controller compensates for any faults and permits the quadcopter to track the desired velocity commands accurately. The proposed approach shows a good tolerance to faults without requiring explicit fault detection. We show that the stability and the performance of the controlled system is maintained, despite the fact that there is no fault detection mechanism involved in the design. The responses are also compared to those obtained with a constant H_2 state feedback controller. Simulation results show that the switched control scheme provides for better recovery than the constant state feedback controller. However, min-switching strategy displays chattering behaviour. A relaxed min-switching strategy was proposed to reduce the chattering on control outputs. Sufficient conditions for controller synthesis are given in terms of LMIs. Simulation results demonstrate that the chattering is significantly reduced by employing the relaxed min-switching strategy. Lastly, it is assumed that the entire state of the quadcopter UAV is not accessible. A switched H_∞ dynamic output feedback controller has been proposed; here, the min-switching strategy is based on only the measured output through the controller state variable. The proposed scheme was tested with the non-linear model of the quadcopter. The switched dynamic output feedback controller has the potential of enabling acceptable performance during heave velocity tracking. However, longitudinal velocity tracking is not as good as that with the switched state feedback controller.

The proposed switched control schemes have been shown to maintain the stability of the quadcopter under various motor fault scenarios. Simulation results show that the switched controllers developed enable the quadcopter to track the desired reference translational velocities in the presence of motor faults. There are some issues to be further investigated. We shall conclude this thesis by providing some future research directions.

8.2 Future Research

1. Asynchronous switched systems are common in many practical engineering applications. Hence, the study of stability and stabilisation of asynchronous switched systems has become a particularly significant research area [143, 154]. An asynchronous switched dynamic output feedback control can be designed for UAV systems using the asynchronous switched stability results of [157] given in Chapter 5.

It would be worth investigating whether a switched dynamic output controller can be designed under a time-varying loss of effectiveness in a motor.

2. The problem of multiple motor faults was not considered in this thesis. A state feedback switched control could be developed to cope with multiple motor and sensor faults.

3. The discrete-time counterpart of Chapter 6 seems a potential and challenging issue that needs to be addressed. The quadcopter subject to the loss of control effectiveness could be described by discrete time-varying polytopic systems. Switched state or output feedback controllers could be designed using modified Riccati-Metzler inequalities.

4. The issue of fault detection for switched time-varying polytopic systems has not yet been taken into account. A robust detection and isolation algorithm for time-varying faults would be worth investigating in instances where fault recovery control based on a min-switching strategy is insufficient.

5. Fixed-order H_∞ controller design [116, 117] in terms of LMIs could be investigated. Furthermore, the problem of stability and stabilisation for switched time-varying polytopic systems based on fixed-order control and state-dependent switching [49] would be an interesting and arduous work.

6. The presented control schemes could be implemented within a real quadcopter UAV system.

REFERENCES

[1] K Alexis, G Nikolakopoulos, and A Tzes. Model predictive quadrotor control: attitude, altitude and position experimental studies. *Control Theory & Applications, IET*, 6(12):1812–1827, 2012.

[2] Liron I Allerhand and Uri Shaked. Robust stability and stabilization of linear switched systems with dwell time. *IEEE Transactions on Automatic Control*, 56 (2):381–386, 2011.

[3] Erdinc Altug, James P Ostrowski, and Robert Mahony. Control of a quadrotor helicopter using visual feedback. In *Robotics and Automation. Proceedings. ICRA. IEEE International Conference on*, volume 1, pages 72–77. IEEE, 2002.

[4] Halim Alwi and Christopher Edwards. Fault tolerant control using sliding modes with on-line control allocation. *Automatica*, 44(7):1859–1866, 2008.

[5] Halim Alwi, Christopher Edwards, and Chee Pin Tan. *Fault detection and fault-tolerant control using sliding modes*. Springer Science & Business Media, 2011.

[6] M Hadi Amoozgar, Abbas Chamseddine, and Youmin Zhang. Experimental test of a two-stage kalman filter for actuator fault detection and diagnosis of an unmanned quadrotor helicopter. *Journal of Intelligent & Robotic Systems*, 70(1-4):107–117, 2013.

[7] Pierre Apkarian and Dominikus Noll. Nonsmooth H_∞ synthesis. *IEEE Transactions on Automatic Control*, 51(1):71–86, 2006.

[8] Denis Arzelier, Deaconu Georgia, Suat Gumussoy, Didier Henrion, et al. H_2 for HIFOO. *International Conference on Control and Optimization With Industrial Applications COIA*, 2011.

[9] Karl Johan Åström and Björn Wittenmark. *Adaptive Control*. Courier Corporation, 2008.

[10] Remus C Avram, Xiaodong Zhang, and Jonathan Muse. Quadrotor actuator fault diagnosis and accommodation using nonlinear adaptive estimators. *IEEE Transactions on Control Systems Technology*, 2017.

[11] C. Satici Aykut, Poonawala Hasan, and W. Song Mark. Robust optimal control of quadrotor UAVs. *Acess*, 1:79–93, 2013.

[12] Gary J Balas. Linear, parameter-varying control and its application to a turbofan engine. *International Journal of Robust and Nonlinear Control*, 12(9):763–796, 2002.

[13] GJ Balas, R Chiang, A Packard, and M Safonov. *Robust Control Toolbox: Getting Started Guide, The MathWorks*. MathWorks, 2012.

[14] Saeed Barghandan, Mohammad Ali Badamchizadeh, and Mohammad Reza Jahed-Motlagh. Improved adaptive fuzzy sliding mode controller for robust fault tolerant of a quadrotor. *International Journal of Control, Automation and Systems*, 15(1): 427–441, 2017.

[15] Christine M Belcastro and John V Foster. Aircraft loss-of-control accident analysis. In *Proceedings of AIAA Guidance, Navigation and Control Conference, Toronto, Canada, Paper No. AIAA-8004*, 2010.

[16] Lénaïck Besnard, Yuri B Shtessel, and Brian Landrum. Quadrotor vehicle control via sliding mode controller driven by sliding mode disturbance observer. *Journal of the Franklin Institute*, 349(2):658–684, 2012.

[17] Samir Bouabdallah and Roland Siegwart. Backstepping and sliding-mode techniques applied to an indoor micro quadrotor. In *Robotics and Automation,ICRA. Proceedings of the IEEE International Conference on*, pages 2247–2252. IEEE, 2005.

[18] Samir Bouabdallah and Roland Siegwart. Full control of a quadrotor. In *Intelligent robots and systems,IROS. IEEE/RSJ international conference on*, pages 153–158. IEEE, 2007.

[19] Samir Bouabdallah, Pierpaolo Murrieri, and Roland Siegwart. Design and control of an indoor micro quadrotor. In *Robotics and Automation. Proceedings. ICRA. IEEE International Conference on*, volume 5, pages 4393–4398. IEEE, 2004.

[20] Samir Bouabdallah, Andre Noth, and Roland Siegwart. PID vs LQ control techniques applied to an indoor micro quadrotor. In *Proceedings of the IEEE/RSJ International Conference on Intelligent Robots and Systems,(IROS)*, volume 3, pages 2451–2456. IEEE, 2004.

[21] Michael S Branicky. Multiple Lyapunov functions and other analysis tools for switched and hybrid systems. *Automatic Control, IEEE Transactions on*, 43(4): 475–482, 1998.

[22] Kemal Büyükkabasakal, Barış Fidan, and Aydoğan Savran. Mixing adaptive fault tolerant control of quadrotor UAV. *Asian Journal of Control*, 2017.

[23] Pedro Castillo, Alejandro Dzul, and Rogelio Lozano. Real-time stabilization and tracking of a four-rotor mini rotorcraft. *Control Systems Technology, IEEE Transactions on*, 12(4):510–516, 2004.

[24] Zhaohui Cen and Hassan Noura. An adaptive thau observer for estimating the time-varying LOE fault of quadrotor actuators. In *Control and Fault-Tolerant Systems (SysTol), Conference on*, pages 468–473. IEEE, 2013.

[25] Abbas Chamseddine, Youmin Zhang, Camille Alain Rabbath, Cedric Join, and Didier Theilliol. Flatness-based trajectory planning/replanning for a quadrotor unmanned aerial vehicle. *Aerospace and Electronic Systems, IEEE Transactions on*, 48(4):2832–2848, 2012.

[26] A Das, K Subbarao, and F Lewis. Dynamic inversion with zero-dynamics stabilisation for quadrotor control. *IET control theory & applications*, 3(3):303–314, 2009.

[27] Grace S Deaecto and José C Geromel. H_∞ control for continuous-time switched linear systems. *Journal of dynamic systems, measurement, and control*, 132(4): 041013, 2010.

[28] Grace S Deaecto and Jose C Geromel. H_∞ state feedback switched control for discrete time-varying polytopic systems. *International Journal of Control*, 86(4): 591–598, 2013.

[29] Grace S Deaecto, José C Geromel, and Jamal Daafouz. Dynamic output feedback H_∞ control of switched linear systems. *Automatica*, 47(8):1713–1720, 2011.

[30] Grace S Deaecto, José C Geromel, and Jamal Daafouz. Switched state-feedback control for continuous time-varying polytopic systems. *International Journal of Control*, 84(9):1500–1508, 2011.

[31] Raymond A DeCarlo, Michael S Branicky, Stefan Pettersson, and Bengt Lennartson. Perspectives and results on the stability and stabilizability of hybrid systems. *Proceedings of the IEEE*, 88(7):1069–1082, 2000.

[32] Jiuxiang Dong, Youyi Wang, and Guang-Hong Yang. H_∞ and mixed H_2/H_∞ control of discrete-time T-S fuzzy systems with local nonlinear models. *Fuzzy Sets and Systems*, 164(1):1–24, 2011.

[33] Chang Duan and Fen Wu. Analysis and control of switched linear systems via modified Lyapunov–Metzler inequalities. *International Journal of Robust and Nonlinear Control*, 24(2):276–294, 2014.

[34] Guy A Dumont and Mihai Huzmezan. Concepts, methods and techniques in adaptive control. In *Proceedings of the American Control Conference*, volume 2, pages 1137–1150. IEEE, 2002.

[35] Zachary T Dydek, Anuradha M Annaswamy, and Eugene Lavretsky. Adaptive control of quadrotor UAVs: A design trade study with flight evaluations. *Control Systems Technology, IEEE Transactions on*, 21(4):1400–1406, 2013.

[36] Christopher Edwards, Thomas Lombaerts, and Hafid Smaili. *Fault tolerant flight control*. Springer, 2010.

[37] Laurent El Ghaoui, Francois Oustry, and Mustapha AitRami. A cone complementarity linearization algorithm for static output-feedback and related problems. *Automatic Control, IEEE Transactions on*, 42(8):1171–1176, 1997.

[38] Thor I Fossen. *Marine control systems: guidance, navigation and control of ships, rigs and underwater vehicles*. Marine Cybernetics, 2002.

[39] A Freddi, S Longhi, and A Monteriu. Actuator fault detection system for a mini-quadrotor. In *Industrial Electronics (ISIE), 2010 IEEE International Symposium on*, pages 2055–2060. IEEE, 2010.

[40] Alessandro Freddi, Alexander Lanzon, and Sauro Longhi. A feedback linearization approach to fault tolerance in quadrotor vehicles. *Proceedings of the IFAC World Congress*, 18(1):5413–5418, 2011.

[41] Pascal Gahinet. Explicit controller formulas for LMI-based H_∞ synthesis. *Automatica*, 32(7):1007–1014, 1996.

[42] Pascal Gahinet and Pierre Apkarian. A linear matrix inequality approach to H_∞ control. *International journal of robust and nonlinear control*, 4(4):421–448, 1994.

[43] Pascal Gahinet and Pierre Apkarian. Decentralized and fixed-structure H_∞ control in MATLAB. In *Decision and Control and European Control Conference (CDC-ECC),50th IEEE Conference on*, pages 8205–8210. IEEE, 2011.

[44] Pascal Gahinet and Pierre Apkarian. Structured H_∞ synthesis in MATLAB. *Proceedings of the IFAC World Cogress*, 18(1):1435–1440, 2011.

[45] Pascal Gahinet and Pierre Apkarian. Frequency-domain tuning of fixed-structure control systems. *UKACC International Conference on Control*, pages 178–183, 2012.

[46] Subhabrata Ganguli, Andres Marcos, and Gary Balas. Reconfigurable LPV control design for boeing 747-100/200 longitudinal axis. In *Proceedings of the American Control Conference*, volume 5, pages 3612–3617. IEEE, 2002.

[47] Zhiqiang Gao and Panos J Antsaklis. Stability of the pseudo-inverse method for reconfigurable control systems. *International Journal of Control*, 53(3):717–729, 1991.

[48] Pedro Castillo Garcia, Rogelio Lozano, and Alejandro Enrique Dzul. *Modelling and control of mini-flying machines*. Springer Science & Business Media, 2006.

[49] Jose C Geromel and Patrizio Colaneri. Stability and stabilization of continuous-time switched linear systems. *SIAM Journal on Control and Optimization*, 45(5): 1915–1930, 2006.

[50] Jose C Geromel, Rubens H Korogui, and J Bernussou. H_2 and H_∞ robust output feedback control for continuous time polytopic systems. *IET Control Theory & Applications*, 1(5):1541–1549, 2007.

[51] José C Geromel, Patrizio Colaneri, and Paolo Bolzern. Dynamic output feedback control of switched linear systems. *Automatic Control, IEEE Transactions on*, 53 (3):720–733, 2008.

[52] K Glover and JC Doyle. State-space formulae for all stabilizing controllers that satisfy an H_∞ norm bound and relations to risk sensitivity. *Systems & control letters*, 11(3):167–172, 1988.

[53] Karolos M Grigoriadis and Robert E Skelton. Low-order control design for LMI problems using alternating projection methods. *Automatica*, 32(8):1117–1125, 1996.

[54] Slawomir Grzonka, Giorgio Grisetti, and Wolfram Burgard. A fully autonomous indoor quadrotor. *Robotics, IEEE Transactions on*, 28(1):90–100, 2012.

[55] Da-Wei Gu, Petko H.Petkov, and Mihail M. Konstantinov. *Robust control design with $MATLAB$*, volume 1. Springer, second edition, 2013.

[56] Suat Gumussoy and Michael L Overton. Fixed-order H_∞ controller design via HIFOO, a specialized nonsmooth optimization package. In *IEEE American Control Conference*, pages 2750–2754. IEEE, 2008.

[57] Suat Gumussoy, Marc Millstone, and Michael L Overton. H_∞ strong stabilization via HIFOO, a package for fixed-order controller design. In *Proceedings of the 47th IEEE Conference on Decision and Control*, pages 4135–4140, 2008.

[58] Suat Gumussoy, Didier Henrion, Marc Millstone, and Michael Overton. Multi-objective robust control with HIFOO 2.0. *IFAC Symposium on Robust Control Design*, 6(1):144–149, 2009.

[59] Mirza Tariq Hamayun, Christopher Edwards, and Halim Alwi. Design and analysis of an integral sliding mode fault tolerant control scheme. In *Fault Tolerant Control Schemes Using Integral Sliding Modes*, pages 39–61. Springer, 2016.

[60] Mirza Tariq Hamayun, Christopher Edwards, and Halim Alwi. *Fault tolerant control schemes using integral sliding modes*. Springer, 2016.

[61] Tomáš Haniš and Martin Hromcık. Lateral control for flexible BWB high-capacity passenger aircraft. In *Proceedings of the 18th IFAC World Congress*, pages 7233–7237, 2011.

[62] Joao P Hespanha and A Stephen Morse. Stability of switched systems with average dwell-time. In *Decision and Control, Proceedings of the 38th IEEE Conference on*, volume 3, pages 2655–2660. IEEE, 1999.

[63] Gabe Hoffmann, Dev Gorur Rajnarayan, Steven L Waslander, David Dostal, Jung Soon Jang, and Claire J Tomlin. The stanford testbed of autonomous rotorcraft for multi agent control (STARMAC). In *Digital Avionics Systems Conference. DASC 04. The 23rd*, volume 2, pages 12–E. IEEE, 2004.

[64] Gabriel M Hoffmann, Haomiao Huang, Steven L Waslander, and Claire J Tomlin. Quadrotor helicopter flight dynamics and control: Theory and experiment. *Proceedings of the AIAA Guidance, Navigation, and Control Conference*, pages 1–20, 2007.

[65] Gabriel M Hoffmann, Steven L Waslander, and Claire J Tomlin. Quadrotor helicopter trajectory tracking control. In *AIAA Guidance, Navigation and Control Conference and Exhibit, Honolulu, Hawaii*, pages 1–14, 2008.

[66] John Y Hung, Weibing Gao, and James C Hung. Variable structure control: A survey. *IEEE transactions on industrial electronics*, 40(1):2–22, 1993.

[67] David Hyland and Dennis Bernstein. The optimal projection equations for fixed-order dynamic compensation. *Automatic Control, IEEE Transactions on*, 29(11): 1034–1037, 1984.

[68] Rolf Isermann. Model-based fault-detection and diagnosis–status and applications. *Annual Reviews in control*, 29(1):71–85, 2005.

[69] Rolf Isermann and Peter Balle. Trends in the application of model-based fault detection and diagnosis of technical processes. *Control engineering practice*, 5(5): 709–719, 1997.

[70] Tetsuya Iwasaki. The dual iteration for fixed-order control. *IEEE Transactions on Automatic Control*, 44(4):783–788, 1999.

[71] Hojjat A Izadi, Youmin Zhang, and Brandon W Gordon. Fault tolerant model predictive control of quad-rotor helicopters with actuator fault estimation. *IFAC Proceedings Volumes*, 44(1):6343–6348, 2011.

[72] Samir Bennani Jean-Francois Magni and Jan Terlouw (Eds). *Robust Flight control: A Design Challenge*. Springer-Verlag Berling Heidelberg New York, Inc., 1997.

[73] Zhenyue Jia, Jianqiao Yu, Yuesong Mei, Yongbo Chen, Yuanchuan Shen, and Xiaolin Ai. Integral backstepping sliding mode control for quadrotor helicopter under external uncertain disturbances. *Aerospace Science and Technology*, 2017.

[74] Jin Jiang. Fault-tolerant control systems-an introductory overview. *Acta Automatica Sinica*, 1:017, 2005.

[75] Tor A Johansen and Thor I Fossen. Control allocationa survey. *Automatica*, 49(5): 1087–1103, 2013.

[76] MA Johnson and MJ Grimble. Recent trends in linear optimal quadratic multivariable control system design. In *IEE Proceedings D-Control Theory and Applications*, volume 134, pages 53–71. IET, 1987.

[77] Colin Jones. Reconfigurable flight control. Technical report, University of Cambridge, 2003.

[78] DA Joosten and JM Maciejowski. MPC design for fault-tolerant flight control purposes based upon an existing output feedback controller. *IFAC Proceedings Volumes*, 42(8):253–258, 2009.

[79] B Jung, Y Kim, and C Ha. Fault tolerant flight control system design using a multiple model adaptive controller. *Proceedings of the Institution of Mechanical Engineers, Part G: Journal of Aerospace Engineering*, 223(1):39–50, 2009.

[80] Hassan K Khalil. *Noninear Systems*. Prentice-Hall, New Jersey, 1996.

[81] Andreas Kwiatkowski and Herbert Werner. PCA-based parameter set mappings for LPV models with fewer parameters and less overbounding. *IEEE Transactions on Control Systems Technology*, 16(4):781–788, 2008.

[82] Alexander Lanzon, Alessandro Freddi, and Sauro Longhi. Flight control of a quadrotor vehicle subsequent to a rotor failure. *Journal of Guidance, Control, and Dynamics*, pages 1–12, 2014.

[83] Robert C Leishman, John Macdonald, Randal W Beard, and Timothy W McLain. Quadrotors & accelerometers :state estimation with an improved dynamic model. *Control Systems*, 34(1):28–41, 2014.

[84] Douglas J Leith and William E Leithead. Survey of gain-scheduling analysis and design. *International journal of control*, 73(11):1001–1025, 2000.

[85] Daniel Liberzon. *Switching in systems and control*. Springer Science & Business Media, 2003.

[86] Daniel Liberzon and A Stephen Morse. Basic problems in stability and design of switched systems. *IEEE Control systems*, 19(5):59–70, 1999.

[87] Daniel Liberzon and Roberto Tempo. Common Lyapunov functions and gradient algorithms. *IEEE Transactions on Automatic Control*, 49(6):990–994, 2004.

[88] Hai Lin and Panos J Antsaklis. Stability and stabilizability of switched linear systems: a survey of recent results. *Automatic control, IEEE Transactions on*, 54(2): 308–322, 2009.

[89] Vincenzo Lippiello, Fabio Ruggiero, and Diana Serra. Emergency landing for a quadrotor in case of a propeller failure: A backstepping approach. In *Intelligent Robots and Systems (IROS), IEEE/RSJ International Conference on*, pages 4782–4788. IEEE, 2014.

[90] Johan Lofberg. YALMIP: A toolbox for modeling and optimization in MATLAB. In *Computer Aided Control Systems Design, International Symposium on*, pages 284–289. IEEE, 2004.

[91] Francisco Ronay López-Estrada, Jean-Christophe Ponsart, Didier Theilliol, Youmin Zhang, and Carlos-Manuel Astorga-Zaragoza. LPV model-based tracking control and robust sensor fault diagnosis for a quadrotor UAV. *Journal of Intelligent & Robotic Systems*, 84(1-4):163–177, 2016.

[92] Dailiang Ma, Yuanqing Xia, Tianya Li, and Kai Chang. Active disturbance rejection and predictive control strategy for a quadrotor helicopter. *IET Control Theory & Applications*, 10(17):2213–2222, 2016.

[93] Jan Maciejowski and Colin Jones. MPC fault-tolerant flight control case study: Flight 1862. In *Proceedings of the International Federation of Automatic Control on Safeprocess Sympoisum*, number EPFL-CONF-169763, pages 119–124, 2003.

[94] Jan Marian Maciejowski. Multivariable feedback design. *Electronic Systems Engineering Series, Wokingham, England: Addison-Wesley*, 1, 1989.

[95] Tarek Madani and Abdelaziz Benallegue. Control of a quadrotor mini-helicopter via full state backstepping technique. In *Proceedings of the 45th IEEE Conference on Decision and Control*, pages 1515–1520. IEEE, 2006.

[96] Jean-François Magni, Samir Bennani, and Jan Terlow. Robust flight control (a design challenge). *Lecture notes in control and information sciences*, 1997.

[97] Aryeh Marks, James F Whidborne, and Ikuo Yamamoto. Control allocation for fault tolerant control of a VTOL octorotor. In *Control (CONTROL), UKACC International Conference on*, pages 357–362. IEEE, 2012.

[98] Abdel-Razzak Merheb, Hassan Noura, and Francois Bateman. Active fault tolerant control of quadrotor UAV using sliding mode control. In *Unmanned Aircraft Systems (ICUAS), International Conference on*, pages 156–166. IEEE, 2014.

[99] Abdel-Razzak Merheb, Hassan Noura, and François Bateman. Design of passive fault–tolerant controllers of a quadrotor based on sliding mode theory. *International Journal of Applied Mathematics and Computer Science*, 25(3):561–576, 2015.

[100] Nathan Michael, Daniel Mellinger, Quentin Lindsey, and Vijay Kumar. The grasp multiple micro-UAV testbed. *Robotics & Automation Magazine, IEEE*, 17(3):56–65, 2010.

[101] Alejandro Montiel-Varela, Omar Santos, Sergio Salazar, Hugo Romero, Adrian Martinez-Vazquez, and Rogelio Lozano. Estimation of velocity and position for a quadrotor aircraft in GPS denied environment. In *Unmanned Aircraft Systems (ICUAS), International Conference on*, pages 430–436. IEEE, 2016.

[102] Mark W Mueller and Raffaello D'Andrea. Stability and control of a quadrocopter despite the complete loss of one, two, or three propellers. In *International Conference on Robotics & Automation (ICRA)*, pages 45–52, 2014.

[103] H Oloomi and B Shafai. Weight selection in mixed sensitivity robust control for improving the sinusoidal tracking performance. In *Decision and Control. Proceedings. 42nd IEEE Conference on*, volume 1, pages 300–305. IEEE, 2003.

[104] Robert Orsi, Uwe Helmke, and John B Moore. A newton-like method for solving rank constrained linear matrix inequalities. *Automatica*, 42(11):1875–1882, 2006.

[105] Konstantinos G Papadopoulos. *PID controller tuning using the magnitude optimum criterion*. Springer, 2015.

[106] Ron J Patton. Fault-tolerant control systems: The 1997 situation. In *IFAC symposium on fault detection supervision and safety for technical processes*, volume 3, pages 1033–1054, 1997.

[107] Wilfrid Perruquetti and Jean-Pierre Barbot. *Sliding mode control in engineering*. CRC Press, 2002.

[108] Paul Pounds, Robert Mahony, and Peter Corke. Modelling and control of a quad-rotor robot. In *Proceedings Australasian Conference on Robotics and Automation*. Australian Robotics and Automation Association Inc., 2006.

[109] Guilhem Puyou and Pierre Ezerzere. Tolerance of aircraft longitudinal control to the loss of scheduling information: toward a performance oriented approach. *7th IFAC Symposium on Robust Control Design*, 7(1):393–399, 2012.

[110] Guilherme V Raffo, Manuel G Ortega, and Francisco R Rubio. An integral predictive/nonlinear H_∞ control structure for a quadrotor helicopter. *Automatica*, 46(1): 29–39, 2010.

[111] M Ranjbaran and K Khorasani. Generalized fault recovery of an under-actuated quadrotor aerial vehicle. In *American Control Conference (ACC)*, pages 2515–2520. IEEE, 2012.

[112] Mina Ranjbaran and Khashayar Khorasani. Fault recovery of an under-actuated quadrotor aerial vehicle. In *Decision and Control (CDC), 49th IEEE Conference on*, pages 4385–4392. IEEE, 2010.

[113] Mickael Rodrigues, Didier Theilliol, Samir Aberkane, and Dominique Sauter. Fault tolerant control design for polytopic LPV systems. *International Journal of Applied Mathematics and Computer Science*, 17(1):27–37, 2007.

[114] Damiano Rotondo, Fatiha Nejjari, Abel Torren, and Vicenc Puig. Fault tolerant control design for polytopic uncertain LPV systems: Application to a quadrotor. In *Control and Fault-Tolerant Systems (SysTol), Conference on*, pages 643–648. IEEE, 2013.

[115] Asif Sabanovic, Leonid M Fridman, and Sarah K Spurgeon. *Variable structure systems: from principles to implementation*, volume 66. IET, 2004.

[116] Mahdieh S Sadabadi and Alireza Karimi. Fixed-order control of LTI systems subject to polytopic uncertainty via the concept of strictly positive realness. In *American Control Conference (ACC)*, pages 2882–2887. IEEE, 2015.

[117] Arash Sadeghzadeh and Alireza Karimi. Fixed structure H_2 controller design for polytopic systems via LMIs. *Optimal Control Applications and Methods*, 36(6): 794–809, 2015.

[118] I. Sadeghzadeh, A. Mehta, A. Chamseddine, and Youmin Zhang. Active fault tolerant control of a quadrotor UAV based on gain-scheduled PID control. In *Electrical Computer Engineering (CCECE), 25th IEEE Canadian Conference on*, pages 1–4. IEEE, 2012.

[119] Iman Sadeghzadeh, Ankit Mehta, and Youmin Zhang. Fault tolerant control of a quadrotor helicopter using model reference adaptive control. In *ASME International Design Engineering Technical Conferences and Computers and Information in Engineering Conference*, pages 997–1004. American Society of Mechanical Engineers, 2011.

[120] Iman Sadeghzadeh Kalat, Abbas Chamseddine, Youmin Zhang, and Didier Theilliol. Control allocation and re-allocation for a modified quadrotor helicopter against actuator faults. In *8th IFAC Symposium on Fault Detection, Supervision and Safety of Technical Processes*, volume 8, pages 247–252, 2012.

[121] S Salazar-Cruz, Juan Escareno, David Lara, and Rogelio Lozano. Embedded control system for a four-rotor UAV. *International Journal of Adaptive Control and Signal Processing*, 21(2-3):189–204, 2007.

[122] Ricardo Sanz, Luis Rodenas, Pedro Garcia, and Pedro Castillo. Improving attitude estimation using inertial sensors for quadrotor control systems. In *Unmanned Aircraft Systems (ICUAS), International Conference on*, pages 895–901. IEEE, 2014.

[123] Michael Schinkel, Yongji Wang, and Ken Hunt. Stable and robust state feedback design for hybrid systems. In *Proceedings of the American Control Conference*, volume 1, pages 215–219. IEEE, 2000.

[124] Kenneth D Sebesta and Nicolas Boizot. A real-time adaptive high-gain EKF, applied to a quadcopter inertial navigation system. *Industrial Electronics, IEEE Transactions on*, 61(1):495–503, 2014.

[125] Tabassom Sedighi, Paul Phillips, and Peter d Foote. Model-based intermittent fault detection. *Procedia CIRP*, 11:68–73, 2013.

[126] Pau Segui-Gasco, Yazan Al-Rihani, Hyo-Sang Shin, and Al Savvaris. A novel actuation concept for a multi rotor UAV. *Journal of Intelligent & Robotic Systems*, 74(1-2):173–191, 2014.

[127] Lakshmi Prabha Nattamai Sekar, Alexander Santos, and Olga Beltramello. IMU drift reduction for augmented reality applications. In *International Conference on Augmented and Virtual Reality*, pages 188–196. Springer, 2015.

[128] Farid Sharifi, Mostafa Mirzaei, Brandon W Gordon, and Youmin Zhang. Fault tolerant control of a quadrotor UAV using sliding mode control. In *Control and Fault-Tolerant Systems (SysTol), Conference on*, pages 239–244. IEEE, 2010.

[129] D Shin, G Moon, and Y Kim. Design of reconfigurable flight control system using adaptive sliding mode control: actuator fault. *Proceedings of the Institution of Mechanical Engineers, Part G: Journal of Aerospace Engineering*, 219(4):321–328, 2005.

[130] Jong-Yeob Shin and Christine M Belcastro. Performance analysis on fault tolerant control system. *Control Systems Technology, IEEE Transactions on*, 14(5):920–925, 2006.

[131] Jong-Yeob Shin, N Eva Wu, and Christine Belcastro. Adaptive linear parameter varying control synthesis for actuator failure. *Journal of Guidance, Control, and Dynamics*, 27(5):787–794, 2004.

[132] Grace Silva Deaecto, Mateus Souza, and José C Geromel. Chattering free control of continuous-time switched linear systems. *Control Theory & Applications, IET*, 8(5):348–354, 2014.

[133] S Skogestad and I Postlethwaite. *Multivariable feedback control: analysis and design*. John Wiley & Sons Ltd., second edition, 2005.

[134] Christoffer Sloth, Thomas Esbensen, and Jakob Stoustrup. Robust and fault-tolerant linear parameter-varying control of wind turbines. *Mechatronics*, 21(4): 645–659, 2011.

[135] Jean-Jacques E Slotine, Weiping Li, et al. *Applied nonlinear control*, volume 60. Prentice-Hall Englewood Cliffs, NJ, 1991.

[136] Manohar B Srikanth, Zachary T Dydek, Anuradha M Annaswamy, and Eugene Lavretsky. A robust environment for simulation and testing of adaptive control for mini-UAVs. In *American Control Conference. ACC.*, pages 5398–5403. IEEE, 2009.

[137] M Staroswiecki. Fault tolerant control: the pseudo-inverse method revisited. *IFAC Proceedings Volumes*, 38(1):418–423, 2005.

[138] Grzegorz Szafranski, Roman Czyba, Wojciech Janusz, and Wojciech Blotnicki. Altitude estimation for the UAV's applications based on sensors fusion algorithm. In *Unmanned Aircraft Systems (ICUAS), International Conference on*, pages 508–515. IEEE, 2013.

[139] Abdelhamid Tayebi and Stephen McGilvray. Attitude stabilization of a VTOL quadrotor aircraft. *IEEE Transactions on Control Systems Technology*, 14(3):562–571, 2006.

[140] David Titterton, John Weston, et al. Strapdown inertial navigation technology. 2-nd edition. *The Institution of Electronical Engineers, Reston USA*, 2004.

[141] Kim-Chuan Toh, Michael J Todd, and Reha H Tütüncü. SDPT3a MATLAB software package for semidefinite programming, version 1.3. *Optimization methods and software*, 11(1-4):545–581, 1999.

[142] Erik Vanhoutte, Stefano Mafrica, Franck Ruffier, Reinoud J Bootsma, and Julien Serres. Time-of-travel methods for measuring optical flow on board a micro flying robot. *Sensors*, 17(3):571, 2017.

[143] Rui Wang, Zhi-Gang Wu, and Peng Shi. Dynamic output feedback control for a class of switched delay systems under asynchronous switching. *Information Sciences*, 225:72–80, 2013.

[144] Tao Wang, Wenfang Xie, and Youmin Zhang. Sliding mode fault tolerant control dealing with modeling uncertainties and actuator faults. *ISA transactions*, 51(3): 386–392, 2012.

[145] Zhengxin Weng, Ron Patton, and Ping Cui. Active fault-tolerant control of a double inverted pendulum. *IFAC Proceedings Volumes*, 39(13):1515–1520, 2006.

[146] Fen Wu and Xuejing Cai. Switching fault-tolerant control of a flexible air-breathing hypersonic vehicle. *Proceedings of the Institution of Mechanical Engineers, Part I: Journal of Systems and Control Engineering*, 227(1):24–38, 2013.

[147] D Xie, Q Wang, and Y Wu. Average dwell-time approach to L_2-gain control synthesis of switched linear systems with time delay in detection of switching signal. *IET Control Theory & Applications*, 3(6):763–771, 2009.

[148] Rongyi Yan, Xiao He, and Donghua Zhou. Detection of intermittent faults for linear stochastic systems subject to time-varying parametric perturbations. *IET Control Theory & Applications*, 10(8):903–910, 2016.

[149] Zhenyu Yang, Mogens Blanke, and Michel Verhaegen. Robust control mixer method for reconfigurable control design using model matching. *Control Theory & Applications, IET*, 1(1):349–357, 2007.

[150] Dan Ye and G-H Yang. Adaptive fault-tolerant tracking control against actuator faults with application to flight control. *IEEE Transactions on control systems technology*, 14(6):1088–1096, 2006.

[151] Alain Yetendje, Maria M Seron, and José A De Doná. Robust MPC multicontroller design for actuator fault tolerance of constrained systems. *IFAC Proceedings Volumes*, 44(1):4678–4683, 2011.

[152] Bin Yu, Youmin Zhang, Ismael Minchala, and Yaohong Qu. Fault-tolerant control with linear quadratic and model predictive control techniques against actuator faults in a quadrotor UAV. In *Control and Fault-Tolerant Systems (SysTol), Conference on*, pages 661–666. IEEE, 2013.

[153] Xiang Yu and Jin Jiang. A survey of fault-tolerant controllers based on safety-related issues. *Annual Reviews in Control*, 39:46–57, 2015.

[154] Chengzhi Yuan and Fen Wu. Asynchronous switching output feedback control of discrete-time switched linear systems. *International Journal of Control*, 88(9): 1766–1774, 2015.

[155] Chengzhi Yuan and Fen Wu. Almost output regulation of switched linear dynamics with switched exosignals. *International Journal of Robust and Nonlinear Control*, 2017.

[156] Juqian Zhang, Laihong Zhou, Cunxu Li, and Bangchun Wen. Binary observers based control for quadrotor unmanned aerial vehicle with disturbances and measurement delay. *Proceedings of the Institution of Mechanical Engineers, Part G: Journal of Aerospace Engineering*, page 0954410017717286, 2017.

[157] Lixian Zhang and Huijun Gao. Asynchronously switched control of switched linear systems with average dwell time. *Automatica*, 46(5):953–958, 2010.

[158] YM Zhang, A Chamseddine, CA Rabbath, BW Gordon, C-Y Su, S Rakheja, C Fulford, J Apkarian, and P Gosselin. Development of advanced FDD and FTC techniques with application to an unmanned quadrotor helicopter testbed. *Journal of the Franklin Institute*, 350(9):2396–2422, 2013.

[159] Youmin Zhang and Jin Jiang. Fault tolerant control system design with explicit consideration of performance degradation. *IEEE Transactions on Aerospace and Electronic Systems*, 39(3):838–848, 2003.

[160] Youmin Zhang and Jin Jiang. Bibliographical review on reconfigurable fault-tolerant control systems. *Annual reviews in control*, 32(2):229–252, 2008.

[161] Q Zhao and J Jiang. Reliable state feedback control system design against actuator failures. *Automatica*, 34(10):1267–1272, 1998.

[162] Kemin Zhou and Pramod P Khargonekar. Robust stabilization of linear systems with norm-bounded time-varying uncertainty. *Systems & Control Letters*, 10(1): 17–20, 1988.

[163] Qing-Li Zhou, Youmin Zhang, C Rabbath, and Didier Theilliol. Design of feedback linearization control and reconfigurable control allocation with application to

a quadrotor UAV. In *Control and Fault-Tolerant Systems (SysTol), Conference on*, pages 371–376. IEEE, 2010.